



저작자표시-비영리-변경금지 2.0 대한민국

이용자는 아래의 조건을 따르는 경우에 한하여 자유롭게

- 이 저작물을 복제, 배포, 전송, 전시, 공연 및 방송할 수 있습니다.

다음과 같은 조건을 따라야 합니다:



저작자표시. 귀하는 원저작자를 표시하여야 합니다.



비영리. 귀하는 이 저작물을 영리 목적으로 이용할 수 없습니다.



변경금지. 귀하는 이 저작물을 개작, 변형 또는 가공할 수 없습니다.

- 귀하는, 이 저작물의 재이용이나 배포의 경우, 이 저작물에 적용된 이용허락조건을 명확하게 나타내어야 합니다.
- 저작권자로부터 별도의 허가를 받으면 이러한 조건들은 적용되지 않습니다.

저작권법에 따른 이용자의 권리는 위의 내용에 의하여 영향을 받지 않습니다.

이것은 [이용허락규약\(Legal Code\)](#)을 이해하기 쉽게 요약한 것입니다.

[Disclaimer](#)

Ph.D. Dissertation of Engineering

Sorption Material Development for
PFAS, BTEX, and Heavy Metals
Removal from Contaminated
Subsurface

오염지반의 과불화화합물, BTEX, 및 중금속제거를
위한 흡착물질 개발

February 2023

Graduate School of Civil and Environmental
Engineering

Seoul National University

Geotechnical and Geoenvironmental Major

Rahim Shahrokhi

Sorption Material Development for PFAS, BTEX, and Heavy Metals Removal from Contaminated Subsurface

Name of Examiner: Professor Junbom Park

Submitting a Ph.D. Dissertation of
Civil Engineering

February 2023

Graduate School of Civil and Environmental
Engineering
Seoul National University
Geotechnical and Geoenvironmental Major

Rahim Shahrokhi

Confirming the Ph.D. Dissertation written by

Rahim Shahrokhi

February 2023

Chair Professor Choong-Ki Chung (Seal)
Vice Chair Professor Junbom Park (Seal)
Examiner Professor Sung-Ryul Kim (Seal)
Examiner Professor Changwon Kwak (Seal)
Examiner Professor Xiaochao Tang (Seal)

Abstract

Rapid industrialization and urbanization have improved the living standards, productivity and economy. However, they have caused adverse consequences to the environment by discharging uncontrolled contaminants from numerous industries. The industrial zones constantly produce considerable amount of wastewater at an alarming rate, which contaminates subsurface from soil to groundwater. South Korea like other developed countries is suffering from this problem with various types of pollutant including inorganic and organic substances releasing to the subsurface in industrial zones. Among the organic contaminants, per and polyfluoroalkyl substances (PFAS) as one the most emerging halogenated hydrocarbons, and commonly utilized industrial solvents of benzene, toluene, ethylbenzene, and xylene (BTEX) have been frequently detected in South Korea. Additionally, due to the extensive application of raw materials by industries, various toxic heavy metals including Pb, Zn, and Cu are introduced into the subsurface in South Korea at high concentration.

Bottom reactive layer can be a remediation technique in which sorbents are added to the soil matrix to prevent spreading contaminants into groundwater by sorbing and stabilizing them inside the soil. In this study some efficient and cost-effective sorbents including recyclable waste materials have been developed for using as bottom reactive layer to stabilize the most common contaminants in South Korea.

In the first section of the present study, potential of pulverized waste tires (PWTs), either on their own or mixed with soil (well graded sand), to act as bottom reactive layer was evaluated by conducting laboratory tests for assessing their adsorption and geotechnical properties. PWT (0, 5, 10, 15, 25, and 100 wt%) was mixed with soil to evaluate the removal of BTEX components and two heavy metal ions (Pb^{2+} and Cu^{2+}). Additionally, tire derived activated carbon (TAC) has been produced using carbonization and chemical activation techniques for the removal of three synthetic heavy metal ions (Pb^{2+} , Cu^{2+} and Zn^{2+}) from an aqueous solution. In the second step of the present research, the most prevalent PFAS substances in South Korea, including two long-chain (PFOA and PFOS) and two short-chain (PFBA and PFBS) PFAS, have been removed from both soil and aqueous phase by developing

chitosan beads (CB) and amine functional grafted chitosan beads (GCB). Furthermore, the solid- liquid distribution coefficient (k_d) for PFAS components has been estimated by performing the column sorption tests.

At each step of this research a series of batch adsorption–desorption experiments including single and competitive isotherm sorption tests, kinetic sorption tests, selectivity sorption, influence of pH, and reusability test has been performed to evaluate the efficiency of each sorbents for removing determined pollutants.

The results demonstrated the developed sorbents from waste materials have potential to be used as an efficient sorbent for removing organic/inorganic contaminants from soil and water.

Keyword: Pollutants, Bottom Reactive layer, Heavy metals, BTEX, PFAS

Student Number: 2017-36819

Table of contents

List of Tables	vii
List of Figures.....	viii
Chapter 1. Background and main objectives	1
1.1 Introduction	1
1.1.1 Discharging of contaminants	1
1.1.2 Remediation method.....	3
1.2 Necessity of research and main objectives	4
1.3. Dissertation organization.....	5
Chapter 2. Literature review	8
2.1 Heavy metal Sorption	8
2.2 BTEX sorption.....	11
2.2.1 BTEX sorption by activated carbon	11
2.2.2 BTEX sorption by mineral sorbents	12
2.2.3 BTEX sorption by other sorbents	13
2.3 PFAS sorption.....	14
2.4 Experimental plans	17
2.4.1 Characterization of adsorbents	17
2.4.2 Zeta potential of sorbents	18
2.4.3 X-ray photoelectron spectroscopy (XPS)	18
2.4.4 Surface functional groups using FT-IR	19
2.4.5 SEM imaging/EDS	19
2.4.6 Powder X-ray diffraction (XRD).....	20
2.4.7 Cation exchange capacity (CEC) and anion exchange capacity (AEC)	20
2.4.8 Compaction tests.....	21
2.4.9 Hydraulic conductivity test.....	21
2.4.10 Compression test.....	21
2.4.11 Shear strength test.....	22
2.5 Data analysis	22
2.5.1 Langmuir model	24
2.5.2 Freundlich model.....	24
2.5.3 Dubinin Radushkevich (D-R) model.....	25
2.5.4 Temkin model.....	25
2.5.5 Kinetic adsorption models	26

Chapter 3. BTEX and heavy metal removal by waste tire and its activated carbon.....	27
3.1 Introduction	27
3.2 Material and Methods.....	29
3.2.1 Raw materials and their characterization.....	29
3.2.2 PWT- soil mixture ratios	30
3.2.3 General procedures for producing activated carbon	30
3.2.4 Preparation of Tire-derived Activated Carbon (TAC)	32
3.2.5 Adsorbate solution	32
3.2.6 Single and competitive isotherm batch adsorption tests.....	33
3.2.7 Chemical stability of PWT and TAC	34
3.2.8 Desorption and reusability potential tests for TAC and CAC	34
3.3 Results and Discussion	35
3.3.1 BTEX removal by S-PWT mixtures.....	35
3.3.2 Heavy metal removal by S-PWT mixtures.....	40
3.3.3 Chemical stability of S-PWT mixtures.....	42
3.3.4 Compaction test results.....	46
3.3.5 Hydraulic conductivity test results	47
3.3.6 Compression test results	47
3.3.7 Shear strength test results	48
3.3.8 Long term settlement of S-PWT mixtures.....	53
3.3.9 Simulation the BTEX movement through modified layer with PWT	56
3.3.10 Cost comparison of PWT with other common sorbents.....	59
3.3.11 Physicochemical characteristics of TAC and CAC	60
3.3.12 Elemental analysis of TAC and CAC.....	65
3.3.13 Zeta potential of TAC and CAC.....	65
3.3.14 FT-IR test results	67
3.3.15 XPS test results.....	70
3.3.16 Single batch sorption of TAC and CAC	75
3.3.17 Competitive sorption of TAC and CAC	80
3.3.18 Kinetic sorption results of TAC and CAC.....	81
3.3.20 Chemical stability of TAC.....	84
3.3.21 Desorption and reusability test of TAC and CAC	86
3.3.22 Possible adsorption mechanisms involved for sorption heavy metals by TAC and CAC	87
3.4 Summary	88

Chapter 4. PFAS removal from contaminated subsurface	92
4.1 Introduction	92
4.1.1 Background.....	92
4.1.2 PFAS removal difficulties and main objectives of present chapter.....	98
4.2 Material and Methods.....	100
4.2.1 Raw materials	100
4.2.2 NaOH concentration	100
4.2.3 Chitosan concentration	101
4.2.4 Grafting of chitosan-based sorbents	101
4.2.5 Preparation of Chitosan Beads (CB)	103
4.2.6 Preparation of Grafted Chitosan Beads (GCB)	104
4.2.7 Preparation of clay chitosan composite	104
4.2.8 Adsorbate solution.....	106
4.2.9 Batch adsorption tests.....	106
4.2.10 Batch adsorption tests by real field water.....	107
4.2.11 Reusability tests for the developed sorbents.....	108
4.2.12 Synthesis of the contaminated soil	109
4.2.13 Leaching tests for stabilized soils.....	109
4.2.14 Rapid Small column test for determining the K_d	110
4.2.15 PFAS measurement	112
4.3 Result and Discussion	112
4.3.1 Characteristics of sorbents.....	112
4.3.2 Zeta potential	114
4.3.3 Isotherm sorption results	115
4.3.4 Kinetic sorption results.....	118
4.3.5 Influence of pH on sorption capacity of sorbents.....	121
4.3.6 Single point adsorption coefficient.....	122
4.3.7 Selectivity sorption test results	123
4.3.8 Batch adsorption tests by real field water results	125
4.3.9 Leaching test results	128
4.3.10 RSCCT results	130
4.3.11 Cost comparison of GCB with other common sorbents	133
4.4. Summary	134
Chapter 5. Conclusions and Recommendations.....	137
5.1 Conclusions	137

5.2 Recommendations for future studies.....	139
Bibliography	141
초 록.....	156
Acknowledgment.....	158

List of Tables

Table 2.1 Previous research for sorption of heavy metals	10
Table 2.2 BTEX components physiochemical properties.....	11
Table 2.3 Previous research for sorption of PFAS substance	15
Table 3.1 Elemental analysis of PWT and soil materials.....	36
Table 3.2 Langmuir and Freundlich parameters for BTEX component sorption by S–PWT mixtures	39
Table 3.3 Physical characteristics of mixtures investigated.....	41
Table 3.4 Langmuir and Freundlich parameters for Pb and Cu sorption by S–PWT mixtures	42
Table 3.5 Released metals from PWT at different pH values.....	43
Table 3.6 XRF chemical analysis for PWT investigated	45
Table 3.7 Effective-stress shear strength parameter values deduced for S–PWT mixtures.....	51
Table 3.8 Shear strength properties of different S–PWT mixtures reported in the literature	52
Table 3.9 Secondary compression index for soft clay in Korea (Suneel et al. 2018)	56
Table 3.10 Sorption and permeability parameters for MODFLOW simulation	58
Table 3.11 Cost comparison of PWT with common adsorbents.....	60
Table 3.12 Physicochemical characteristics of TAC and CAC samples	62
Table 3.13 EDS results for CAC and TAC.....	64
Table 3.14 Zeta Potential (ZP) of TAC and CAC samples before and after Pb ion adsorption	66
Table 3.15 XPS elemental composition of the TAC and CAC before and after Pb (II) adsorption	74
Table 3.16 Langmuir, Freundlich, D-R, and Temkin isotherm parameters for Pb, Cu and Zn sorption by TAC and CAC samples.....	77
Table 3.17 Adsorption capacities for different types of adsorbents reported in literature	80
Table 3.18 Pseudo first-order and pseudo second-order parameters for Pb, Cu and Zn sorption by TAC and CAC samples.....	83
Table 3.19 Fitting parameters of the intra-particle diffusion model for heavy metal adsorption on TAC and CAC	84
Table 3.20 Released metals from TAC at different pH values	85
Table 3.21 Desorption rate from ion loaded TAC and CAC samples	86
Table 4.1 Previous research about PFAS distribution in Korea.....	96
Table 4.2 Most detected PFAS contaminants in Korea with their basic properties.....	97
Table 4.3 Properties of soils used for column tests.....	112
Table 4.4 Physicochemical characteristics of developed sorbents.....	114
Table 4.5 Langmuir and Freundlich parameters for PFAS substance sorption by each sorbent	118
Table 4.6 Pseudo first-order and pseudo second-order parameters for PFAS sorption by sorbents...	120
Table 4.7 Present anions and cations in the Han river water	125
Table 4.8 Obtained K_d and K_{oc} values for each PFASs from column tests	132
Table 4.9 Cost comparison of GCB with common adsorbents.....	134

List of Figures

Fig. 1.1 Spreading the contaminated zone into subsurface.....	2
Fig. 1.2 A systematic categorisation of contaminants including the most released pollutants in South Korea.....	3
Fig. 1.3 Bottom Reactive layer for stabilizing the contaminants inside the soil.....	4
Fig. 2.1 CEC extraction equipment.....	20
Fig. 3.1 Images of PWT material: (a) individual PWT particles; (b) surface morphology as revealed by scanning electron microscopy.....	30
Fig. 3.2 Grain size distributions of the soil and PWT materials	30
Fig. 3.3 BTEX component sorption by S–PWT mixtures: a) Benzene, b) Toluene, c) Ethylbenzene and d) Xylene.....	36
Fig. 3.4 Heavy metals adsorption by S–PWT mixtures, a) Lead and b) Copper	40
Fig. 3.5 SEM–EDS results for PWT investigated.....	45
Fig. 3.6 Standard Proctor-compaction results for various S–PWT mixtures	46
Fig. 3.7 One-dimensional compression test results, a) Void ratio versus effective vertical stress, b) Variation of compression and swelling indices with PWT content	47
Fig. 3.8 Drained direct-shear test results for various S–PWT mixtures: shear stress against horizontal displacement traces for σ'_v of a) 40 kPa, b) 80 kPa and c) 160 kPa; d) Peak shear stress against effective vertical stress	48
Fig. 3.9 Drained direct-shear test results for various S–PWT mixtures: vertical displacement against horizontal displacement traces for σ'_v of a) 40 kPa, b) 80 kPa and c) 160 kPa; d) Angle of dilation for the three applied normal stress levels. Note: following convention, negative vertical displacement indicates dilative behavior	49
Fig. 3.10 Time-dependent volumetric strains for sand and mixed sand with tire chips ($v=80$ kPa) (Wartman et al. 2007)	54
Fig. 3.11 Secondary compression index versus waste tire content (Wartman et al. 2007).....	54
Fig. 3.12 Creep behavior of tire shreds and clayey soil.....	55
Fig. 3.13 Imaginary landfill for MODFLOW simulation	57
Fig. 3.14 Concentration of BTEX versus time at points A and B.....	59
Fig. 3.15 (a-b) N_2 adsorption-desorption isotherms at 77 K, (c-d) pore size distribution of the CAC and TAC samples.....	61
Fig. 3.16 SEM Images of the TAC sample at (a) 5,000 \times , (b) 10,000 \times and (c) 50,000 \times magnification and the CAC sample at (d) 5,000 \times , (e) 10,000 \times and (f) 50,000 \times magnification.....	63
Fig. 3.17 XRD patterns for TAC and CAC samples.....	64
Fig. 3.18 FT-IR spectra of TAC and CAC (a) before and (b-c) after adsorption of heavy metals	68
Fig. 3.19 XPS characterization of TAC and CAC samples (a): XPS survey spectra of TAC and CAC before and after adsorption Pb ion; (b) and (c): C1s and O1s XPS spectra of TAC before loading Pb ion; (d), (e) and (f) : C1s ,O1s and Pb 4f XPS spectra of TAC after loading Pb ion; (g) and (h): C1s and O1s XPS spectra of CAC before loading Pb ion; (k), (l) and (m) : C1s ,O1s and Pb 4f7 XPS spectra of CAC after loading Pb ion.....	72
Fig. 3.20 Relative contents of oxygen functional groups for TAC and CAC samples before and after Pb ion adsorption	74
Fig. 3.21 (a-b) Heavy metals adsorption by TAC and CAC samples, (c-d) heavy metals adsorption from loaded TAC and CAC samples	76
Fig. 3.22 Comparison of the maximum adsorption capacity of the heavy metals in competitive and single adsorption isotherms for TAC and CAC samples (initial concentration of ions: 500 $mg \cdot L^{-1}$)	81
Fig. 3.23 (a-b) Kinetics of heavy metals adsorption by TAC and CAC samples	82
Fig. 3.24 The piecewise fitting curves of heavy metals adsorption kinetics of TAC and CAC by the intra-particle diffusion model	84

Fig. 3.25 TAC and CAC adsorption capacities for heavy metals after three successive adsorption-desorption cycles	87
Fig. 3.26 Comparison of TAC and CAC for their dominant sorption mechanism for heavy metals....	88
Fig. 4.1 Human exposure to PFASs contaminants.....	93
Fig. 4.2 PFASs concentration and distribution in soil, water, and sediment near Asan lake.....	94
Fig. 4.3 PFASs concentration and distribution in industrial, urban, and agricultural soils throughout the Korea.....	94
Fig. 4.4 Concentration and distribution of PFASs in the human's blood (n=786) from the general Korean population (Seo et al., 2018)	95
Fig. 4.5 FT-IR results for modified montmorillonite with different cationic surfactants	102
Fig. 4.6 Zeta potential results for modified montmorillonite with different cationic surfactants	103
Fig. 4.7 Preparation of chitosan beads (CB) and grafted chitosan beads (GCB).....	104
Fig. 4.8 Preparation of montmorillonite grafted chitosan beads (MT-GCB).....	105
Fig. 4.9 Location of taking sample from Han river.....	108
Fig. 4.10 Grain size distribution of soil	109
Fig. 4.11 Schematic plan of RSSCT column at this study	111
Fig. 4.12 Zeta potential of sorbents at different pH values	115
Fig. 4.13 Isotherm sorption results for (a) PFOA, (b) PFOS, (c) PFBA, and (d) PFBS substances ..	117
Fig. 4.14 Kinetic sorption results for (a) PFOA, (b) PFOS, (c) PFBA, and (d) PFBS substances	119
Fig. 4.15 Influence of pH on sorption of (a) PFOA, (b) PFOS, (c) PFBA, and (d) PFBS substances	122
Fig. 4.16 Single point adsorption coefficients for each sorbent at environmentally relevant concentration.....	123
Fig. 4.17 Performance of each sorbents (a) CB, (b) GCB, (c) PAC, and (d) AER for PFAS sorption in single and multi-solute	124
Fig. 4.18 Performance of each sorbents for PFAS sorption in DI an and Han river water	127
Fig. 4.19 PFAS stabilization by MT-GCB and GAC inside the soil at (a) contamination level of 1.5 $\mu\text{g.g}^{-1}$, and (b) contamination level of 10 $\mu\text{g.g}^{-1}$	129
Fig. 4.20 (a-c) Breakthrough curves for PFAS components.....	131
Fig. 4.21 Relationship between K_{oc} and K_{ow} values for each PFAS substance along with the derived equations	133

Chapter 1. Background and main objectives

1.1 Introduction

1.1.1 Discharging of contaminants

Huge quantities of hazardous wastes produced with the fast development of industrialization are inadvertently discharged into the soil. Consequently, due to rainwater infiltration the released contaminants will spread from soil to the groundwater, and as a result, nearby subsurface can become contaminated with mixed wastes of organic/inorganic pollutants (Figure 1.1)

The contaminants that may be released to the subsurface near industrial zones are classified into two categories: inorganic pollutants and organic pollutants. Each of these two groups has its own subgroups, with inorganic pollutants being divided into metal and nonmetal, and organic pollutants classified as hydrocarbons (non-halogenated) and halogenated organic pollutants. Furthermore, both non-halogenated and halogenated organic pollutants are separated into aromatic and aliphatic subgroups (Figure 1.2) (Swartjes 2011).

South Korea (hereafter, Korea) like other developed countries is suffering from this problem with a variety type of pollutant including inorganic and organic substances releasing to the subsurface in industrial zones. Following the above mentioned systematic categorisation of contaminants (Figure 1.2), among the organic contaminants, per and polyfluoroalkyl substances (PFAS) as one the most emerging halogenated hydrocarbons, and commonly utilized industrial solvents of benzene, toluene, ethylbenzene, and xylene (BTEX) have been frequently detected in Korea (Ministry of Environment Korea 2017). Additionally, due to the extensive application of raw materials by industries, various toxic heavy metals including Pb, Zn, and Cu are introduced into the subsurface in Korea at high concentration. According to the Ministry of Environment Korea (2017), 15.3% of investigated industrial zones were in the warning level of heavy metal contamination.

These contaminants are toxic, mostly nonbiologically degradable, and cause significant threats to the ecosystem and human health by accumulating in the groundwater (Chowdhury et al. 2017). For example, PFAS and BTEX components can cause several adverse health

outcomes in humans such as cancer, thyroid hormone disruption, immunotoxicity, hepatotoxicity, and neurodevelopmental problems (Eichler and Little 2020). Moreover, despite being essential of some metals for living organisms and important for the proper function of enzymes in humans, excessive concentrations of copper and zinc ions in the human body can lead to kidney/liver damage as well as Alzheimer’s disease (Li et al. 2019). Similarly, lead can disturb many systems of the human body, such as the nervous system, and may cause diseases such as anemia (Zhang et al. 2020).

Therefore, inadvertent discharge of inorganic/ organic contaminants is a pressing environmental issue that must be remediated before releasing any type of contaminated water back into the ecosystem.

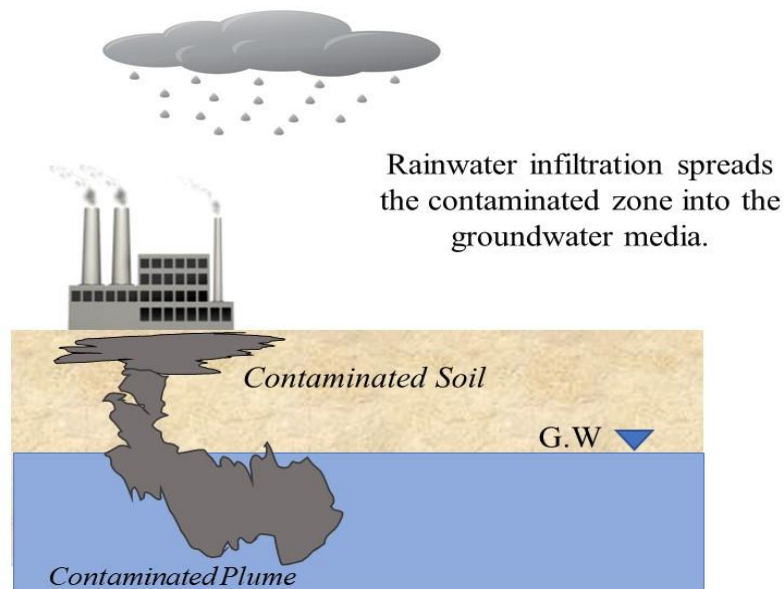


Fig. 1.1 Spreading the contaminated zone into subsurface

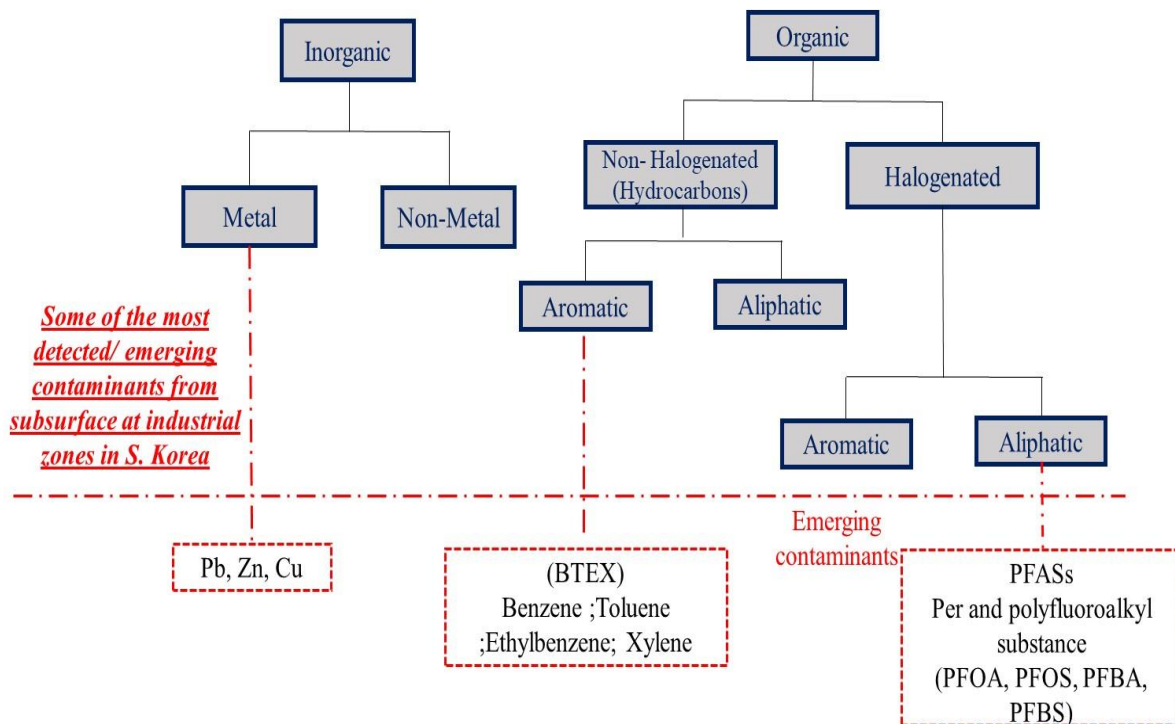


Fig. 1.2 A systematic categorisation of contaminants including the most released pollutants in South Korea

1.1.2 Remediation method

Numerous techniques have been applied for removing inorganic and organic contaminants. For instance, dissolved heavy metals can be removed by ion exchange, chemical precipitation, flocculation, ultrafiltration, reverse osmosis, and/or electrolytic removal (Yadav et al. 2019). Air stripping, bioremediation, chemical oxidation and adsorption have been reported as the most practical techniques for removing organic contaminants (Hou et al. 2021).

However, most of these treatment techniques are environmentally damaging and suffer from lower efficiency, limitation in operation, and high cost, all of which restrict their application (Shan et al. 2020). Of the mentioned methods, adsorption is considered to be the most effective physicochemical technique for the reduction of both organic and inorganic pollutants due to the simplicity of operation, cost-effectiveness, and regenerative nature of the adsorbents (Baimenov et al. 2020).

Bottom reactive layer is a sorption-based remediation technique where sorbents are added to the soil matrix to prevent contaminants from spreading into groundwater by sorbing and

stabilizing them within the soil (Figure 1.3). From geoenvironmental perspective, the sorbents used as a bottom reactive layer should satisfy sufficient environmental protection capacity while maintaining the bearing capacity of foundation after mixing.

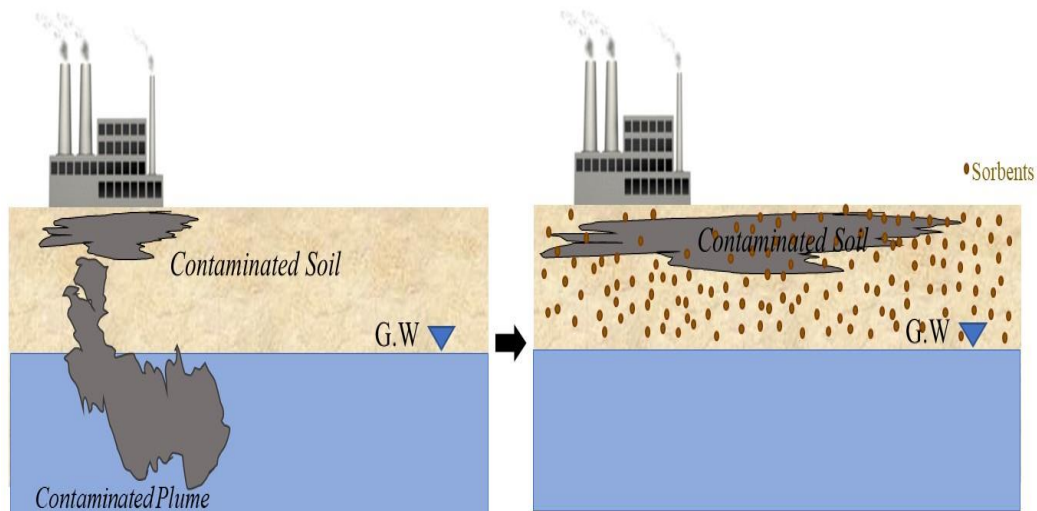


Fig. 1.3 Bottom Reactive layer for stabilizing the contaminants inside the soil

Many different types of sorbents have been used to treat inorganic and organic pollutants, with the most common adsorbents studied being granular/ powdered activated carbon, clay minerals, agro-industrial waste materials, biochar, zerovalent iron (ZVI), and ion exchange resins (Vardhan et al. 2019; Varsha et al. 2022). Efficiency and performance of these sorbents for removing inorganic/organic pollutants including PFAS, BTEX, Pb, Zn, and Cu as the most common contaminants in Korea have been examined by several previous researches, which will be briefly stated in the following section.

1.2 Necessity of research and main objectives

As stated in the literature review section, performance of the most common sorbents with highly efficient removal capacity has been already proved by previous research for removing the heavy metals and organic contaminants. Previous research, however, has some limitations, and other factors should be considered before using these sorbents as the bottom reactive layer. For examples:

1. These commercial sorbents have not been examined when used as fill materials (no specific report for geotechnical properties and sorption efficiency simultaneously).
2. Development of some efficient recyclable materials as adsorptive fill materials for removing emerging contaminants including PFAS substances has not been considered.
3. In Korea, most of the studies have focused on PFAS detection and its distribution. However, PFAS sorption by considering some influential factors (e.g. pH, selectivity sorption) has not been evaluated yet.
4. Distribution coefficient (K_d) of PFAS as one of the most influential parameters for predicating the fate and transport of PFAS substances in the subsurface has not been reported yet.

Therefore, conducting research while taking the aforementioned factors into account is necessary to determine the interaction of sorbents including recyclable sorbents with the mostly released contaminants into the subsurface.

Given the research needs described above, the overarching goal of the research is to elucidate the interactions between the most common contaminants in Korea and sorbents while they are used as bottom reactive layer by conducting laboratory-scale sorption and desorption experiments. Three specific objectives were further defined in the proposed research.

Objective 1 was the development of efficient and cost-effective sorbents including recyclable materials for removing the most common contaminants in Korea.

Objective 2 was to find the optimum mixing ratio of these sorbents as using fill materials while satisfying sorption and bearing capacities at the same time.

Objective 3 was to find the distribution coefficient (K_d) of PFAS contaminants by developing sorption equation.

1.3. Dissertation organization

Chapter 1 provides the overview of the study background, main objectives, and structure of the dissertation.

Chapter 2 provides a detailed literature review on sorption of the most detected contaminants in Korea by commonly used sorbents. Also, the experimental plans and models which have been used at the present dissertation are described in this chapter.

Chapter 3 provides information on the world's and Korea's waste tire disposal problems, as well as the use of these waste materials as a recyclable sorptive fill material. Detail information on using waste tires as engineering fill materials for removing BTEX components and heavy metals while simultaneously examining the geotechnical performance of the soil–pulverized waste tire (S–PWT) mixtures is provided. Making tire activated carbon and using it as a sorbent for removing heavy metals in comparison of commercial activated carbon is also presented. Additionally, detailed discussion on interactions between heavy metals and tire activated carbon by considering the possible adsorption mechanisms is also presented. This chapter addresses objectives 1 and 2. This chapter has been published in two articles:

1. Shahrokhi-Shahraki, R., Kwon, P.S., Park, J., O’Kelly, B.C., Rezania, S., 2020. BTEX and heavy metals removal using pulverized waste tires in engineered fill materials. *Chemosphere* 242, 125281. <https://doi.org/10.1016/j.chemosphere.2019.125281>.
2. Shahrokhi-Shahraki, R., Benally, C., Gamal El-din, M., Park, J., 2021. High Efficiency Removal of Heavy Metals Using Tire-derived Activated Carbon vs Commercial Activated Carbon: Insights into the Adsorption Mechanisms. *Chemosphere* 264, 128455. <https://doi.org/10.1016/j.chemosphere.2020.128455>.

Chapter 4 addresses Objectives 1, 3 and begins by providing information about PFAS problems in Korean environments, including the most commonly detected PFAS components and their basic properties. Efficiency of chitosan and grafted chitosan beads for removing of PFAS contaminants in comparison of two other commercial sorbent (pulverized activated carbon and anion exchange resin) has been provided on the basis of experimental observations and statistical analysis. Detailed information on stabilization of PFAS contaminants inside the soil by using two sorbents including clay composite and granular activated carbon is provided as well. Moreover, at this chapter the solid- liquid distribution coefficient (k_d) for PFAS components has been estimated by performing the column sorption tests.

Chapter 5 finally presents the main conclusions of the present study and recommendations for further researches.

Chapter 2. Literature review

2.1 Heavy metal Sorption

Heavy metals are defined as elements with atomic weights ranging from 63.5 to 200.6 g. mol⁻¹ and densities greater than 5 g. cm⁻³ (Raychaudhuri et al. 2021). They are accumulating in the environment and are not biodegradable due to their similar qualities to those of metals. The International Agency for Research on Cancer (IARC) and the United States Environmental Protection Agency (US EPA) both classify heavy metals as human carcinogens (Srivastava et al. 2021).

Sorption of heavy metals from both soil and water have been already examined at different concentrations from ppb to ppm ranges. Some previous research including different types of adsorbents for heavy metal removal are presented in Table 2.1. As shown in Table 2.1 activated carbon showed higher sorption capacity for heavy metal removal in comparison of other sorbents with the reported adsorption capacity ranging from 23.42 to 295.3 mg. g⁻¹. Also, biochar had sorption capacities comparable to the activated carbon. Zeolite as one of the most common clayey sorbents displayed sorption capacity at range of 25.8 to 109.89 mg. g⁻¹ for heavy metals with higher removal for Pb (Table 2.1).

Agro-industrial wastes have also been used for heavy metal removal in some studies. For instance, at the study by Singh et al. (2021) waste biomass and waste plastics were pyrolyzed and tested for heavy metal removal from aqueous phase. The adsorption capacity of both biochar and plastic chars was maximized at pH 4 with a removal rate of 99.9%. Furthermore, the isothermal sorption models revealed that biochar has greater sorption capacity than plastic chars. In other research the brewed tea waste *Camellia sinensis* was tested for the removal of four heavy metals, namely lead (Pb), zinc (Zn), nickel (Ni), and cadmium (Cd) from simulated aqueous solution by considering the influence of pH. According to the results, brewed tea waste showed heavy metal removal potential, with maximum adsorption capacities of 1.197, 1.457, 1.163, and 2.468 mg. g⁻¹ for Pb, Zn, Ni, and Cd, respectively, obtained at optimum pH of 4.0 to 5.0 (Çelebi et al. 2020).

Additionally, efficiency of sorbents for immobilizing the metals inside the soil has been reported by some researchers. For example, in one study the amended soil with modified zeolite has decreased the leaching of Pb, Cd, and Zn in the soil by 21%, 10%, and 19% , respectively (Ma et al. 2022). In another research the P fertilizer stabilized soil has reduced the Pb, Cu, and Zn concentration by 85%, 74.3%, and 91.9%, respectively (Wu et al. 2017).

Islam et al. (2017) investigated the effectiveness of calcined cockle shell (CCS) as a stabilizer sorbent to immobilize heavy metals (Cd, Pb, and Zn) in mine tailing soil. After amending the soil with 5% CCS and incubating it for 28 days, it was subjected to a leaching test with 0.1M HCl. The leaching tests results revealed discharge of Cd, Pb, and Zn was reduced by 85, 85, and 91%, respectively.

Some geomaterials (CaCl₂-modified zeolite and bentonite) and nanoparticles (ZnO and MgO) were used to stabilize heavy metals in alkaline soil treated with three sewage sludges (SS). In Rasht and Shiraz SS-treated soil, zeolite and MgO were the best Cu stabilizers, while ZnO and MgO performed better in Isfahan SS-treated soil. Furthermore, the nanoparticles had a higher Zn sorption capacity than the geomaterials (Feizi et al. 2019).

Table 2.1 Previous research for sorption of heavy metals

Adsorbent	Contaminant (s)	Contaminated media	Concentration range	Maximum adsorption capacity (mg·g ⁻¹)	Reference
Zeolite	Pb	Water	100-500 mg. L ⁻¹	109.89	(Joseph et al. 2020)
	Zn			36.76	
	Cu			57.80	
NaOH modified fly ash	Pb	Water	30-500 mg. L ⁻¹	126.55	(Huang et al. 2020)
Biochar	Pb	Water	10-3000 µg. L ⁻¹	0.766	(Esfandiar et al. 2022)
	Zn			0.159	
	Cu			0.110	
Cauliflower leaves biochar	Pb	Water	50-500 mg. L ⁻¹	177.82	(Ahmad et al. 2018)
	Cu			53.96	
Granular Activated Carbon	Cu	water	0- 80 mg. L ⁻¹	23.42	(Zheng et al. 2018)
Coconut derived activated carbon	Pb	Industrial wastewater	10-300 mg. L ⁻¹	92.72	(Anirudhan and Sreekumari 2011)
	Cu			73.60	
Carbon nanotube sheets	Pb	Water	100-1200 mg. L ⁻¹	117.64	(Tofighy and Mohammadi 2011)
	Zn			74.62	
	Cu			64.90	
Activated carbon supported by ZVI	Pb	water	10- 300 mg. L ⁻¹	295.3	(Qu et al. 2021)
Biopolymer	Pb	Soil	0.15- 4mM	38.3	(Ko et al. 2022)
	Zn			7.2	
	Cu			8.5	

2.2 BTEX sorption

BTEX is a class of Volatile Organic Compounds (VOCs) that includes benzene, toluene, ethylbenzene, and xylene. Every year, by using volatile organic compounds as raw chemical components in manufacturing, a large amount of BTEX contaminated wastewater is produced and discharged into the aqueous environment (Su et al. 2010). BTEX are also classified as priority contaminants regulated by the US EPA (EPA 1986). According to the Republic of Korea (hereafter, Korea) Ministry of Environment, the maximum allowable levels of BTEX in soil are 1, 20, 50 and 15 mg. kg⁻¹, respectively (Ministry of Environment Korea 2017). BTEX is classified as Light Non-Aqueous Phase Liquid (LNAPL) and non-polar organic contaminants. Some physiochemical properties of BTEX are presented at Table 2.2.

Table 2.2 BTEX components physiochemical properties (Mitra and Roy 2011)

Parameters	Benzene	Toluene	Ethylbenzene	Xylenes
Formula	C ₆ H ₆	C ₆ H ₅ CH ₃	C ₆ H ₅ CH ₂ CH ₃	C ₆ H ₄ (CH ₃) ₂
Molar weight	78.12	92.15	106.18	106.18
Density (g. mL ⁻¹)	0.8765	0.8669	0.8670	0.8685
Polarity	Non-polar	Non-polar	Non-polar	Non-polar
Solubility (mg. L ⁻¹)	1780	500	150	150
Octanol- water partition coefficient (log K _{ow})	2.13	2.69	3.15	3.15
Henry's law constant (kPa. m ³ . Mol ⁻¹)	0.55	0.67	0.7	0.8

2.2.1 BTEX sorption by activated carbon

At the study by Yakout (2014) the phosphoric acid activated carbon prepared from rice husk showed adsorption capacity of 365 mg. g⁻¹ for benzene. In other study a KOH activated coal with high surface area of 3200 m². g⁻¹ showed adsorption values of 860 mg. g⁻¹ and 1200 mg. g⁻¹ for the adsorption of benzene and toluene, respectively (Asenjo et al. 2011).

At the study by (Wibowo et al. 2007) a commercial coal-based activated carbon F-400 was chosen, and modified through chemical treatment with HNO_3 and thermal treatment under nitrogen flow for removing benzene and toluene. The results showed thermally treated activated carbon had the highest sorption capacities among examined activated carbon with sorption capacity of $257.74 \text{ mg. g}^{-1}$ and $240.07 \text{ mg. g}^{-1}$ for toluene and benzene, respectively.

The produced activated carbon from *Aesculus hippocastanum* L. biomass using carbonization and chemical activation had sorption capacity ranges $423\text{-}1114 \mu\text{g. g}^{-1}$ for BTEX components (Isinkaralar et al. 2022).

The efficiency of surface modified activated carbon with green oxidizing agents has been studied by Anjum et al. (2019) for up taking the BTEX components. The result showed surface modification of activated carbon can increase its sorption capacity where the maximum sorption capacity was computed to be $260.78 \text{ mg. g}^{-1}$, $263.16 \text{ mg. g}^{-1}$, and $269.55 \text{ mg. g}^{-1}$ for benzene, toluene, and p-xylene respectively.

2.2.2 BTEX sorption by mineral sorbents

At the study by (Vidal et al. 2012) a hexadecyltrimethyl ammonium (HDTMA) surfactant-modified zeolite was examined for its efficiency for removing BTEX from aqueous solution. The surfactant-modified zeolite showed sorption capacity of 12.13 , 13.75 , 13.86 , and 13.98 mg. g^{-1} for benzene, toluene, ethylbenzene, and o-xylene, respectively.

The sorption removal of BTEX from aqueous solution by montmorillonite modified with poly ethylene glycol were investigated by (Nourmoradi et al. 2012). The results showed sorption capacity of 5.92 , 6.71 , 7.35 , and 8.19 mg. g^{-1} for benzene, toluene, ethylbenzene, and o-xylene, respectively.

Vaezihir et al. (2020) evaluated the efficiency of natural zeolite as physical permeable reactive barrier (PRB) for migration of BTEX plume in a bench-scale. The results indicated high removal rates (up to 90%) of BTEX by passing through the zeolite.

A modified vermiculite by magnetite nanoparticles (VMT-mag) has been developed by Bartilotti et al. (2021) for BTEX removal from wastewater. The VMT-mag showed 85% removal for BTEX components only after 5 min of contacting time with wastewater.

The raw diatomite, and modified diatomite using thermally, chemically, and both chemically and thermally modification has been studied by Aivalioti et al. (2012) for the BTEX removal from aqueous solutions. It was demonstrated that the diatomite samples were efficient for BTEX removal, while the sample treated with HCl being the most effective with adsorption capacity of 0.0006 mmol. g⁻¹, 0.0006 mmol. g⁻¹, 0.0008 mmol. g⁻¹, and 0.0018 mmol. g⁻¹ for benzene, toluene, ethylbenzene and *m*-xylene, respectively.

2.2.3 BTEX sorption by other sorbents

The efficiency of polystyrenic resin for BTEX removal from aqueous phase has been evaluated by Makhathini and Rathilal (2017). The results showed sorption removal of 98% of benzene, 88% of toluene, 59% of ethylbenzene, 84% *p*-xylene and 90% *o*-xylene at initial concentration of 14.47 mg. l⁻¹ and temperature of 25 °C for resin.

At the study by (Shakeri et al. 2016) the application of ostrich bone waste modified by a cationic surfactant (OBW-OH-CTABr) has been evaluated for the BTEX removal from the synthetic and real waters. The results showed BTEX sorption is dependent to adsorbent dosage, and while the adsorbent dosage increased from 0.1 to 0.5 g, the removal capacity of BTEX ions increased from 18% to 37%, 20% to 63%, 34% to 69.5%, and 38.9% to 78% for benzene, toluene, ethylbenzene and *p*-xylene, respectively.

In other study the synthesized compost materials from the organic matter of the municipal solid waste of the Chania Prefecture, Crete, Greece has been applied for sorption of BTEX from aqueous solution. The results showed produced composite materials had sorption capacity of 22.21mg.g⁻¹, 12.2 mg.g⁻¹, 9.18 mg.g⁻¹, and 4.08 mg.g⁻¹ for benzene, toluene, ethylbenzene and *m*-xylene, respectively (Simantiraki and Gidakos 2015).

the biochar derived from municipal solid waste (termed “MSW-BC”) has been examined as adsorptive materials for toluene and ethylbenzene removal from the aqueous media at initial concentration of 10-600 µg. L⁻¹ and different pH. The adsorption of toluene and ethylbenzene on the MSW-BC was slightly dependent on the pH, with the obtained maximum sorption capacity ranges 44- 47 µg. g⁻¹ at pH 8 (Jayawardhana et al. 2021).

Waste tire as one of the frequently produced waste rubbers has been also examined for removal of BTEX components. For example, at study by Alamo-Nole et al. (2011) efficiency of tire crumb rubber (TCR) and its main components including the carbon black (CB) and styrene-butadiene polymer (SBP) has been evaluated for Sorption of toluene and xylene. A removal of 60% of toluene and 81% of xylene for initial concentration of mg. L⁻¹ and 30 minutes contacting time was obtained using 5 g.L⁻¹ of TCR. CB and SBP also showed almost similar removal rate as obtained values for TCR.

In another study by Banaszekiewicz and Badura (2019) recycled tire polymer fibers (RTPF) has been used as a stabilizer of BTEX compounds in treated soil with cement. It was found while the RTPF percentage is increasing in mixture the BTEX immobilization efficacy also is increasing in comparison to Portland cement alone. The removal of BTEX compounds were from 7 to 33% with the obtained maximum percentage reduction for toluene.

2.3 PFAS sorption

As shown in Table 2.3, the reported adsorption capacity of activated carbon ranges from 0.006 to 560 mg. g⁻¹ at various initial concentration of PFAS substance. Moreover, it has been demonstrated that powdered activated carbon has more sorption capacity in comparison to granular activated carbon which also has been confirmed by Zhang et al. (2019).

Anion exchange resins showed efficient performance for sorption of PFAS components. As an example, IR67 had sorption capacity of 2390 mg. g⁻¹ for PFOS which is higher than sorption capacity of powdered activated carbon (Table 2.3).

Various kind of minerals including silica, kaolinite, montmorillonite have been examined for PFAS sorption, while the reported sorption capacities for these materials were lower than resins and activated carbon. At the study by Elanchezhiyan et al. (2021) efficiency of chitosan as one the most common biopolymers has been evaluated for PFOS, and PFOA removal from aqueous solution. The synthesized chitosan showed sorption capacity of 16.07 and 21.64 mg. g⁻¹ for PFOA and PFOS, respectively.

Table 2.3 Previous research for sorption of PFAS substance

Adsorbent	Contaminant (s)	Contaminated media	Concentration range	Maximum adsorption capacity (mg. g ⁻¹)	Reference
Powdered activated carbon	Mix PFAS	Water	1.64 - 55.7 ng. L ⁻¹	2.990	(Murray et al. 2019)
Granular activated carbon	Mix PFAS	Water	1.64 - 55.7 ng. L ⁻¹	0.006	(Murray et al. 2019)
Powdered activated carbon	PFOS	Water	10 mg. L ⁻¹	2.9	(Qian et al. 2017)
Powdered activated carbon	PFOA	Water	50 mg. L ⁻¹	290	(Yu et al. 2009)
	PFOS			560	
Anion-exchange resin (AI400)	PFOA	water	50 mg. L ⁻¹	1263.9	(Yu et al. 2009)
	PFOS			226.2	
Anion-exchange resin (IR67)	PFOS	Water	200 mg. L ⁻¹	2390	(Gao et al. 2017)
Anion-exchange resin (A532E)	Mixed PFAS	Water	0.74 – 97.7 µg. L ⁻¹	6.71-99.9 % removal	(Fang et al. 2021)
	PFOA			0.11	
Clay minerals	PFOS	water	400 mg. L ⁻¹	0.31	(Zhao et al. 2014)
	PFHxS			0.31	
	PFHxA			0.059	

Ochoa-Herrera and Sierra-Alvarez (2008) investigated the removal of PFAS surfactants from aqueous solutions by sorption onto various types of granular activated carbon, zeolite with different Si/Al ratios, and sludge materials. According to the results, GAC had the highest sorption capacity among the other sorbents, with maximum sorption capacities of 182 mg. g⁻¹, 57 mg. g⁻¹, and 48 mg. g⁻¹ for PFOS, PFOA, and PFBS, respectively. Furthermore, zeolite with a higher Si/Al ratio was more influential in PFAS adsorption, with the NaY80 (zeolite with a

Si/Al ratio of 80) having the highest sorption removal among all examined zeolite. NaY80 had a maximum sorption capacity of 114.7 mg. g⁻¹, which was nearly comparable to GAC's sorption capacity.

In study by Yan et al. (2020) bentonite has been modified by intercalating quaternary ammonium cations in the exchangeable interlayer sites of smectite, and used for PFAS pollutants removal in real groundwater. The removal efficiency of modified bentonite (FLUORO-SORB®200 (Fluoro200)) was at range 95~99%, which was superior to those of granular activated carbon or hard-wood biochar and comparable to an ion exchange resin. Furthermore, selectivity sorption results showed that at environmentally relevant concentrations, the performance of Fluoro200 is not affected by potential organic co-contaminants (e.g., diesel, BTEX, TCE, and 1,4 dioxane) or water chemistry (Ca²⁺ and Na⁺).

In other study for improving PFAS sorption, Montmorillonite clays were functionalized with either poly (diallyldimethylammonium) chloride (PDADMAC) or poly(4-vinylpyridine-co-styrene) (PVPcoS). In comparison to nonmodified clay, the PDADMAC and PVPcoS polymers increased PFOA and PFOS sorption by two orders of magnitude. Furthermore, polymer-clay composites outperformed biochar in terms of PFAS substance removal (Ray et al. 2019).

To selective sorption of perfluorooctanesulfonate (PFOS) and perfluorooctanoate (PFOA) from water, a novel fluorinated montmorillonite (F-MT) was synthesized by exchanging cationic fluorinated surfactant. At concentrations below 10 g. L⁻¹, F-MT demonstrated fast and high sorption for PFOS and PFOA with better performance than activated carbon and resin. The equilibrium sorption capacity of PFOS and PFOA were 116.1 mg. g⁻¹, and 51.7 mg. g⁻¹, respectively. Furthermore, in the presence of other organic pollutants, the F-MT demonstrated excellent selectivity for PFOS and PFOA. The presence of phenol, pyridine, dodecylbenzenesulfonate (SDBS), and phenanthrene (PHE) had no effect on the sorption of PFOS and PFOA. The novel F-MT demonstrated renewability potential, with constant sorption capacity after five sorption-desorption cycles (Du et al. 2016).

Additionally, some studies have examined efficiency of some sorbents for stabilizing the PFAS contaminants inside the soil. For example, amended soil by activated carbon has reduced the leaching of long chain PFAS (PFOA, PFOS) by 81-86% (Söregård et al. 2019)

Aly et al. (2019) investigated two cationic polymers, polydiallyldimethyl ammonium chloride (polyDADMAC) and polyamine (a co-polymer of epichlorohydrine and dimethyl amine), to improve sorption capacity of soil against six PFAS (PFBS, PFBA, PFH_xS, PFNA, PFOS, PFOA). The treatability tests were conducted on natural soil excavated from an Air Force base in the south-central United States. Based on batch sorption results, the coagulants increased the soil's PFAS sorption capacity by a factor of 2.0-6.1. The reason was that polymers increased soil hydrophobicity while also imparting a positive charge on soil particles. Furthermore, at an initial PFAS concentration of 100 µg. L⁻¹, one-dimensional columns test for treated soil delayed PFAS breakthrough by 20 times the pore volume.

2.4 Experimental plans

2.4.1 Characterization of adsorbents

The physical properties of the adsorbents were characterized using N₂ adsorption-desorption isotherms at 77 K using a Micromeritics ASAP 2020 surface area analyzer. The adsorbent samples were outgassed at 350 °C for 240 min prior to analysis. From the N₂ adsorption-desorption isotherms, the specific surface areas of the all sorbents were estimated using the Brunauer, Emmett and Teller (BET) equation (Brunauer et al. 1938). Additionally, their cumulative pore volume, average pore size, and the pore size distribution were obtained by applying the Barrett–Joyner–Halenda (BJH) method (Barrett et al. 1951). The morphology of the adsorbent particles was characterized using scanning electron microscopy (SEM) with an energy dispersive spectroscopy (EDS) microanalysis system. The crystallinity or amorphous nature of adsorbents was assessed using X-ray diffraction (XRD) analysis. A Thermo Scientific Flash 2000 elemental analyzer was used to determine the elemental contents (oxygen, carbon, hydrogen, nitrogen and sulfur) of the adsorbent's particles. The elemental composition of the sorbents was evaluated by X-ray fluorescence spectrometer (XRF).

2.4.2 Zeta potential of sorbents

Zeta potential is a method for measuring the surface charge of adsorbents and is used to determine the electrostatic interaction between the ions and the adsorbents (Peng et al. 2017). To obtain the zeta potential of Tire -derived activated carbon (TAC) and commercial activated carbon (CAC), either on their own or in the presence of Pb ions, the following approach was used. First, CAC was manually ball milled in a porcelain mortar and passed through sieve # 200 (opening: 75 μm). Then, 0.1 g of each of the TAC and CAC powders (<0.075 mm particle size) were added to 50 mL of DI water (Zhao et al. 2015). For samples with Pb ions, the concentration of Pb in the suspension was 100 mg L⁻¹. The suspensions were agitated at 180 rpm for 24 h, centrifuged at 3900 rpm for 20 min, and filtered. The initial pH value for all suspensions was adjusted to neutral. Since the pH level changed during the Pb adsorption, the pH levels were remeasured after filtering and recorded as the final pH.

Zeta potential at various pH values was measured following the method as described by Deng et al. (2015). Briefly, 50 mg of each sorbent was suspended into 50ml polypropylene centrifuge tubes containing 25ml of DI. The suspensions were agitated at 150rpm for 24h under at ambient temperature, and centrifuged at 3900 rpm for 20 min and then filtered (pore size 0.45 μm). The pH value of supernatants was adjusted at range of 3-11 with 0.5 N HCl or NaOH solutions.

Zeta potential of each supernatant was analyzed by Electrophoretic Light Scattering Spectrophotometer (ELSZ-1000, Japan). For each sample, the zeta potential was measured twice, and the mean was calculated.

2.4.3 X-ray photoelectron spectroscopy (XPS)

X-ray photoelectron spectroscopy (XPS) provides information on the composition and chemical bonding state of elements for sorbent by measuring the binding energy of the interior electrons. For XPS analysis, the CAC samples before and after Pb adsorption (the loaded samples with initial Pb concentration of 5000 mg L⁻¹) were manually ball milled in a porcelain mortar and passed through sieve # 200 (opening: 75 μm). Then both TAC and CAC powders

(<0.075 mm particle size) were pelleted (diameter size <10 mm) using manual hydraulic pellet press. After preparing the pellets the XPS measurements were performed with X-ray photoelectron spectroscopy (XPS; ESCAII, AXIS SUPRA (Kratos, UK)) in an ultra-high vacuum chamber of mu-metal construction. Wide scan spectra were taken with 1 eV step intervals in the binding energy range of 0 –1200 eV, while spectra of C1s, O1 s, Pb 4f were measured with 0.1 eV step intervals. The peak fitting was performed with AVANTAGE 5.99 software by using Smart algorithm.

2.4.4 Surface functional groups using FT-IR

Fourier Transform Infrared Spectroscopy (FT-IR) was used to analyze surface functional groups present on each sorbent. For TAC and CAC adsorbents the FT-IR has been used for samples before and after adsorption of heavy metals (the loaded samples with the initial metal concentration of 5000 mg. L⁻¹). Each adsorbent was dried at ambient temperature, and then were mixed with KBr in a ratio of 1:100. The mixtures were compressed using manual FT-IR KBr hydraulic pellet press to make the pellets with size of almost 10 mm diameter and 1 mm thickness. Finally, the pellets were placed in the Nicolet 6700, Thermo Scientific (USA), and were analyzed in the spectral range of 4000-400 cm⁻¹.

2.4.5 SEM imaging/EDS

The surface morphology of raw adsorbents was evaluated using a scanning electron microscope (SEM) equipped with an energy dispersive spectroscopy (EDS). For this aim, two-sided adhesive carbon tape was placed on an SEM stub, and a small amount of dried adsorbents were sprinkled on its surface. Then the samples were coated in a vacuum with a thin layer of gold, and examined in SEM chamber under accelerating voltage of 15 kV. The morphology of adsorbents was evaluated at three different scales of magnification (x5000, x10000, and x50000). After the SEM analysis, the samples were transferred to EDS system to allow the chemical analysis of observed adsorbents in SEM monitor.

2.4.6 Powder X-ray diffraction (XRD)

X-ray diffraction analysis was performed in order to determine the crystallinity or amorphous nature of sorbents. The analysis was performed by SmartLab Intelligent X-ray Diffraction System with diffraction angle (2θ) range of 5° to 80° .

2.4.7 Cation exchange capacity (CEC) and anion exchange capacity (AEC)

For this study the ammonium acetate extraction method was used for measuring the Cation exchange capacity (CEC) values of sorbents. Firstly, 5g of dried adsorbent was saturated by percolating 5 mL of 1N ammonium acetate, and placed in CEC extraction equipment (Figure 2.3). Then the upper syringe was filled by 50mL of 1N ammonium acetate as the first extraction solution. After extracting the ammonium acetate through the adsorbents (~8h), the upper syringe was re-filled with 99% isopropyl alcohol, which was used for rinsing off any extra ammonium acetate left on the adsorbent material. As a secondary extraction solution, the CEC extraction equipment was filled with 10% sodium chloride solution. By extracting the sodium chloride through the adsorbents, the cation exchange capacity of sorbents was quantified using Kjeldahl distillation.

Anion exchange capacity (AEC) of sorbents was measured following the study of (Saeidi et al. 2020). For each sorbents the CEC and AEC experiment were performed in duplicate, and the mean value was reported as the final values.

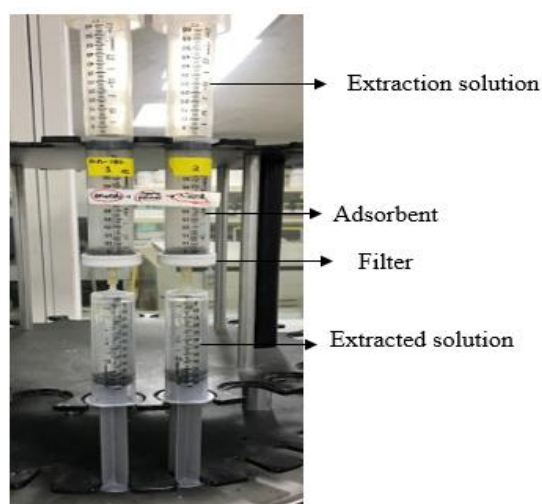


Fig. 2.1 CEC extraction equipment

2.4.8 Compaction tests

To obtain the compaction characteristics of all soil–pulverized waste tire (S–PWT) mixtures investigated, standard-Proctor compaction testing, employing a 1-l compaction mold, was performed in accordance with ASTM D698-12e2 (ASTM 2007). Air-dried soil, PWT and water in the required amounts were thoroughly mixed to produce the various S–PWT mixtures which were allowed to achieve moisture uniformity in waterproof storage containers before performing the compaction tests. From the experimental results, the values of optimum moisture content for compaction and corresponding maximum dry unit weight were determined for each mixture.

2.4.9 Hydraulic conductivity test

Hydraulic conductivity testing was performed on the test soil (S–PWT0) material in accordance with ASTM D2434-68 (ASTM 2006). The 10 cm dia. × 12 cm long test specimen was prepared by compaction of the S–PWT0 material at its identified standard-Proctor optimum moisture content to achieve 95% of its associated maximum dry unit weight. Before performing the permeability testing, the compacted specimen was fully submerged in water for a 24-h period to reduce its air voids content. After the specimen saturation stage in the permeameter apparatus, permeability testing was performed at various hydraulic gradients (0.2 to 2.0), with the average value reported as the specimen hydraulic conductivity.

2.4.10 Compression test

To investigate the compressibility behavior of the various S–PWT mixtures, one-dimensional consolidation testing was performed in accordance with ASTM D2435M-11 (ASTM 2011). These mixtures were placed in 60 mm dia. × 20 mm high confinement rings at 90% of their identified maximum dry unit weight and incrementally loaded in 24-h duration stages from 20 to 640 kPa (20, 40, 80, 160, 320 and 640 kPa), before unloading using the same sequence, to investigate the change in specimen void ratio against effective vertical stress (e – $\log \sigma'_v$).

Values of compression (C_c) and swelling (C_s) indices were calculated from the gradients of the experimental e - $\log \sigma'_v$ loading and unloading curves, respectively, for each S-PWT mixture.

2.4.11 Shear strength test

For assessing the shear strength properties of the various S-PWT mixtures, drained direct-shear testing was performed in accordance with ASTM D3080M-11 (ASTM 2002), thereby allowing the determination of their respective effective-stress shear strength parameter (ϕ) values. For each S-PWT mixture, test specimens were prepared by compaction of the material in three equal-height layers into the 60 mm dia. \times 40 mm high shearbox apparatus, each layer compacted to achieve 95% of the identified standard-Proctor maximum dry unit weight value. For each mixture, direct shear tests were performed for σ'_v levels of 40, 80, and 160 kPa, displacing the top half of the shearbox relative to its bottom half at a horizontal displacement rate of 0.8 mm/min, which was deemed sufficiently slow to allow practically complete dissipation of excess pore pressure. Specimen shearing was continued for 15 min, by the end of which 12 mm horizontal (shear) displacement had occurred. This approach is consistent with ASTM D3080M-11, which reported a minimum required time of failure with dissipating pore pressure for these classes of soils (SP, SW) of ≥ 10 min. These experiments were performed in triplicate and the average values of effective cohesion, c' , and effective friction angle, ϕ , reported as the final results.

2.5 Data analysis

The sorption capacities of each sorbent at any certain time, and under equilibrium conditions have been determined by equation (2.1) and (2.2), respectively.

$$q_t = \frac{(C_i - C_t)V}{m} \quad (2.1)$$

$$q_e = \frac{(C_i - C_e)V}{m} \quad (2.2)$$

Where, q_t (mg. g⁻¹ or µg. g⁻¹) and q_e (mg. g⁻¹) are the adsorption capacities at any certain time, and under equilibrium phase, respectively. $V(L)$ is the volume of adsorbate, and m (g) is the dry mass of sorbent. Additionally, C_i (mg·L⁻¹ or µg. L⁻¹), C_t (µg·L⁻¹), and C_e (mg·L⁻¹) are the concentrations at initial, any certain time, and equilibrium phase of the adsorbate, respectively.

The removal rate of each sorbent was calculated as described in equation (2.3):

$$R = \frac{(C_i - C_e)}{C_i} \quad (2.3)$$

Where R (%) is the removal rate of each sorbent.

The desorption rate (D , %) was calculated for each metal according to (2.4):

$$D (\%) = \frac{q_{des}}{q_t} \times 100 \quad (2.4)$$

where q_{des} (mg. g⁻¹ or µg. g⁻¹) is the concentration of desorbed solute from the surface of the adsorbents.

The single point adsorption coefficient (distribution factor K_d) was determined as:

$$K_d = \frac{q_e}{C_e} \quad (2.5)$$

Where K_d (L. g⁻¹) is distribution factor.

The flow rate of solute (ml. min⁻¹) through the soil columns was calculated using the equation (2.6):

$$\text{Flow Rate} = \frac{\text{Bed Volume}}{\text{EBCT}} \quad (2.6)$$

Where EBCT and bed volume are empty bed constant time (ml. min⁻¹), and bed volume (ml) of column samples, respectively.

The retardation factor (R), distribution coefficient, and organic carbon partition coefficient values for each PFAS substances was calculated using equations (2.7) and (2.8), respectively.

$$R = 1 + \frac{\rho_b}{n} K_d \quad (2.7)$$

$$K_d = f_{oc} K_{oc} \quad (2.8)$$

Where R is retardation factor, ρ_b is density of soil ($\text{kg} \cdot \text{L}^{-1}$), n is porosity of soil, f_{oc} is organic carbon content of soil (%), K_d is distribution coefficient ($\text{L} \cdot \text{kg}^{-1}$), and K_{oc} is organic carbon partition coefficient ($\text{L} \cdot \text{kg}^{-1}$).

The isotherm adsorption data were analyzed by Langmuir, Freundlich, Dubinin Radushkevich, and Temkin models. Moreover, for describing the mass transfer from solute to the solid sorbent, the kinetic results were analyzed with pseudo-first-order, pseudo-second-order, and intra-particle diffusion models. Details about these models are provided below.

2.5.1 Langmuir model

The Langmuir model (Langmuir 1916) makes the assumption that each of the adsorption sites on the adsorbent surface can be occupied only by one molecule; that is, the adsorbed molecules do not interact with each other, and consequently the adsorption occurs as a monolayer phenomenon. The Langmuir model is expressed as:

$$q_t = \frac{q_{\max} K_L C_e}{(1 + K_L) C_e} \quad (2.9)$$

where q_t ($\text{mg} \cdot \text{g}^{-1}$) is the amount of adsorbate that is sorbed on the solid, C_e ($\text{mg} \cdot \text{l}^{-1}$) is the solute concentration at equilibrium, q_{\max} ($\text{mg} \cdot \text{g}^{-1}$) is the maximum monolayer capacity of the adsorbent, and K_L ($\text{l} \cdot \text{mg}^{-1}$) is the Langmuir adsorption constant, which is related to the affinity of adsorption. Note that the both empirical coefficient of q_{\max} and K_L can be obtained by plotting C_e/q_t as a function of parameter C_e .

2.5.2 Freundlich model

The Freundlich model (Freundlich 1907) states that the adsorption occurs as a multilayer process following the empirical expression given by equation 2.10, and is based on the adsorption on non-homogeneous surfaces having dissimilar adsorption sites, where sites of higher adsorption capacity are occupied first, with the adsorption quantity declining as the surface coverage rises.

$$q_t = K_F C_e^{1/n} \quad (2.10)$$

where q_t and C_e have the same definitions as given for equation 2.9, K_F ($\text{mg}\cdot\text{g}^{-1}$) is the Freundlich adsorption isotherm coefficient, and n is the Freundlich exponent, which is related to the intensity of adsorption.

2.5.3 Dubinin Radushkevich (D-R) model

The (D-R) model was proposed by Dubinin and Radushkevich (1947) based on assumption of heterogenous surface, which provides characteristic of adsorption related to the porous structure of sorbents. The linear D-R model is presented as equation (2.11):

$$\ln q_t = \ln q_{max} - \beta \varepsilon^2 \quad (2.11)$$

where q_t is the amount of ion adsorbed per unit weigh of adsorbent ($\text{mg}\cdot\text{g}^{-1}$), q_{max} is the maximum adsorption capacity obtained from D-R model, β is the activity coefficient which is useful for obtaining the mean energy sorption E , and ε ($\text{J}\cdot\text{mol}^{-1}$) is the Polanyi potential which is calculated form equation (2.12):

$$\varepsilon = RT \ln \left(1 + \frac{1}{C_e} \right) \quad (2.12)$$

where R is the gas constant ($8.314 \text{ J}\cdot\text{mol}^{-1}\cdot\text{K}^{-1}$) and T is the temperature (K). The q_{max} and β parameters were determined by plotting the $\ln q_t$ versus ε^2 . Also, the mean energy E ($\text{mol}\cdot\text{J}^{-1}$) of sorption can be obtained from equation (2.13):

$$E = \sqrt{\frac{1}{2\beta}} \quad (2.13)$$

2.5.4 Temkin model

The Temkin model (Temkin and Pyzhev, 1940) ignores the extremely high and low concentration values of adsorbate, and presumes the heat of adsorption trends to decrease linearly rather than logarithmically with coverage. The Temkin model is expressed by (2.14):

$$q_t = \frac{RT}{b} \ln A + \frac{RT}{b} \ln C_e \quad (2.14)$$

where C_e is the equilibrium concentration ($\text{mg}\cdot\text{L}^{-1}$), T is absolute temperature (K), R is the gas constant ($8.314 \text{ J}\cdot\text{mol}^{-1}\cdot\text{K}^{-1}$), b is the Temkin constant, which is related to the heat of sorption ($\text{J}\cdot\text{mol}^{-1}$), and A is the Temkin isotherm constant ($\text{L}\cdot\text{g}^{-1}$). The A and b values were calculated by plotting the q_t experimental data versus $\ln C_e$.

2.5.5 Kinetic adsorption models

The kinetic results were analyzed with pseudo first-order, pseudo second-order, and intraparticle diffusion models to describe the ion mass transfer from solution to the solid adsorbents. These models are described by following equations. Pseudo first-order (2.15), pseudo second-order (2.16), and intraparticle diffusion (2.17) models (Xiao et al., 2019).

$$\log(q_e - q_t) = \log(q_e) - \frac{K_1 t}{2.303} \quad (2.15)$$

$$\frac{t}{q_t} = \frac{1}{k_2 q_e^2} + \frac{t}{q_e} \quad (2.16)$$

$$q_t = k_p t^{0.5} + C \quad (2.17)$$

where q_t ($\text{mg}\cdot\text{g}^{-1}$) is the amount of adsorption at time t , q_e ($\text{mg}\cdot\text{g}^{-1}$) is the equilibrium adsorption capacity obtained by pseudo first-order and pseudo second-order models, k_1 (min^{-1}) and k_2 ($\text{g}\cdot\text{mg}^{-1}\cdot\text{min}^{-1}$) are the first order kinetic and the second order kinetic adsorption constants, and k_p ($\text{mg}\cdot\text{g}^{-1}\cdot\text{min}^{-0.5}$) is the intraparticle diffusion rate constant, and C is constant which reflects the boundary layer effect.

Chapter 3. BTEX and heavy metal removal by waste tire and its activated carbon

3.1 Introduction

The abundance of waste tires, with current annual worldwide generation of approximately one billion scrap tires, is expected to progressively increase (Sekhar 2014). In Korea alone, for instance, about 20 million waste tires are generated annually (Kim and Kang 2013). Since waste tires cannot be degraded and presently fill up landfill space, the final disposal of waste tires could be a critical environmental concern worldwide (Abbaspour et al. 2019). An environmentally-friendly solution for dealing with waste tires would be to reuse them as worthy products, such as recyclable additives in some engineering applications (Manchón-Vizuete et al. 2005).

Recently, the beneficial reuse of waste tires in the fields of geotechnical and geoenvironmental engineering has shown promise, including for soil reinforcement applications, as retaining-wall backfill, lightweight foundation fill and landfill cover materials (Reddy et al. 2018; Soltani et al. 2019), as well as the adsorption of organic and inorganic contaminants from an aqueous phase (Babiker et al. 2019). As reported by Bhatti et al. (2017), the waste-tire additive removed various types of chromium, with adsorption capacities of 105.8 mg. g⁻¹ and 174.6 mg. g⁻¹ for Cr(VI) and Cr(III), respectively. The limited research in this area suggests that tire chips are also effective as adsorptive materials in removing Pb and Cu ions (Calisir et al. 2009; Deng et al. 2016; Oladoja et al. 2010).

Furthermore, pyrolysis has recently been considered as one of the state of the art recycling method for dealing with waste tires, wherein waste tires are converted to char, hydrophobic liquids, and volatile fractions (Martínez et al. 2013). In industrial manufacturing, oil is the main product from waste tire pyrolysis (Martínez et al. 2013), and depending on the pyrolysis conditions, 30 to 40% of the initial weight of the waste tires is converted to char as a side product (Acosta et al. 2016). Tire pyrolysis char is an extremely carbonaceous material and can

be used as a precursor to make activated carbon for heavy metal adsorption (Saleh and Gupta 2014), which is an economical way to reduce waste tire disposal challenges. In fact, tire pyrolysis char has already shown promising results in the sorption of inorganic and organic pollutants (Acosta et al. 2016; Acosta et al. 2018; Gupta et al. 2012; Shaid et al. 2019). For instance, Acosta et al. (2018) noted that KOH-activated tire pyrolysis char with a monolayer capacity of 123 mg g⁻¹ can remove Bisphenol A from aqueous solutions. Nieto-Márquez et al. (2017) modified adsorbents from waste tires by using different activating agent/waste tire ratios for the removal of Pb²⁺, Cd²⁺ and Cr³⁺ ions.

Based on the authors' knowledge, the utilization of pulverized waste tire (PWT) mixed with soil as a matrix for removing BTEX components and heavy metals while simultaneously examining the geotechnical performance of the soil–pulverized waste tire (S–PWT) mixtures as engineering fill materials has not been evaluated yet. Also, to date, the efficiency of heavy metal removal by tire-derived activated carbons in comparison to that by commercial activated carbon (CAC), after taking into consideration the adsorption mechanisms, has not been considered in the literature.

Therefore, the main goals of this chapter are to investigate:

1. The adsorption capability and capacity of PWT for removal of BTEX components.
2. The effectiveness of PWT for removal of two specific heavy metals, namely Pb and Cu.
3. The geotechnical performance of various S–PWT mixtures as engineering fill materials, in order to find the optimum mixing ratio of S–PWT mixtures while satisfying sorption and bearing capacities at the same time.
4. Producing tire-derived activated carbon (TAC) by sequential carbonization and chemical activation techniques, and evaluate the adsorption capacity of TAC for the removal of three specific heavy metals (Pb, Cu, Zn) in comparison to that of commercial activated carbon (CAC).
5. Identify the adsorption mechanisms involved in the adsorption of heavy metals using TAC and CAC

A series of batch adsorption–desorption experiments using PWT, TAC and CAC samples were carried out for removing three heavy metals (Pb, Cu, Zn), and BTEX component from aqueous solutions. The adsorption capacities of these materials for toxic ion removal was assessed by Langmuir, Freundlich, Dubinin- Radushkevich (D-R), and Temkin adsorption isotherm models. Special attention was paid to the adsorption mechanisms of TAC and CAC by characterization of their properties using Brunauer–Emmett–Teller (BET), zeta potential, cation exchange capacity (CEC), Fourier transform infrared spectroscopy (FT-IR), and X-ray photoelectron spectroscopy (XPS) analyses.

3.2 Material and Methods

3.2.1 Raw materials and their characterization

The PWT material used in this study either for making TAC or mixing with soil had the gradation of poorly graded sand (SP) and was composed of irregular rubber particles with rough surfaces. (Figures 3.1 and 3.2.). The locally sourced test soil (classified as well graded sand (SW)) employed for synthesizing the S–PWT mixtures investigated had characteristic grain sizes d_{10} , d_{30} and d_{60} of 0.30, 0.81 and 1.78 mm, respectively, and coefficients of uniformity (C_u) and curvature (C_c) of 5.9 and 1.2, respectively. In other words, as evident from Figure 3.2, the test soil was marginally coarser than the PWT material.

Granular CAC (CAS No. 7440- 44-0) with a 20-40 mesh particle size was sourced from Jesung Chemical Company (Korea) to be used as a reference material in the adsorption–desorption tests. Potassium hydroxide (KOH, 85% pure), which was purchased from Duksan (Korea), was used as the chemical activating agent. For synthesizing the BTEX solution, benzene (purity, 99.7%), toluene (purity, 99%), ethylbenzene (purity, 99%), and m-xylene (purity, 99%) were sourced from the Merk corporation. Also, $\text{Pb}(\text{NO}_3)_2$, $\text{Zn}(\text{NO}_3)_2 \cdot 6\text{H}_2\text{O}$ and $\text{CuCl}_2 \cdot 2\text{H}_2\text{O}$ were obtained from Merk corporation and used to synthesize the metal ions. HCl (purity 35%), HNO_3 (purity 65%), and NaOH were purchased from Duksan and were used to wash the produced TAC and for adjusting the solution pH.

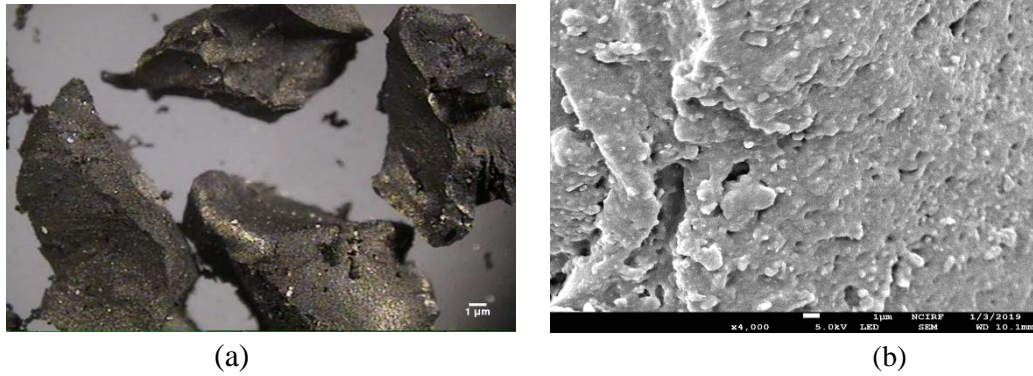


Fig. 3.1 Images of PWT material: (a) individual PWT particles; (b) surface morphology as revealed by scanning electron microscopy

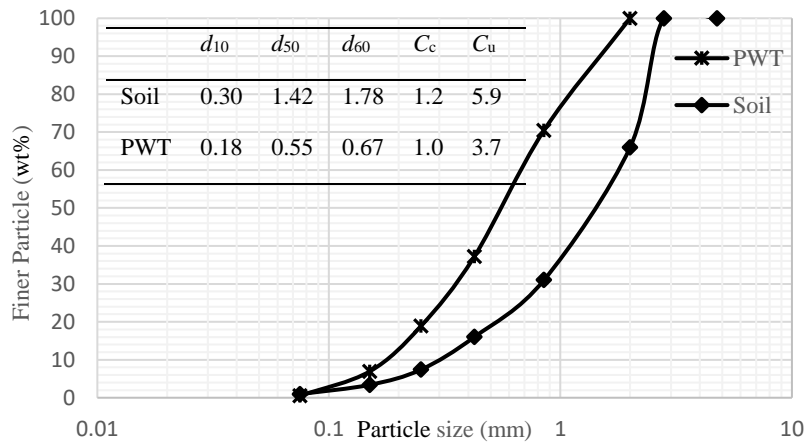


Fig. 3.2 Grain size distributions of the soil and PWT materials

3.2.2 PWT- soil mixture ratios

The PWT material was washed using deionized water for 24 h, allowed to dry at ambient laboratory temperature and then mixed at proportions of 0, 5, 10, 15, 25 and 100 wt% with the air-dried soil. These mixtures were named S-PWT0, S-PWT5, S-PWT10, S-PWT15, S-PWT25 and S-PWT100, respectively, with S-PWT0 and S-PWT100 identifying soil alone and pure PWT material, respectively.

3.2.3 General procedures for producing activated carbon

Activated carbon (AC) is typically produced based on two basic processes: carbonization and activation. The purpose of carbonization is to pyrolyze the carbon precursor in the temperature

range of 300-900 °C to reduce the content of volatile raw materials and produce primary porous charcoal combined with a high content of carbon. The activation process aims to improve the specific surface area and increase the pore volume of AC by modifying the chemical properties of AC. Usually, two main techniques including physical and chemical activation methods are used to produce the activated carbon (Martínez et al. 2013).

Physical activation is a two-step process that begins with carbonization in the presence of an inert gas (N₂ or Ar) and ends with activation in the 800 - 1200°C temperature range using steam or an oxidizing gas (O₂, CO₂, H₂O vapor). An alternative single-step carbonization method called chemical activation allows both carbonization and activation to occur at the same time in the 450–850 °C temperature range. Chemical activation involves impregnating the precursor with a dehydrating reagent (such as KOH, NaOH, H₃PO₄ and K₂CO₃, ZnCl₂, and H₃PO₄.) followed by carbonization at the appropriate temperature (Martínez et al. 2013). In comparison to physical activation, chemical activation has two significant advantages. One advantage is that less energy is consumed, and the other is that pyrolysis and activated carbon production can be completed in a single stage (Teng et al. 2000).

Each physical or chemical activation process has its own influence on the produced AC. Physical activation can result in AC with a higher surface area, whereas chemical activation creates AC with large pore volumes. Furthermore, both feedstock precursor (type of feedstock and particle size) and activation preparation process parameters (gas flow, heating rate, carbonization time, and carbonization temperature) have been shown the influence on the properties and characteristics of the produced activated carbon in both physical and chemical activation (Naji and Tye 2022). Therefore, selecting the appropriate activation techniques with its preparation process parameters is one of the most important issues in producing proper activated carbon for using as an adsorbent.

Considering these points in the present research, a combination of physical and chemical activation processes has been investigated for producing activated carbon from waste tire with sufficient surface area and pore volumes at the same time. Other main activation parameters including activation agent, gas type and its flow rate, heating rate, carbonization time, and

carbonization temperature has been chosen from previous recommendation and used for making tire activated carbon as described below (Acosta et al. 2016; Acosta et al. 2018).

Even though several previous studies have considered producing activated carbon from waste tire, evaluating the combination of physical and chemical activation processes in producing waste tire can be mentioned as the main difference between this research with the previous researches.

3.2.4 Preparation of Tire-derived Activated Carbon (TAC)

TAC was synthesized using a two-step sequence: carbonization and chemical activation. First, the PWT material was washed using DI water and dried at ambient laboratory temperature for 24 h. Then, the carbonization step was initiated by heating the dried PWT in a tube furnace (OTF-1200X) to 570 °C at a rate of 30 °C·min⁻¹. The PWT was held at 570 °C for 100 min in a N₂ environment, with nitrogen gas flow in the furnace at a rate of 200 mL·min⁻¹ (Acosta et al. 2016). The subsequent chemical activation step was performed by physically mixing the carbonized PWT with KOH at ratio of 1 to 6 (this impregnation ratio was selected based on the work of Acosta et al. (2016)). To enhance the chemical reaction, the mixture was diluted with DI water, mixed for 1 h and soaked overnight. Afterwards, the dried mixture was placed into the tube furnace and heated at a rate of 3° C·min⁻¹ to 750 °C and was maintained for 60 min in a N₂ environment with a gas flow of 200 mL·min⁻¹ (Acosta et al. 2016). After cooling the activated sample under nitrogen flow, it was washed with 1 N HCl and then rinsed using DI water to remove any remaining KOH. Finally, the product was dried at 105 °C for 24 h and passed through a 75-µm sieve (U.S. standard sieve NO. 200). The final product was denoted as TAC and tested as an adsorbent for heavy metals.

3.2.5 Adsorbate solution

For isotherm sorption tests using S-PWT sorbents dilution of each BTEX component was achieved by adding the required volume of distilled water to produce solutions of adsorbate with various initial concentrations within the range of 10–200 mg. L⁻¹. Simultaneously, for

metal ions, a synthetic mixing-stock solution ($1000 \text{ mg} \cdot \text{L}^{-1}$) of Cu and Pb was prepared by using $\text{CuCl}_2 \cdot 2\text{H}_2\text{O}$ and $\text{Pb}(\text{NO}_3)_2$ in distilled water. The stock solution was further diluted by distilled water as experimental solutions. Five concentrations of Cu–Pb solution (50, 250, 500, 750 and 1500 ppm) were prepared as adsorbate solutions to evaluate the sorption capacity of either S-PWT mixtures.

For TAC and CAC adsorption tests three stock solutions of $5000 \text{ mg} \cdot \text{L}^{-1}$ Pb^{2+} , Zn^{2+} and Cu^{2+} were synthesized by dissolving $\text{Pb}(\text{NO}_3)_2$, $\text{Zn}(\text{NO}_3)_2 \cdot 6\text{H}_2\text{O}$ and $\text{CuCl}_2 \cdot 2\text{H}_2\text{O}$ in the required volume of deionized (DI) water. The prepared stock solutions were further diluted with appropriate amounts of DI water to obtain the working experimental solutions with concentrations of 100, 500, 1000, 2000, 3000 and $4000 \text{ mg} \cdot \text{L}^{-1}$. All the prepared adsorbate solutions had a neutral pH of 7.

3.2.6 Single and competitive isotherm batch adsorption tests

For determining the adsorption capacity of each S–PWT mixture, single batch adsorption experiments (solid to liquid ratio of 1: 10) were performed by following the EPA/530-SW-87-006-F standard, as described in (Roy et al. 1986). For organic adsorbate, these experiments were performed in 60 ml gas-tight glass vials, minimizing the headspace inside each vial to avoid vaporization of BTEX solution. Batch samples were prepared by adding 5 g of each S–PWT mixture to 50 ml of the BTEX or heavy metal aqueous solution at desired concentration.

The same batch adsorption method was also performed for TAC and CAC with different solid to liquid ratios. Batch samples were prepared by adding 0.2 g and 2.5 g of TAC and CAC to 50 mL of each of the heavy metal ion solutions at the desired concentration.

Samples were mechanically agitated at 180 rpm at ambient laboratory temperature ($20 \pm 2 \text{ }^\circ\text{C}$) for 24 h. After agitation, the suspensions were centrifuged at 4000 rpm for 20 min and then filtered. The BTEX and heavy metal supernatants were analyzed for measuring their equilibrium concentration using a gas chromatograph device with flame ionization detection (GC-FID) and atomic absorption spectroscopy (Analytik Jena AG, DE/novAA 300), respectively.

To check the reproducibility, each test specimen was prepared in triplicate. Control samples (adsorbate solution only) were also prepared to assess the quantity of BTEX or metals that can be volatilized and adsorbed on the vial surface. Additionally, the competitive adsorption tests for TAC and CAC were conducted in a same procedure as the single adsorption test using a multi-metal solution of Pb, Cu and Zn ions at concentration of 500 mg·L⁻¹.

3.2.7 Chemical stability of PWT and TAC

One substantive issue regarding the field application of PWT or TAC material is the potential leaching of various tire components. Therefore, in order to account for the presence of toxic ions either on PWT itself or during the pyrolysis of PWT, and to check their stability, a leaching test was performed at acidic and alkaline conditions according to the study of Alamo-Nole et al. (2011). That is, 0.5 g of PWT or TAC was soaked in 50 mL of DI water with adjusted pH value ranges 1-10 using HNO₃ and NaOH solutions. After 24 h of agitation at ambient temperature (22 ± 2 °C), the solutions were filtered. The clear supernatants were taken from each sample and were analyzed using inductively coupled plasma mass spectrometry (ICP-MS) for the Pb, Cu, Zn, cadmium (Cd), and arsenic (As) ions. All these experiments were also performed in triplicate, with the average value reported as the final value.

3.2.8 Desorption and reusability potential tests for TAC and CAC

To evaluate the possibility of recovering heavy metals from the loaded TAC and CAC surfaces as well as their reusability for subsequent use, one-step desorption experiments were performed at the end of the sorption experiments. Several studies have reported that HCl is the most efficient eluent for desorbing loaded ions from activated carbon surfaces (Gautam et al. 2014; Smičiklas et al. 2006) and was therefore selected as the eluent agent in this study. After batch adsorption tests, the supernatant was decanted from each sample, and the metal-loaded samples were dried at 60 °C for 24 h. A total of 50 mL of 0.01 M HCl (pH ~ 2) was added to the dried samples, which were placed on a shaker for 24 h at 180 rpm and then centrifuged at 3900 rpm for 20 min. The supernatant was extracted, and the released metal concentrations were analyzed

by atomic absorption spectroscopy. The actual desorbed concentrations for each sample were corrected by subtracting their known concentrations before the desorption step and their remaining concentration after the desorption test.

At the end of one cycle of desorption tests, the exhausted sorbents with heavy metals with initial concentration of $500 \text{ mg}\cdot\text{L}^{-1}$ were used to assess the reusability potential of the sorbents. For this aim, after finishing the first desorption cycle, the next adsorption cycle began by drying the used sorbents in an oven at $60 \text{ }^\circ\text{C}$ for 24 h. The used and dried adsorbent material was placed into a fresh solution containing $500 \text{ mg}\cdot\text{L}^{-1}$ of all three metals. The adsorption-desorption tests were continued for three cycles. Each test was performed twice and the mean was calculated.

3.3 Results and Discussion

3.3.1 BTEX removal by S-PWT mixtures

Figure 3.3 presents the amount of adsorbed BTEX components per unit mass of adsorbent plotted against equilibrium concentration for all S–PWT mixtures. Based on these results, PWT has the potential to adsorb BTEX components.

Referring to Figure 3.3, the sorption capacity of the various mixtures was dependent on their proportion of PWT. That is, the adsorption of BTEX increases with increasing percentage of PWT, with the maximum and minimum removal rates considering each BTEX component achieved for S–PWT100 and S–PWT0, respectively. The reason can be attributed to the high component of carbon (81.4 wt%, see Table 3.1) in the PWT's structure, which can be an attracting source for aromatic hydrocarbons.

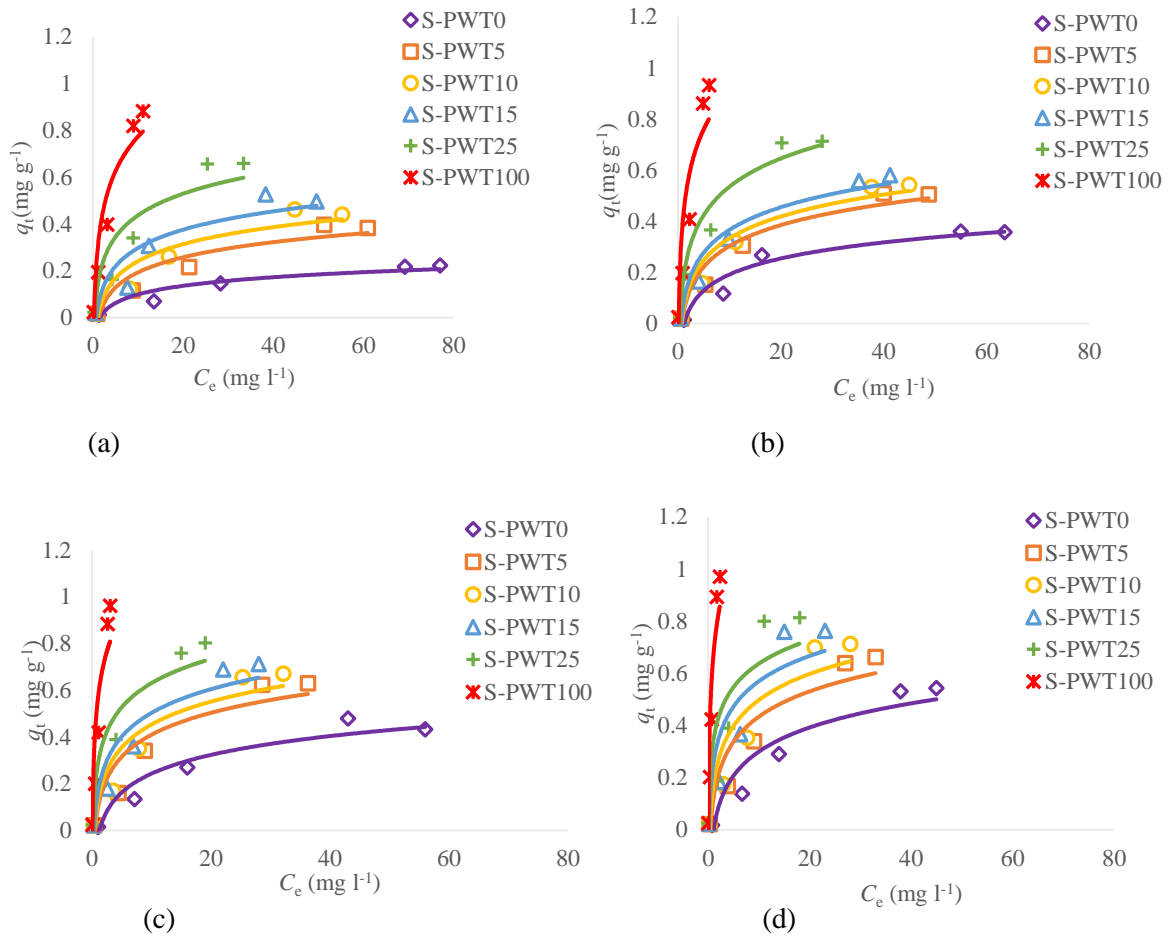


Fig. 3.3 BTEX component sorption by S–PWT mixtures: a) Benzene, b) Toluene, c) Ethylbenzene and d) Xylene

Table 3.1 Elemental analysis of PWT and soil materials

	Element (wt%)				
	Carbon	Hydrogen	Nitrogen	Sulfur	Oxygen
PWT	81.4	7.41	0.47	2.38	3.02
Soil	0.05	0.56	ND	ND	1.93

NOTE: ND: not detected

The removals of benzene, toluene, ethylbenzene and xylene by the S–PWT100 mixture were 78, 83, 93 and 96%, respectively. This is better than that achieved (although reasonably consistent) with previous studies which showed tire efficiency for removing toluene and xylene from aqueous phase of 60 and 81%, respectively (Alamo-Nole et al. 2011). With the sorption efficiency of tire chips affected by particle size (Bogliainenko and Tansel 2017), the higher removal rates achieved for the present investigation can be related to the PWT’s finer gradation.

For instance, Lu et al. (2015) employed equidimensional scrap tire pieces (2-mm side width) for the removal of BTEX, with removal efficiencies of 53, 70, 95 and 82% for benzene, toluene, ethylbenzene and xylene, respectively.

In the present study, the adsorption of BTEX compounds indicated the following order for adsorption affinity of BTEX: xylene > ethylbenzene > toluene > benzene. The same order has been reported for the adsorption of BTEX employing other adsorbent types (Almeida et al. 2012; Lu et al. 2015; Yakout and Daifullah 2014). This favorable sorption of xylene and ethylbenzene compared to toluene and benzene can arise for the following reasons: (i) higher hydrophobicity based on their octanol-water partition coefficient, such as the values of 3.15 for both xylene and ethylbenzene, 2.73 for toluene and 2.13 for benzene (Aivalioti et al. 2010); (ii) higher molecular weight (size), such as 106 g mol⁻¹ for both xylene and ethylbenzene compared to 92 and 78 g mol⁻¹ for toluene and benzene, respectively (Su et al. 2010); (iii) lower water solubility for xylene and ethylbenzene compared to toluene and benzene (Zhang et al. 2013). Generally, it seems that compared to toluene and benzene, xylene and ethylbenzene are more hydrophobic, such that they have greater tendencies for adsorption onto the PWT particle surfaces.

For better theoretical assessment of the adsorption mechanisms, the Langmuir and Freundlich models were fitted to the experimental data, with the deduced values of the model parameters listed in Table 3.2. The Freundlich K_F value, which is related to the loading factor of sorbate, indicates the uptake capacity of sorbent. Referring to Table 3.2, the estimated K_F values demonstrated that S-PWT100 had the highest uptake capacity of sorbent (K_F value) among all mixtures. The respective uptake capacity for xylene, ethylbenzene, toluene and benzene by S-PWT100 were 526.0, 376.9, 206.6 and 126.8 $\mu\text{g. g}^{-1}$ of sorbent. These deduced uptake capacities for 100% PWT material are consistent with previous experimental studies. For instance, Alamo-Nole et al. (2011) employed 14–20 mesh size tire-crumb rubber to remove xylene and toluene from aqueous solution, with reported uptake capacities of 723 and 239 $\mu\text{g. g}^{-1}$, respectively. Kim et al. (1997) investigated the sorption of organic components into rubber and found that its uptake capacity was 303 $\mu\text{g. g}^{-1}$ for toluene, with higher K_F values obtained for ethylbenzene and *m*-xylene.

The maximum adsorption capacity (q_{\max}) obtained from the Langmuir isotherm is used to calculate the adsorbed amount of BTEX by the PWT material before its surface becomes occupied. The S-PWT100 had the greatest q_{\max} values, consistent with its expected higher adsorption capacity, as compared to the other mixtures investigated. For S-PWT100, the maximum monolayer capacities were 1.91, 2.50, 2.69 and 2.91 mg. g⁻¹ for benzene, toluene, ethylbenzene and xylene, respectively. These deduced adsorption capacity values are essentially in line with BTEX removal using scrap tire pieces investigated by Lu et al. (2015).

Based on relatively higher values of the coefficient of determination (R^2) listed in Table 3.2 for the various S-PWT mixtures, the Freundlich model appears to fit the experimental data better than the Langmuir model. As such, it can be suggested that the adsorption of BTEX by PWT occurred by a multi-layer adsorption pattern, rather than a monolayer phenomenon.

Table 3.2 Langmuir and Freundlich parameters for BTEX component sorption by S-PWT mixtures

Material	Mixture	Langmuir model			Freundlich model		
		q_{\max} ($\text{mg} \cdot \text{g}^{-1}$)	K_L ($\text{l} \cdot \text{mg}^{-1}$)	R^2	K_F ($\mu\text{g} \cdot \text{g}^{-1}$)	$1/n$	R^2
Benzene	S-PWT0	0.34	0.023	0.959	10.65	0.72	0.990
	S-PWT5	0.67	0.024	0.976	17.92	0.78	0.989
	S-PWT10	0.75	0.029	0.939	24.10	0.77	0.988
	S-PWT15	0.79	0.039	0.852	34.21	0.73	0.974
	S-PWT25	0.98	0.064	0.917	63.78	0.70	0.994
	S-PWT100	1.91	0.080	0.928	126.79	0.88	0.983
Toluene	S-PWT0	0.57	0.029	0.896	16.67	0.80	0.934
	S-PWT5	0.74	0.048	0.987	34.03	0.75	0.967
	S-PWT10	0.78	0.054	0.993	39.64	0.74	0.967
	S-PWT15	0.80	0.064	0.997	46.78	0.73	0.967
	S-PWT25	0.99	0.100	0.934	83.60	0.72	0.906
	S-PWT100	2.50	0.099	0.889	206.60	0.87	0.998
Ethylbenzene	S-PWT0	0.81	0.025	0.853	19.51	0.85	0.962
	S-PWT5	0.94	0.060	0.962	54.00	0.73	0.987
	S-PWT10	0.97	0.070	0.979	64.20	0.72	0.989
	S-PWT15	0.99	0.094	0.988	78.97	0.70	0.988
	S-PWT25	1.00	0.198	0.986	135.67	0.65	0.988
	S-PWT100	2.69	0.180	0.824	376.85	0.87	0.999
Xylene	S-PWT0	1.12	0.022	0.968	25.15	0.85	0.988
	S-PWT5	0.99	0.062	0.977	58.60	0.73	0.993
	S-PWT10	1.03	0.080	0.951	77.00	0.70	0.995
	S-PWT15	1.03	0.120	0.908	110.90	0.656	0.995
	S-PWT25	1.06	0.190	0.886	161.28	0.59	0.989
	S-PWT100	2.91	0.230	0.913	526.02	0.91	0.995

3.3.2 Heavy metal removal by S-PWT mixtures

Figure 3.4 shows the adsorption of Cu–Pb solution by the various S–PWT mixtures. These results indicate that compared to the soil alone (S–PWT0), the adsorption capacity was greater for up to 10 wt% PWT, but decreased for higher proportions, with ~5 wt% PWT identified as optimum among the various mixtures. That is, the S–PWT5 mixture had the highest removal of selected ions from aqueous phase, with the removal of Pb and Cu at 62.8 and 37.7%, respectively. The S–PWT100 achieved relatively lower average removal values for Pb and Cu of 40.6 and 25.9%, respectively. This can be due to the lower surface area and mainly lower pore void volume of PWT compared to the soil particles (see Table 3.3 for BET surface area and pore void volume of each mixture). That is, the BET surface area of PWT is generally in the range of 0.06–3.5 m².g⁻¹ (Selbes et al. 2015), substantially lower than that measured for the test soil of 11.96 m².g⁻¹.

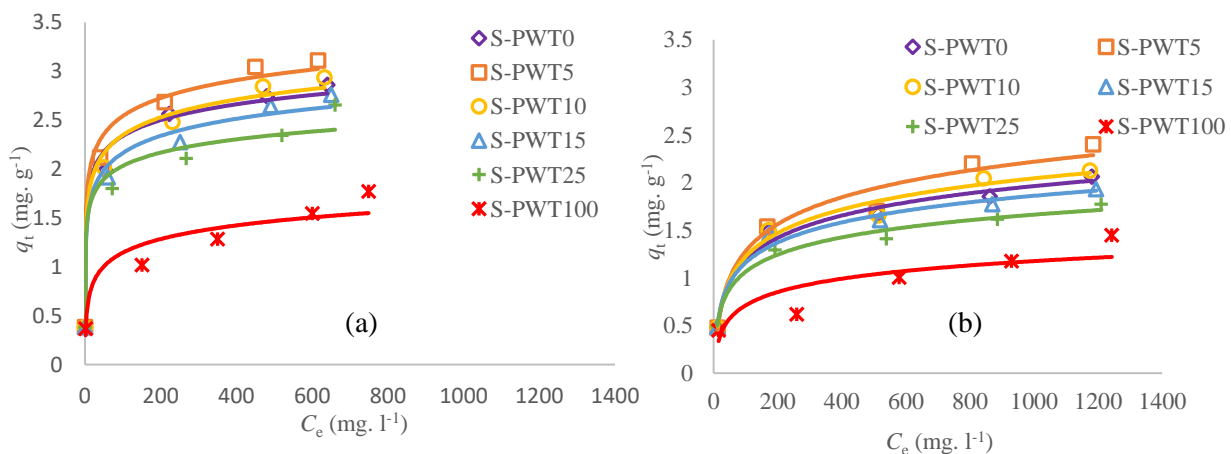


Fig. 3.4 Heavy metals adsorption by S–PWT mixtures, a) Lead and b) Copper

Table 3.3 Physical characteristics of mixtures investigated

Mixture	Surface area (m ² . g ⁻¹) ^a	Pore void volume (cm ³ . g ⁻¹) ^b
S-PWT0	11.96	0.026181
S-PWT5	3.5	0.026021
S-PWT10	0.29	0.012783
S-PWT15	0.41	0.011892
S-PWT25	1.48	0.010575
S-PWT100	0.13	0.008866

NOTE: ^a Brunauer–Emmett–Teller (BET) surface area; ^b Barrett, Joyner and Halenda (BJH) model desorption data.

The adsorption sequence of the examined heavy metals for all S–PWT mixtures was Pb > Cu, indicating that Pb was more adsorbed by the S–PWT mixtures than Cu. A logical justification for this result from the multi-solute adsorption isotherm is the smaller hydrated radius of the Pb²⁺ ion (4.01 Å) compared to Cu²⁺ (4.19 Å). Pb (7.71) also has a lower negative logarithm of hydrolysis constant (pKH) value than Cu (8.00). Thus, Pb has a greater tendency to be hydrolyzed (Boostani et al. 2019).

The experimental sorption data were also analyzed using the Langmuir and Freundlich isotherm models, with the deduced parameter values listed in Table 3.4. For S–PWT100, the maximum monolayer capacity (q_{max}) values for Pb²⁺ and Cu²⁺ were 1.81 and 1.57 mg. g⁻¹, respectively. Similar results were reported in the study by Calisir et al. (2009), which investigated crumb tire for adsorbing Cu²⁺ with the capacity of 1.52 mg. g⁻¹.

Table 3.4 Langmuir and Freundlich parameters for Pb and Cu sorption by S-PWT mixtures

Material	Mixture	Langmuir model			Freundlich model		
		q_{\max} (mg. g ⁻¹)	K_L (l. mg ⁻¹)	R^2	K_F (μg. g ⁻¹)	$1/n$	R^2
Pb ²⁺	S-PWT0	2.88	0.060	0.997	847.50	0.19	0.996
	S-PWT5	3.16	0.060	0.997	866.00	0.20	0.993
	S-PWT10	2.98	0.048	0.995	763.60	0.21	0.993
	S-PWT15	2.79	0.040	0.993	697.46	0.21	0.994
	S-PWT25	2.61	0.033	0.986	797.23	0.18	0.997
	S-PWT100	1.81	0.012	0.961	332.87	0.24	0.989
Cu ²⁺	S-PWT0	2.11	0.012	0.990	224.24	0.32	0.949
	S-PWT5	2.53	0.008	0.974	204.92	0.35	0.967
	S-PWT10	2.23	0.011	0.987	224.50	0.33	0.961
	S-PWT15	1.97	0.014	0.993	248.10	0.30	0.947
	S-PWT25	1.80	0.012	0.988	268.60	0.26	0.972
	S-PWT100	1.57	0.004	0.908	202.50	0.25	0.864

3.3.3 Chemical stability of S-PWT mixtures

The leaching test results are given in Table 3.5. Based on these results, there was no detectable arsenic and cadmium present at the end of the 24-h contact period for pH ranging 1–10. The only detectable level for Pb was for a pH of unity, with a concentration of 0.45 mg. l⁻¹, which is higher than the maximum contaminant level (MCL) requirement for drinking water according to a US EPA regulation (EPA 2009).

Table 3.5 Released metals from PWT at different pH values

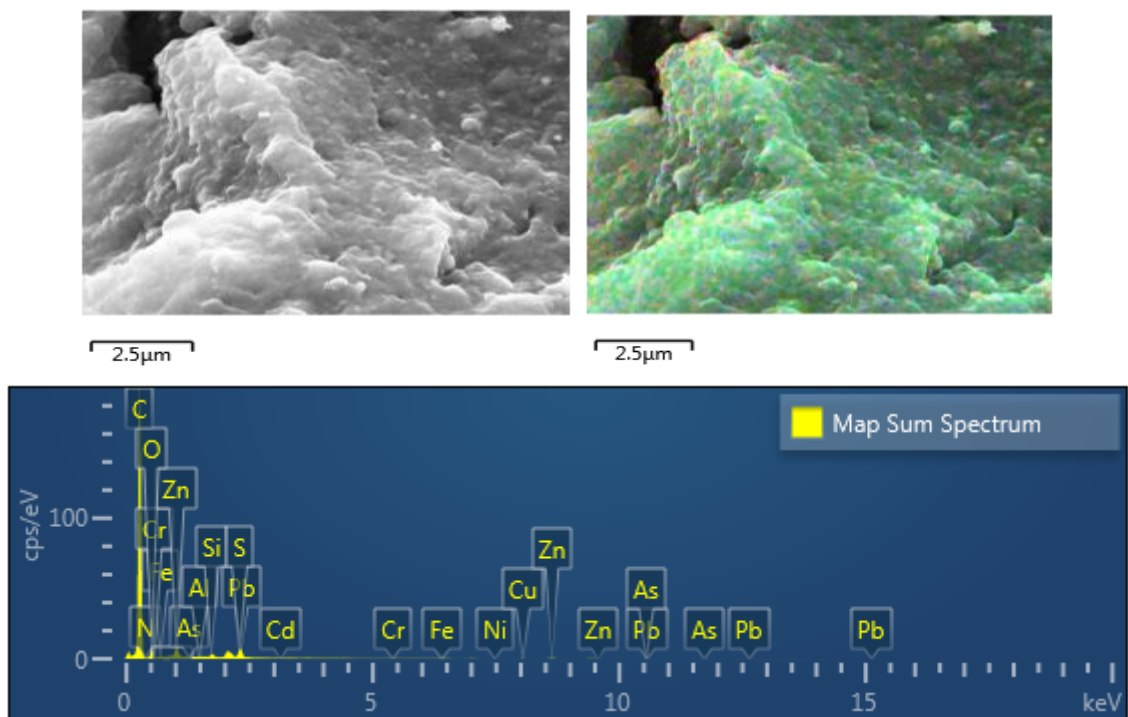
Ions	Concentration (mg. l ⁻¹) at different pH value of solution				MCL (mg. l ⁻¹) (EPA 2009)
	1	4	7	10	
Zn	126.85	4.83	3.67	2.26	5.0
Cu	15.52	0.0014	0.0009	0.0010	1.3
Pb	0.45	ND	ND	ND	0.015
As	ND	ND	ND	ND	0.010
Cd	ND	ND	ND	ND	0.005

NOTE: ND, not detected; MCL, maximum contaminant level requirement for drinking water

For Zn and Cu ions, leaching occurred for acidic and alkaline conditions, although the leaching for the highly acidic condition (pH 1) was substantially more noticeable, apart from which the levels measured for the all other pH values were below the US EPA MCL drinking-water regulation requirements. In other words, the results demonstrate that the release of Zn and Cu from PWT increases for increasing pH, although only the highly acidic condition produced a warning level of these metals. Among the heavy metals, zinc had the highest leachable amounts, because of the leaching of zinc oxide, which is the main component of waste tire (Wik and Dave 2009). For instance, Selbes et al. (2015) exposed different sizes of tire chips to leaching solutions with pH ranging 3–10 and found that the inorganic leaching was independent of tire-chip size, decreasing continuously with increasing pH. Their results showed that Zn had the highest leaching value (79.4 mg over 28 d period), whereas Pb, Cd, As, and Cr were below their maximum residue limit (MRL) value requirements for drinking water. Gualtieri et al. (2005) investigated the leaching of Zn ions from tire debris for pH values ranging 3–7, reporting that the leaching of Zn increases for reducing pH value, with observed maximum and minimum elutes of 44.7 and 1.2 mg. l⁻¹ for pH 3 and 7, respectively. In the study by Depaolini et al. (2017), the leaching values of 0.6040 ± 1.36 and 0.0050 ± 0.0007 mg. l⁻¹ for Zn and Pb, respectively, were obtained from granulated tire in deionized water. Li et al. (2010) employed acidified water (pH 4) to simulate the effect of normal acid rainwater for leaching of nine metals from crumb rubber, with results demonstrating that Zn ($0.7 - 3.6 \mu\text{g. l}^{-1}$

¹) was the highest leachable metal in the extraction fluid. Based on these studies, and considering the results of the present investigation, it is evident that zinc is the most leachable metal from waste tires.

In addition, the SEM EDS analyzing (Figure 3.5) and XRF test (Table 3.6) were performed to investigate the elements and possible trace of any toxic heavy metals in the PWT. The results showed that among the heavy metals present, zinc had the highest percentage (~3 wt%), which can be the main source for releasing and contamination of the soil body.



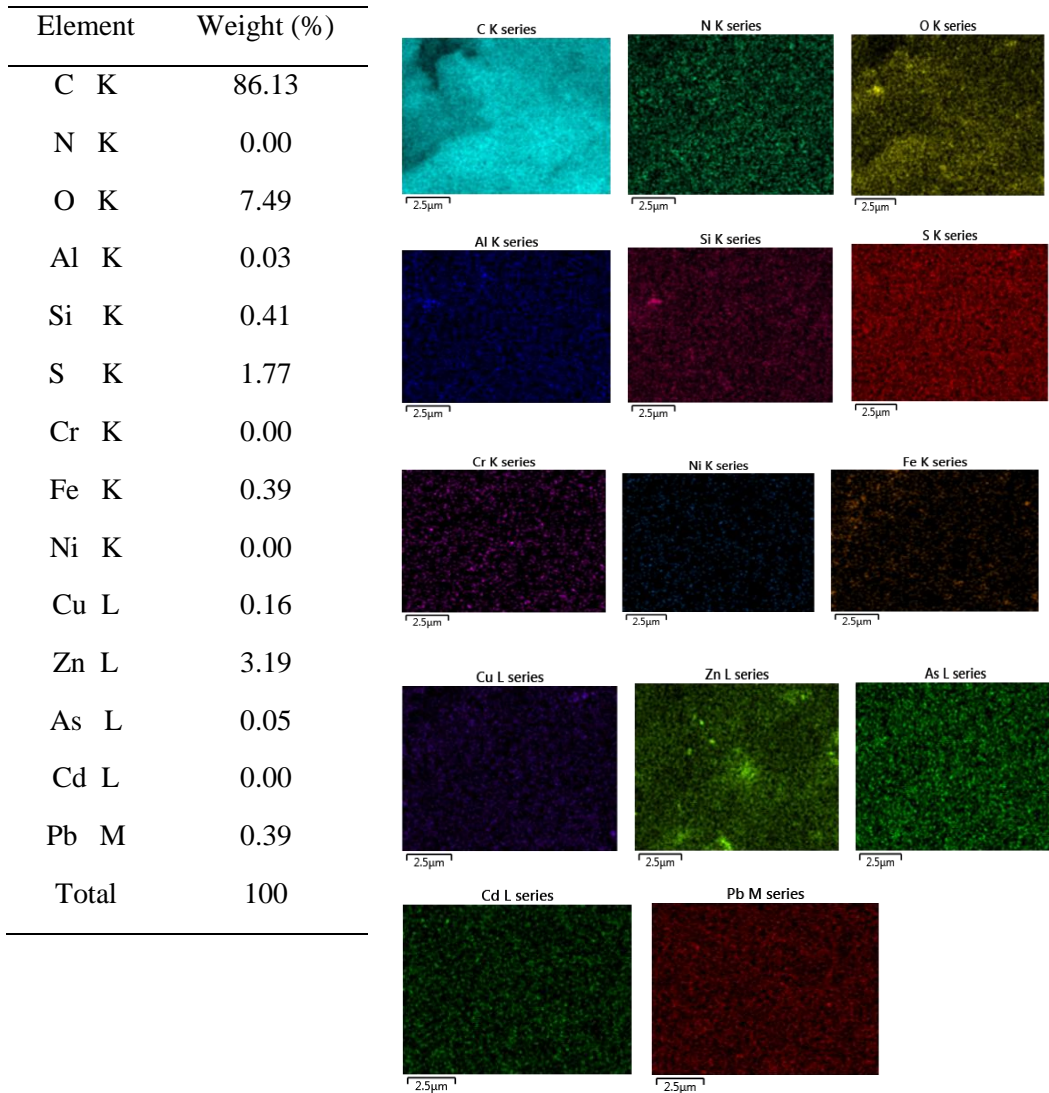


Fig. 3.5 SEM–EDS results for PWT investigated

Table 3.6 XRF chemical analysis for PWT investigated

Compound	SiO ₂	Al ₂ O ₃	TiO ₂	Fe ₂ O ₃	MgO	CaO	Na ₂ O	K ₂ O	MnO	P ₂ O ₅	LOI
wt%	0.69	0.10	ND	0.19	0.07	0.13	ND	0.07	ND	0.2	91.84

NOTE: ND: not detected; LOI, loss of ignition

As such, when the PWT is employed within fill materials, the main stimulus for releasing heavy metals (especially Zn) from its body and spreading them to the groundwater media is infiltration of acidic rainwater. The pH value of acidic rain typically ranges 4.0–4.2 (EPA 2006), but the detected level for zinc over this pH range was found lower than the MCL level requirement for drinking water (see Table 3.5). Consequently, even though tire has zinc, using

PWT as fill material is environmentally safe for the acidic rainwater condition in nature. However, the highly acidic (pH 1) leaching solution condition must also be considered cautiously for using PWT in the field.

3.3.4 Compaction test results

Figure 3.6 presents the standard Proctor-compaction test results for all S–PWT mixtures investigated. The value of maximum dry unit weight substantially decreased and the optimum moisture content for compaction increased with increasing PWT content.

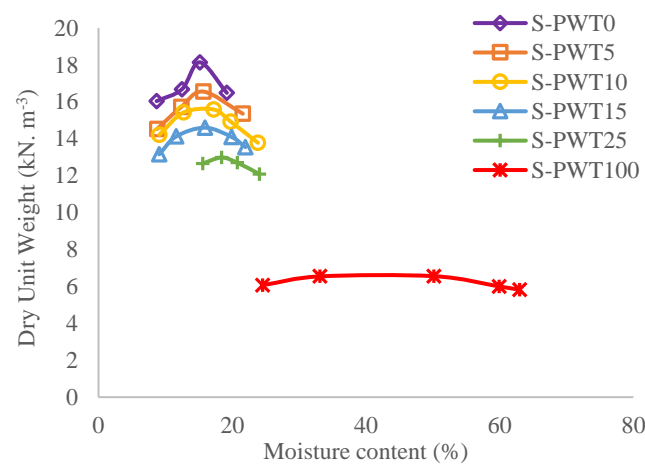


Fig. 3.6 Standard Proctor-compaction results for various S–PWT mixtures

The maximum dry unit weight values for the soil and PWT materials (i.e., S–PWT0 and S–PWT100, respectively) were 18.1 and 6.6 kN. m⁻³, respectively. Their substantial difference can be attributed to the lower specific gravity of tire chips (1.02–1.24 (Reddy et al. 2018)) compared to the soil solids (~2.67). The increase in optimum moisture content for compaction with increasing PWT content occurs on account of the reduction in energy absorption by the soil–PWT skeleton due to the presence of the pulverized tire additive (Gelder and Fowmes 2016).

The presented experimental results are in line with previous studies, including investigations of the compaction characteristics of clay and clayey soil materials mixed with fine and coarse tire chips (Cetin et al. 2006), clayey and sandy soils with different percentages of waste tire

(Abbaspour et al. 2019), sand–tire chip mixtures (Reddy et al. 2015) and both sand and fly ash mixed with a particulate rubber (Amuthan et al. 2018) .

3.3.5 Hydraulic conductivity test results

The standard Proctor-compacted S–PWT0 material had a measured permeability coefficient value of $3 \times 10^{-6} \text{ m. s}^{-1}$, typical of fine sand.

3.3.6 Compression test results

Figure 3.7a shows the compressibility behaviors of the various standard Proctor-compacted S–PWT mixtures. As evident from this figure, the compressibility and rebound of the mixtures for one-dimensional loading and unloading, respectively, both substantially increased with increasing PWT content. This is confirmed by the compression and swelling index values computed from the gradients of the e – $\log \sigma'_v$ loading and unloading curves, respectively, for each S–PWT mixture (see Figure 3.7b). As expected, the PWT material (S–PWT100) behaved essentially elastically.

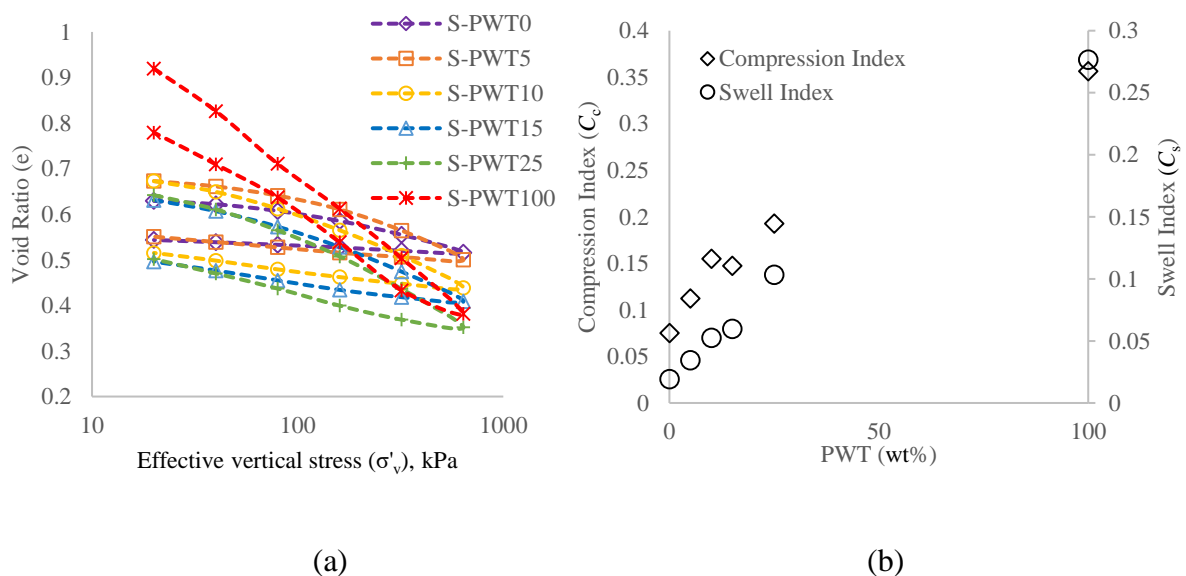


Fig. 3.7 One-dimensional compression test results, a) Void ratio versus effective vertical stress, b) Variation of compression and swelling indices with PWT content

3.3.7 Shear strength test results

Figures 3.8 and 3.9 present the results of the drained direct-shear tests performed on the various standard Proctor-compacted S–PWT mixtures. As evident from Figures 3.8 (a–c), the stiffness and peak shear stress (τ_{\max}) both substantially decreased in value with increasing PWT content, while the horizontal (shear) displacement corresponding to τ_{\max} progressively increased. That is, for an increasing proportion of PWT, the test specimens exhibited more ductile responses owing to the increase in rubber-to-rubber grain contacts for the soil–PWT skeleton (Kim and Santamarina 2008). Similar experimental behavior has been reported for soil–tire chip mixtures (Amuthan et al. 2018; Disfani et al. 2017; Madhusudhan et al. 2017; Reddy et al. 2015).

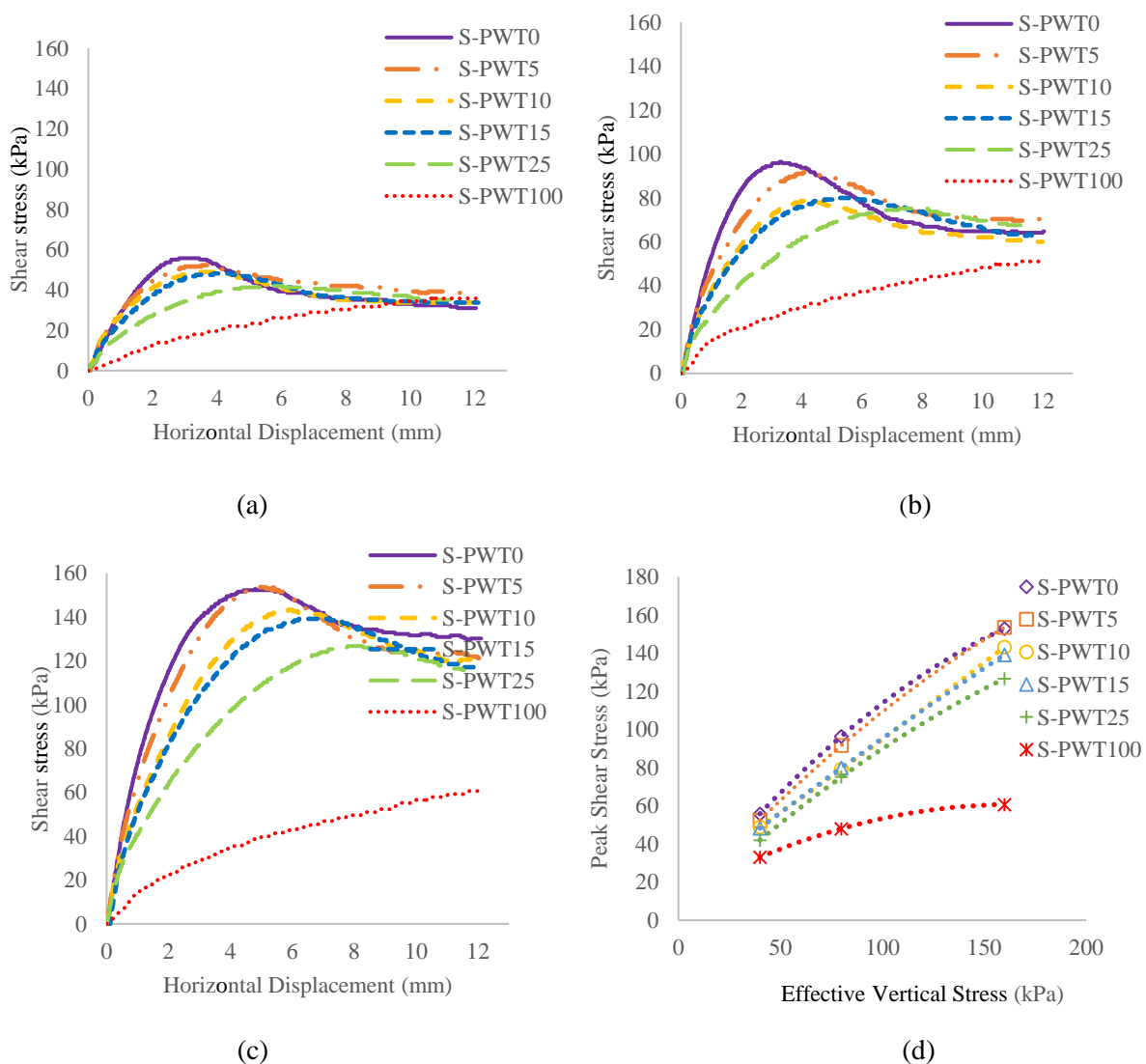


Fig. 3.8 Drained direct-shear test results for various S–PWT mixtures: shear stress against horizontal displacement traces for σ'_v of a) 40 kPa, b) 80 kPa and c) 160 kPa; d) Peak shear stress against effective vertical stress

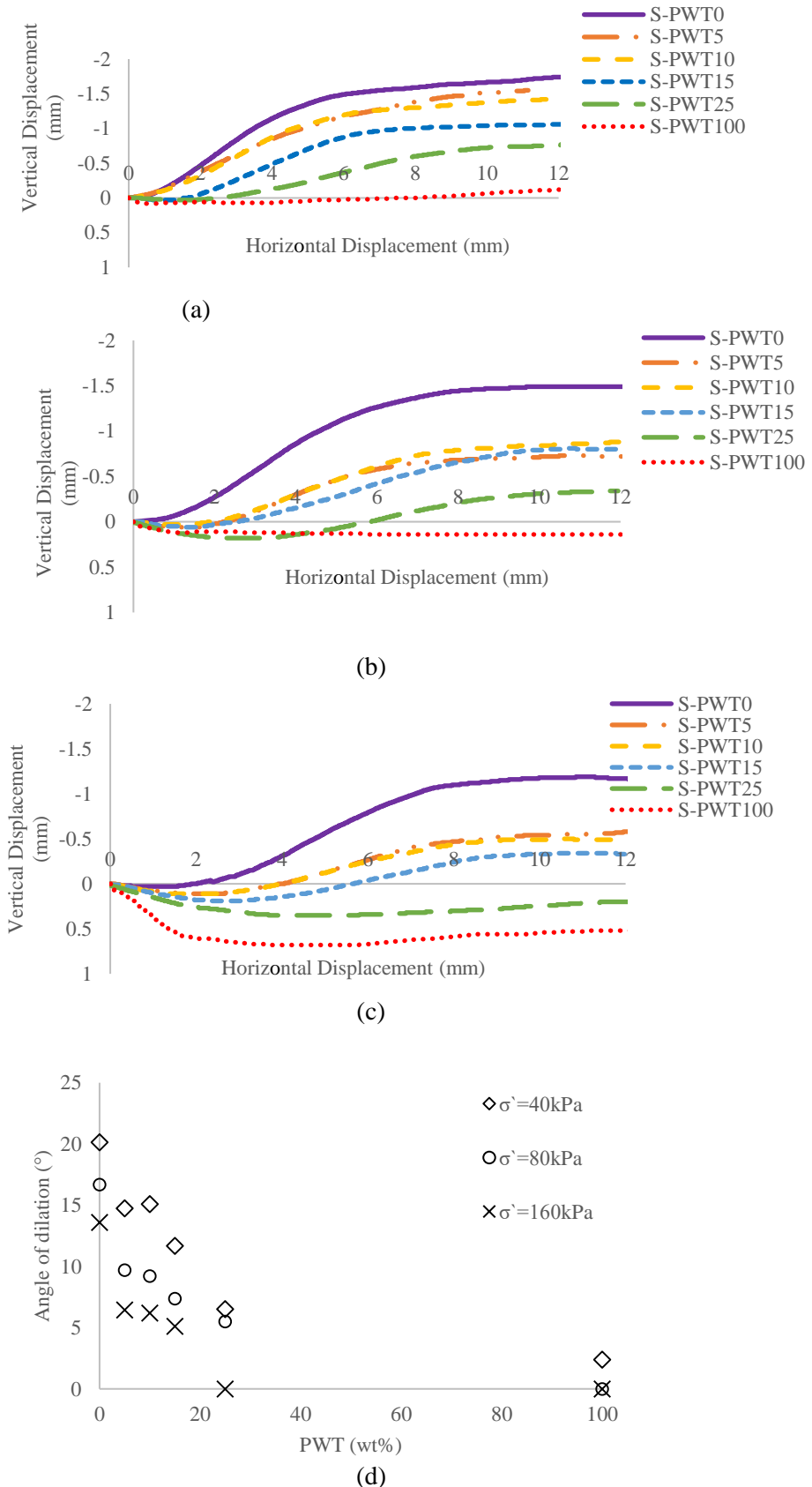


Fig. 3.2 Drained direct-shear test results for various S–PWT mixtures: vertical displacement against horizontal displacement traces for σ'_v of a) 40 kPa, b) 80 kPa and c) 160 kPa; d) Angle of dilation for the three applied normal stress levels. Note: following convention, negative vertical displacement indicates dilative behavior

Due to their compacted state and characteristic sand sized particles, the S–PWT mixtures generally experienced dilative behavior under shear, with the amount of specimen dilation reducing overall for higher applied normal stress and increasing PWT content. The angle of dilation values computed for the various S–PWT mixtures are presented in Figure 3.9d. For 100% PWT under shear, however, the test specimens experienced a small contractive behavior that increased for higher applied normal stress, indicative of their inferior compaction (see comparatively lower dry unit weight values achieved in Figure 3.6). The same was true to a lesser extent for the S–PWT25 mixture, such that its behavior changed from dilative to contractive over the increasing σ'_v range from 40 to 160 kPa.

The peak shear stresses mobilized at the applied normal stresses of $\sigma'_v = 40, 80$ and 160 kPa for the various S–PWT mixtures are plotted in Figure 3.8d. The fitted Mohr–Coulomb failure envelopes for all S–PWT mixtures produced extrapolated values of $c' > 0$ for $\sigma'_v = 0$ kPa. Although the $\tau_{\max} - \sigma'_v$ envelopes were slightly curved, the best-fit linear regression analysis was employed to deduce values of c' and ϕ' for the various mixtures. Based on the results presented in Table 3.7, the c' value decreased from 27.5 to 16.2 kPa with increasing PWT content from 0 to 25 wt%. In terms of friction angle, the ϕ' value increased marginally for PWT content increasing from 0 to 5 wt%, but then decreased for greater PWT content. The initial increase in ϕ' for the inclusion of 5 wt% PWT particles arises from their angularity (irregular shape), which enhances interlocking of the matrix of soil (fine sand) and PWT particles. The inferior compaction behavior of mixtures with greater PWT content (see Figure 3.6) produced more void space, causing the shearing resistance mobilized between the soil and PWT particles to decrease, thereby affecting a progressive reduction in the friction angle. However, compared to the soil alone (38.4°), the reduction in friction angle value was not overly significant, with ϕ' decreasing to 37.0° and 34.9° for 15 and 25 wt% PWT, respectively.

Table 3.7 Effective-stress shear strength parameter values deduced for S–PWT mixtures

Parameter	Material					
	S–PWT0	S–PWT5	S–PWT10	S–PWT15	S–PWT25	S–PWT100
c' (kPa)	27.5	21.4	18.6	16.9	16.2	26.7
ϕ (°)	38.4	39.9	38.3	37.0	34.9	12.4

A comprehensive review of the pertinent literature for direct shear testing showed that PWT addition to soil may cause a decrease or increase in the shear strength parameter values of soil–PWT mixtures (refer to Table 3.8). The majority of these studies, however, reported that the shear strength parameter values increased for the addition of tire chips up to an optimum PWT content of ~20–35 wt%, decreasing beyond this optimum range (Anbazhagan et al. 2017; Ghazavi et al. 2011; Reddy et al. 2015; Soganci 2015). There are some differences between the strength characteristics reported in this study and previous studies, which may be a result of the different gradation and particle shapes of PWT materials investigated and differences in the sample preparation methods employed for the strength tests performed in these studies. Overall, however, the ϕ range of 12.4–38.4° (Table 3.7) deduced for the present investigation is in line with the typical range of 18–49° reported for various soil and PWT mixing ratios investigated in previous studies (Table 3.8). Apart from the pure PWT material (S–PWT100), the ϕ values for all other S–PWT mixtures investigated were in the range of dense sand. It suggested that these soil–PWT mixtures could be used as adsorptive fill material for load-bearing engineering applications.

Table 3.8 Shear strength properties of different S–PWT mixtures reported in the literature

Parameter	Tire mixing ratio (wt% unless otherwise stated)											Reference	Comments	
	0	5	10	15	20	25	30	40	50	70	100			
c' (kPa)	49.3	45.7	43.0										Gong et al. (2019)	Railway ballast and tire derived aggregate (both passing 63.5-mm sieve). Tire mixing ratio as vol% Direct shear testing (500×500×350 mm shearbox) at 2 mm/min horizontal displacement rate
ϕ' (°)	38.7	34.6	29.5											
c (kPa)	nr											Madhusudhan et al. (2019)	Poorly graded sand and shredded tire (<2 mm) Drained triaxial testing (50 mm dia. × 100 mm long specimens) at confining pressure of 100 kPa and 0.6%/h axial strain rate	
ϕ' (°)	49		41				37		37		37			
c' (kPa)	nr											Amuthan et al. (2018)	Sand and 0.425–2 mm sized particulate rubber Direct shear testing (60×60×30 mm shearbox) at 0.625 mm/min horizontal displacement rate	
ϕ' (°)	45		34				30		30		26			
c' (kPa)	2	14	26		32		41						Noorzad and Raveshi (2017)	Poorly graded sand and 0.1–1mm sized powder rubber Drained triaxial testing (38 mm dia. × 76 mm long specimens) at 18%/h axial strain rate
ϕ' (°)	40	39	38		36		33							
c' (kPa)	7.5		11		10		11	25		23	17		Reddy et al. (2015)	Poorly graded sand and tire chips, each 10×10×20 mm long Direct shear testing (30×30×30 cm shearbox) at 1.25 mm/min horizontal displacement rate
ϕ' (°)	46		47.5		49		53	44		18	18			
c' (kPa)	0	1.5	4.5		7		3					3.5	Soganci (2015)	Compacted poorly graded sand and 1–3 mm sized tire chips Direct shear testing (shearbox 60×60 mm in plane)
ϕ' (°)	40.4	42.1	45.6		47.1		42.8					24.3		
c' (kPa)	0.8			5.1		6.8	7.3	9.4				2.5	Ghazavi et al. (2011)	Poorly graded sand and granular tire chips (<10mm sized) Tire mixing ratio as vol% Direct shear testing (shearbox 300×300 mm in plane) at 1 mm/min horizontal displacement rate
ϕ' (°)	30.2			35.8		38.2	39.7	38.2				24.2		

NOTE: nr, not reported

3.3.8 Long term settlement of S-PWT mixtures

The total settlement of any fill materials can be divided into two parts: the initial settlement, which occurs after compaction and loading by the superstructure, and the secondary settlement. The secondary settlement which is occurring for long time is considered as creep settlement. Although performing long-term compression tests on S-PWT mixtures was beyond the scope of this study, this section attempted to look at possible long-term settlement of waste tires and their mixtures with soils by looking at previous research.

At the study by (Wartman et al. 2007) the time-dependent compression of tire derived aggregate and tire-soil composites has been evaluated.

Waste tire chips with size less than 3cm has been selected, and were mixed at different ratios (0, 50, 65, 85, and 100 %) with a uniformly graded, medium subangular sand classified as SP. Experiments were performed under one dimensional confined compression on tire chip specimens in a triaxial cell under fully saturated conditions. The long- term settlement for each waste tire (WT)-soil composites were based on the Figure 3.10.

According to their findings, the time-dependent compression reached a steady rate after 10 to 20 hours of testing and remained roughly constant for the rest of the experiment. This suggests that representative time-dependent compression characteristics of waste tire can be determined within the first few days of an experiment, and that longer duration tests (5 days) may not be required in practice. Also, the time-dependent compression was a function of WT content and time, where time-dependent compression of 100% WT was much higher than sand. However, based on their results, for mixed sand with less than 50% WT, the compression rate was almost close to the sand. Moreover, they reported the secondary compression index of 100% WT is nearly an order of magnitude greater than sand (Figure 3.11). Secondary compression index varied from low level of 0.001 for 50% WT, to a higher value of 0.0074 for 100% WT.

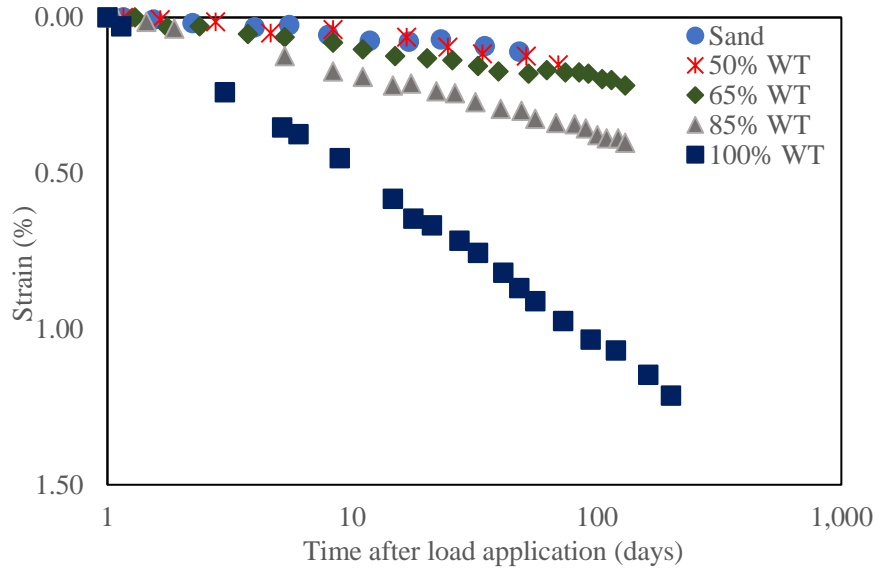


Fig. 3.3 Time-dependent volumetric strains for sand and mixed sand with tire chips ($\nu=80$ kPa) (Wartman et al. 2007)

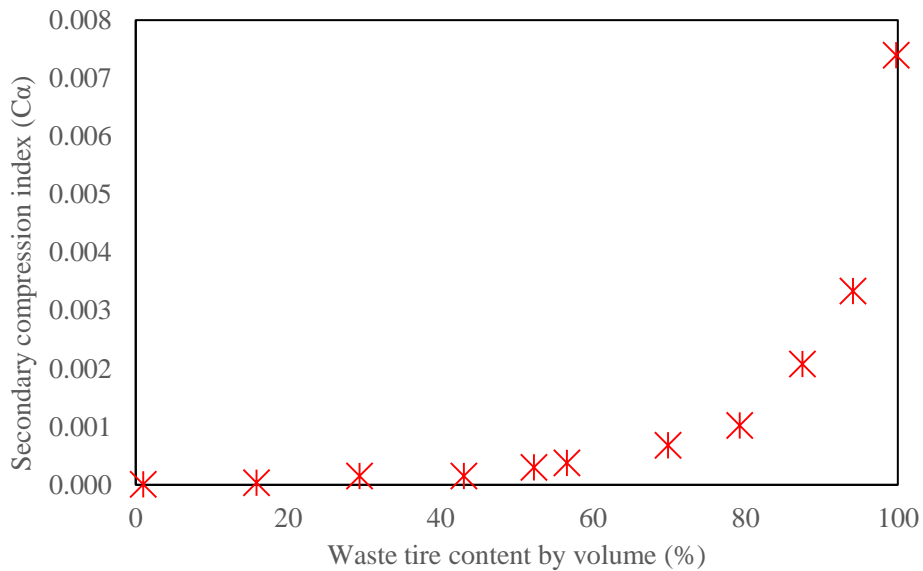


Fig. 3.4 Secondary compression index versus waste tire content (Wartman et al. 2007)

Drescher et al. (1999) studied creep in experiments ranging up to 400 days under vertical stress of 83kPa on 50 mm large tire shreds. Their results were based on the Figure 3.12.

According to their results, the strain-rate has fluctuated for several days and decreased with time until 30 days after loading. After 30 days the strain rate started to increase, where the reported average strain-rate for the period from 60 to 365 days beyond loading was 0.0362 % per week.

Also, the average strain-rates for the period from 330 to 360 days beyond loading were 0.0093 % per week. The authors reported that shredded tire pieces exhibit progressive creep when subject to long-term loading, with a noticeable rate of creep settlement occurring even after one year. The approached creep strain for tire shreds was reported near to 6%.

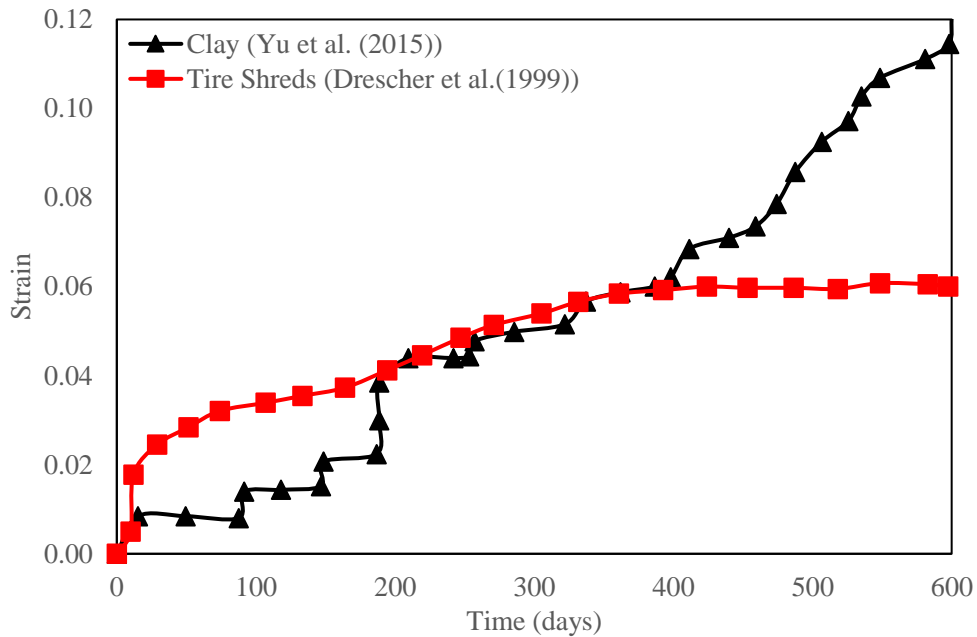


Fig. 3.5 Creep behavior of tire shreds and clayey soil

Several other researches have performed creep experiments on waste tire with different size. Based their results, it can be concluded that the time-dependent deformations of waste tire is dependent to the tire size, and generally constant rate over logarithmic cycles time will approach strains of ~5-8% after 1 to 2 years (Dickson et al. 2001; Hoppe and Mullen 2004; Humphrey et al. 2000; Salgado et al. 2003; Zornberg et al. 2004).

The obtained secondary compression index for waste tire composites were compared with obtained creep parameters for clayey soil in Korea (Table 3.9). It was obtained that the reported secondary compression index for waste tire composites were in range of secondary compression index of clayey soil in Korea. Also, the creep behavior for clayey soil over 600 days which has

been performed with Yu et al. (2015) (Figure 3.12), demonstrated the creep stain for clays was in the same pattern as the waste tire.

Table 3.9 Secondary compression index for soft clay in Korea (Suneel et al. 2018)

Location	C_{α}
Pusan New Port	0.003- 0.06
Nakdong	0.025- 0.14
Noksan	0.009- 0.020
Pohang	0.009- 0.015
Kwangyang	0.008-0.013
Mokpo	0.007- 0.020
Yongsan	0.009- 0.022

Totally it can conclude that waste tire exhibits high constant rate degrees of time-dependent compression (creep strains of ~5-8%) which is similar to clayey soil compression. However, the long-term properties of waste tire-soil composites require further investigation.

3.3.9 Simulation the BTEX movement through modified layer with PWT

Based on the obtained results adding the waste tire to the soil increases the sorption rate of the soil, while the permeability of the mixture may either increase or decrease. If the permeability changed more than sorption capacity, contaminants may move through the bottom reactive layer without having proper sorption by the S-PWT mixture.

In order to determine how permeability changes affect the sorption and movement of BTEX through the modified layer with PWT, the movement of released BTEX from one imaginary landfill (Figure 3.13) through subsurface has been assessed by MODFLOW software.

Based on the performed batch sorption and geotechnical experiments for S-PWT mixtures, for satisfying both geotechnical and environmental properties of Soil/Tire mixture, the mixing ratio less than 15% is recommended. Therefore, the bottom layer under the landfill has been modified with 15 % PWT, and the concentration of BTEX for both modified and non-modified layers has been estimated at points A and B (points located under the landfill).

The required sorption and permeability parameters for MODFLOW simulation were based on table 3.10.

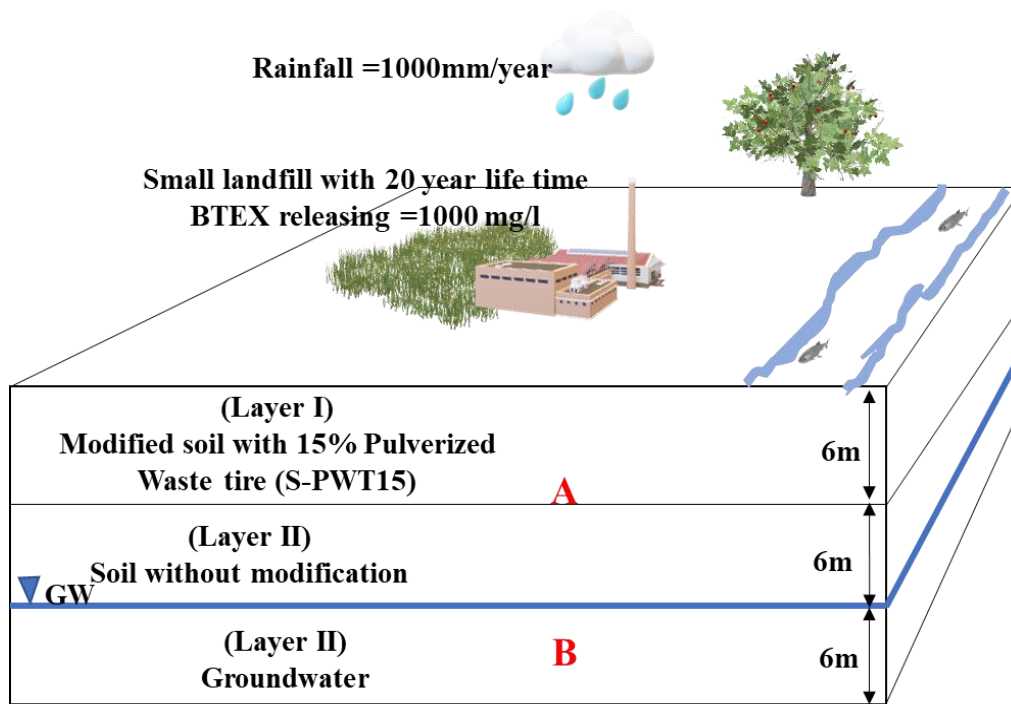


Fig. 3.6 Imaginary landfill for MODFLOW simulation

Table 3.10 Sorption and permeability parameters for MODFLOW simulation

Mixture	Permeability (Boominathan and Banerjee 2019)	Obtained sorption parameter (from present study)	
		q_{\max} ($\text{mg. } g^{-1}$)	K_L ($l. \text{ } mg^{-1}$)
S-PWT0	6.58×10^{-5}	0.34	0.023
S-PWT5	6.1×10^{-5}	0.94	0.06
S-PWT10	5.7×10^{-5}	0.97	0.07
S-PWT15	5.09×10^{-5}	0.99	0.094
S-PWT25	4.3×10^{-5}	1.00	0.198
S-PWT100	2.6×10^{-5}	2.69	0.180

Figure 3.14 depicts the concentration of BTEX at points A and B over a 20-year period. As can be seen from this graph, the modified layer with 15% PWT has delayed the BTEX releasing. With 15% PWT, BTEX reached to the groundwater media after 10 years, whereas without any modification, groundwater was contaminated in 4 years. Furthermore, the concentration of released BTEX to the groundwater using the modified layer with 15% PWT was half of the non-modified layer after 20 years.

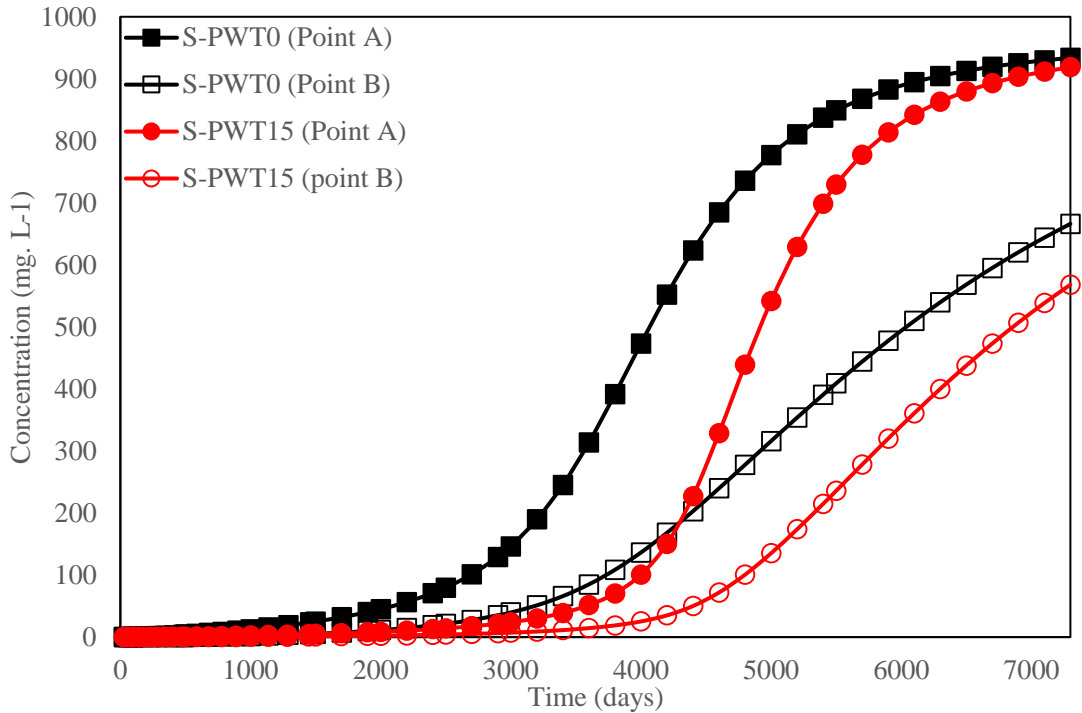


Fig. 3.7 Concentration of BTEX versus time at points A and B

3.3.10 Cost comparison of PWT with other common sorbents

The experimental results indicate that these compacted S–PWT mixtures have relatively low dry unit weight (Figure 3.6), low compressibility ($C_c = 0.11$ – 0.19 : Figure 3.7(b)), adequate shear capacity for many load-bearing field applications, and satisfactory adsorption of organic/inorganic contaminants. As such, these characteristics make compacted S–PWT materials worthy candidates for many fields geotechnical and the geoenvironmental applications. For instance, due to their lightweight, S–PWT mixtures produce lower self-weight vertical and horizontal effective stresses *in-situ*, which is advantageous for using as backfill materials behind retaining walls and bridge abutments. Other notable applications for compacted S–PWT materials may include as bottom layers in landfills and industrial foundation fills, where they have sufficient bearing capacity and high adsorption of contaminants. Due to the large volumes of additives typically required for such fill materials, S–PWT mixtures have potential to drastically reduce the financial costs in field applications. The cost of PWT has been reported as ~ 0.065 US\$/kg (Lin et al., 2008), generally

substantially cheaper compared to other adsorptive fill materials, including commercial activated carbon, biosorbents, zeolite, and clay (see Table 3.11). Based on reported unit costs, using PWT instead of these common adsorbents could produce estimated cost savings of the order of 65.9 to 98.9% at 1m³ scale (Table 3.11).

Table 3.11 Cost comparison of PWT with common adsorbents

Material	Cost (US\$.kg ⁻¹)	Average Bulk Density (Mg. m ⁻³)	Mass of fill material for 1m ³ scale (kg)	Average cost of fill material for 1m ³ scale (US\$)	Saving (%)
PWT	0.065 (Lin et al. 2008)	0.67	670	44	—
CAC	9 (Kurniawan et al. 2006)	0.48 (Acosta et al. 2016)	480	4320	98.9
Zeolite	0.04–0.90 (Wen et al. 2018)	1.45 (Kwon et al. 2019)	1450	682	93.6
Biosorbents	0.02–15.43 (Bhattacharyya and Gupta 2008)	0.32 (Bhattacharya et al. 2013)	320	2471	98.2
Clay	0.04–0.12 (Bhattacharyya and Gupta 2008)	1.6 (Holtz et al. 2011)	1600	128	65.9

Note: CAC, commercial activated carbon

3.3.11 Physicochemical characteristics of TAC and CAC

Figure 3.15 (a-b) shows the N₂ adsorption-desorption isotherms for the CAC and TAC samples. According to the IUPAC classification, the N₂ adsorption-desorption isotherm of TAC resembles the Type IV isotherm with a H₃ hysteresis loop (Rouquerol et al. 2013). This isotherm suggests the presence of mesopores, for which the adsorption mechanism begins with the formation of a monolayer-multilayer on the surface of the TAC followed by pore condensation. The N₂

adsorption-desorption isotherm of CAC exhibited a Type I isotherm with the existence of narrow micropores, where adsorption is occurring only via the formation of a monolayer on the surface of the CAC.

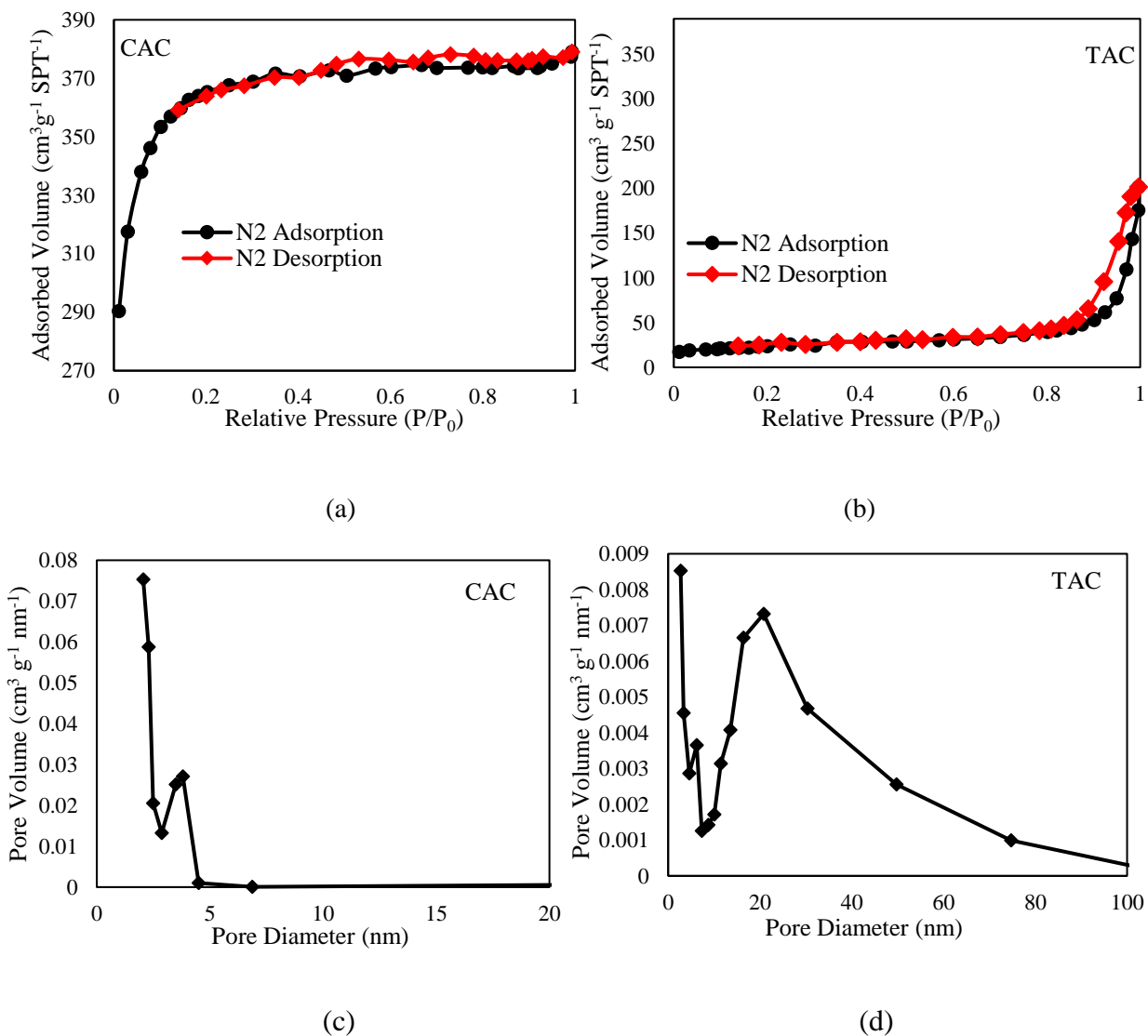


Fig. 3.15 (a-b) N₂ adsorption-desorption isotherms at 77 K, (c-d) pore size distribution of the CAC and TAC samples

Figure 3.15 (c-d) shows the pore size distribution of the CAC and TAC samples obtained from their N₂ desorption isotherm curves. The pore size distribution curves confirm that the pore sizes of the CAC sample are distributed in a narrow range from just below 2 nm to approximately 6 nm,

which includes micropores (<2 nm) and small mesopores (Bansal and Goyal 2005). For TAC, the pore sizes were well distributed over the range of micro- and mesopores. The BET specific surface area for TAC (82 m²·g⁻¹) was less than that of CAC (1241m²·g⁻¹). Moreover, the cumulative pore volume of CAC 0.445069 cm³·g⁻¹ was higher than the TAC cumulative pore volume of 0.302377 cm³·g⁻¹ (Table 3.12). The higher surface area may be because CAC had a higher pyrolysis temperature than TAC (Li et al. 2017).

Table 3.9 Physicochemical characteristics of TAC and CAC samples

Properties	TAC	CAC
Carbon %	80.45	83.17
Hydrogen %	1.04	1.32
Nitrogen %	ND	ND
Sulfur %	0.91	0.07
Oxygen %	11.28	8.66
H/C	0.013	0.015
(O+N)/C	0.141	0.104
BET surface area (m ² ·g ⁻¹)	82	1241
Cumulative pore volume (cm ³ ·g ⁻¹) ^a	0.302377	0.445069
Pore size (nm) ^b	19.756	2.781
CEC (cmoL·kg ⁻¹)	8.45	56.89

NOTE: ND, not detected; ^a P/P0=0.99; ^b Barrett-Joyner-Halenda (BJH) model, desorption data

SEM images of the TAC and CAC samples (Figure 3.16) confirm that TAC has a porous morphology while CAC is a flat adsorbent. Moreover, the XRD analysis for CAC (Figure 3.17) displayed more sharp diffraction peaks with larger peak areas as compared to TAC, which suggests that CAC is a more crystalline material while TAC is less crystalline and a more amorphous adsorbent material (Liang et al. 2017). Additionally, the SEM-EDS results (Table 3.13) for the adsorbents show that the TAC surface has a higher content of oxygen (14.8%) and sulfur (0.9%)

when compared with CAC, which indicates that TAC may have more surface functional groups or active sites, where potential binding of heavy metals can occur. This can also be potentially attributed to the higher pyrolysis temperature of CAC compared to that of TAC. Previous studies have documented that adsorbents with higher pyrolysis temperatures result in a decrease in elements such as H and O as well as surface functional groups (Kwak et al., 2019; Li et al., 2017).

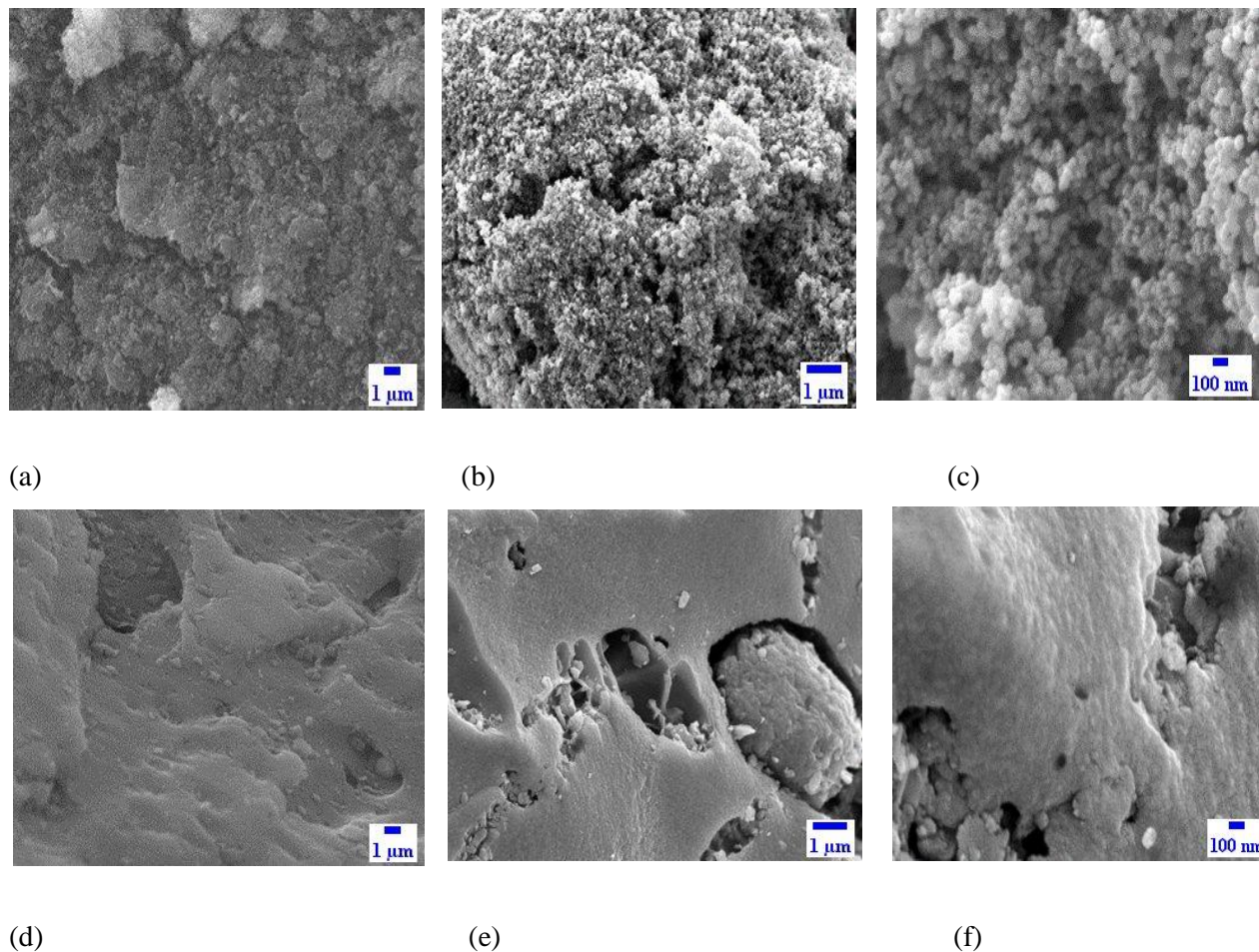


Fig. 3.16 SEM Images of the TAC sample at (a) 5,000 \times , (b) 10,000 \times and (c) 50,000 \times magnification and the CAC sample at (d) 5,000 \times , (e) 10,000 \times and (f) 50,000 \times magnification

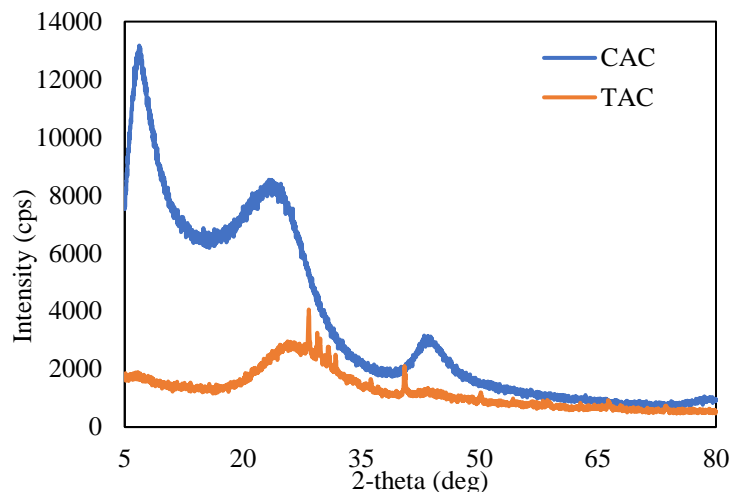


Fig. 3.17 XRD patterns for TAC and CAC samples

Table 3.10 EDS results for CAC and TAC

CAC		TAC	
Element	Weight (%)	Element	Weight (%)
C K	90.54	C K	80.45
N K	0	N K	0
O K	8.73	O K	14.78
Al K	0	Al K	0.04
Si K	0.06	Si K	1.63
S K	0.16	S K	0.92
Cr K	0	Cr K	0
Fe K	0	Fe K	0.13
Ni K	0	Ni K	0
Cu L	0	Cu L	0
Zn L	0	Zn L	0.91
As L	0.03	As L	0
Cd L	0	Cd L	0
Pb M	0.48	Pb M	1.16
Total	100	Total	100

The cation exchange capacity (CEC) values for the CAC and TAC samples were 56.89 and 8.45 $\text{cmol}\cdot\text{kg}^{-1}$, respectively. The higher CEC value for CAC reveals that CAC has higher amounts of cations, such as K^+ , Ca^{2+} , and Mg^{2+} , that are available for exchange with toxic metal ions.

Consequently, more heavy metals can be adsorbed on the surface of CAC via the ion exchange adsorption mechanism. The increased cation concentration indicates that cation exchange is a predominant mechanism for Pb(II) adsorption on biochar adsorbents (Kwak et al., 2019). The CEC value for CAC was comparable to that of wheat straw biochar (26.8 – 175.9 mg·g⁻¹), which primarily adsorbed Pb(II) by cation exchange (Kwak et al., 2019). The low CEC value for TAC indicates that ion exchange plays only a small part in heavy metal adsorption and that there are other more predominating adsorption mechanisms.

3.3.12 Elemental analysis of TAC and CAC

Table 3.12 displays the elemental analysis result for TAC and CAC. In comparison to CAC, TAC had lower carbon and higher oxygen contents. During pyrolysis, high temperatures are used and the carbon content of activated carbon increases (Kwak et al. 2019; Li et al. 2017). Pyrolysis for CAC occurred at higher temperature than that for TAC; which may explain the higher carbon content of CAC. The aromaticity and polarity of the adsorbents were evaluated by calculating the H/C and (O+N)/C molar ratios, respectively. The molar ratio of H/C for CAC and TAC were 0.015 and 0.013, respectively. The resulting low molar ratios for both TAC and CAC suggest that they both have high aromaticity and strong carbonization, which make them efficient adsorbent materials (Chen et al. 2014). The polarity index [(O + N)/C] for CAC and TAC were 0.104 and 0.141, respectively. The higher polarity index for TAC compared to that for CAC implies that TAC is more hydrophilic and contains more polar functional groups for coordination with heavy metals, as was also confirmed by SEM-EDS results (He et al., 2017b).

3.3.13 Zeta potential of TAC and CAC

Zeta potential values for TAC and CAC samples before and after adsorption of Pb ions are shown in Table 3.14. Both TAC and CAC samples have highly negative zeta potential values. This indicates that TAC and CAC are carrying negative charges on their surfaces, which increases the

possibility for Pb sorption due to increasing electrostatic interaction between the positive Pb ions and the negatively charged adsorbent surface (Tan et al. 2020). After adsorption of the Pb ions, the zeta potential of CAC drastically increased, however, the zeta potential of TAC did not change significantly. In other words, after reacting with Pb ions, the negative charge of CAC decreased, and changed to a positive value, while the surface charge of TAC remained negative. This can be attributed to the formation of an Electric Double Layer (EDL) and/or altering the initial pH values of adsorbents by loading the Pb ions.

Table 3.14 Zeta Potential (ZP) of TAC and CAC samples before and after Pb ion adsorption

Sample	ZP before adsorption	ZP after Pb adsorption	Initial pH	Final pH
TAC	-34.5	-34.01	7	10.2
CAC	-36.1	+18.9	7	7

EDL is formed due to surface charge distribution near the adsorbent particles. The EDL consists of two layers; the stern layer, which is fixed to the solid surface of the adsorbents, and the diffuse layer, which is located on top of the stern layer. The Zeta potential is the electric potential of the EDL between these two layers. Non-specific adsorption of ions occurs in the diffuse layer by electrostatic attraction, whereas specific adsorption occurs at the stern layer by chemical bonding between the adsorbents and the adsorbate (Wakatsuki et al. 1974). Therefore, nonspecific adsorption (electrostatic adsorption) of ions will not change the surface charge of the adsorbents. However, due to the formation of chemical bonds, specifically adsorbed ions in the stern layer will change the surface charge of the adsorbent, which will alter the value of the zeta potential (Xu et al. 2011). Thus, it seems that for the TAC sample, the Pb ions are entering the diffuse layer, and are adsorbed nonspecifically. Therefore, the zeta potential of Pb-loaded TAC is not changing relative to its initial value. However, for CAC, the concentration of Pb ions is higher than the electrostatic interaction capacity, thus the extra ions are entering the stern layer, and adsorption occurs by both specific and nonspecific processes. As a result, the value of the zeta potential for

CAC changes after reacting with Pb ions. Therefore, under the investigated concentrations of Pb ($\sim 100 \text{ mg}\cdot\text{L}^{-1}$), both specific and nonspecific adsorption processes were fulfilled for CAC, whereas TAC still had an additional capacity for specific adsorption to occur at higher concentrations.

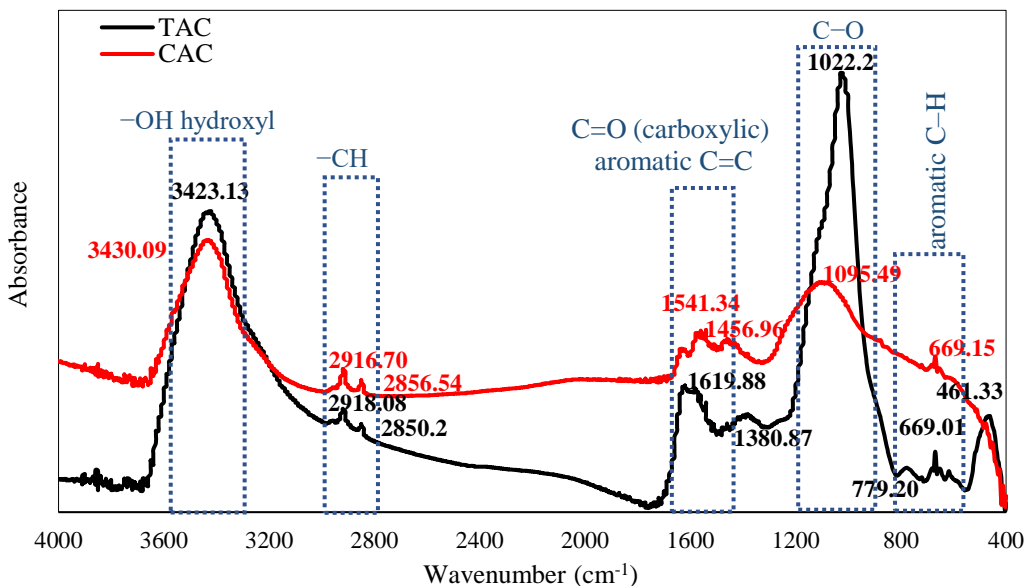
Moreover, the pH value of the TAC sample was increased after loading Pb on its surface. Deprotonation of surface functional groups due to higher pH generally increases the zeta potential value (Eeshwarasinghe et al. 2019). Thus, increasing the pH of TAC after loading Pb on its surface can explain the lower change in the TAC zeta potential.

3.3.14 FT-IR test results

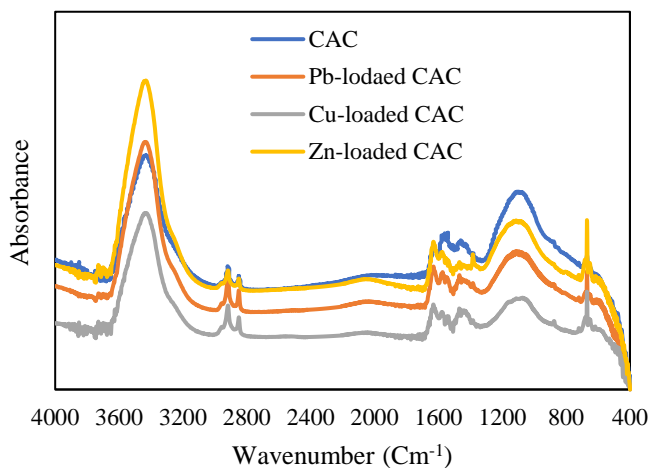
The FT-IR spectra of the TAC and CAC before and after adsorption of heavy metals are presented in Figure 3.18. As illustrated in Figure 3.18a, FT-IR spectra of the raw TAC and CAC show that each adsorbent has functional groups that may act as proton donors, which is important for coordination with heavy metals. The functional group represented by the bands at $3450 - 3200 \text{ cm}^{-1}$ is assigned to $-\text{OH}$ stretching vibration of the hydroxyl group (Uchimiya et al. 2011; Zhang et al. 2020). The peaks at a range $3000 - 2840 \text{ cm}^{-1}$ are attributed to aliphatic $-\text{CH}$ stretching (Uchimiya et al. 2011). The $\text{C}=\text{O}$ (carboxylic) groups are at $1750 - 1540 \text{ cm}^{-1}$, and the aromatic $\text{C}=\text{C}$ group is at $1600 - 1450 \text{ cm}^{-1}$ (Merck KGaA 2020; Sikder et al. 2013). The peaks observed at 1380.87 cm^{-1} (almost range $1383 - 1250 \text{ cm}^{-1}$) are attributed to phenolic $\text{O}-\text{H}$ bending in TAC (Uchimiya et al. 2011). The bands at $1200 - 1000 \text{ cm}^{-1}$ are corresponded to $\text{C}-\text{O}$ stretching in alcohols and phenols (Kołodzyńska et al. 2017; Tan et al. 2020); the peaks at a range $900 - 650 \text{ cm}^{-1}$ represent aromatic $\text{C}-\text{H}$ bending vibrations (Liu et al. 2020; Wu et al. 2019; Zhang et al. 2020).

As is evident from Figure 3.18a, the peak areas of the formed functional groups (especially the carboxylic, hydroxyl and phenolic groups) for TAC showed higher intensities than those for CAC. Additionally, in comparison to CAC, TAC showed another peak at 461.33 cm^{-1} , representing $\text{S} - \text{S}$ bonds (Stuart 2004). The extra peak and the higher intensities of the functional groups may increase the possibility of TAC coordination with heavy metals. After heavy metals loading, the

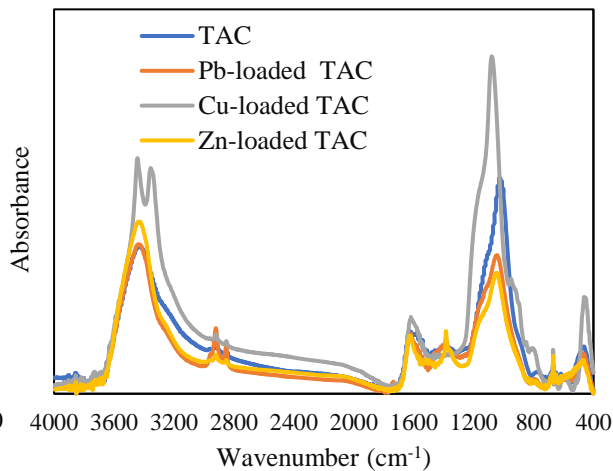
peaks for both TAC and CAC either shifted to a new position or became weaker/stronger. Coordination interaction of heavy metals is mostly achieved by complexation with oxygen functional groups or/and interaction with aromatic π - electrons (Hotová et al. 2020).



(a)



(b)



(c)

Fig. 3.18 FT-IR spectra of TAC and CAC (a) before and (b-c) after adsorption of heavy metals

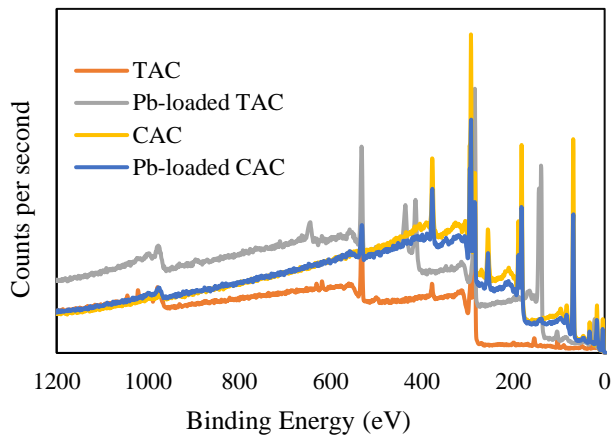
According to the FT-IR spectra shown in Figures 3.18b and 3.18c, the shift of the carboxylic and hydroxyl bands after loading heavy metals with weaker/stronger intensities, is due to the surface complexation of the heavy metals with these functional groups. For example, the shift of the band at 1619.88 and 1380.87 cm^{-1} for TAC to 1618.23 and 1383.78 cm^{-1} for Pb-loaded TAC and that at 3423.13 cm^{-1} for TAC to 3440.45 cm^{-1} for Pb-loaded TAC, support the surface complexation of lead by carboxylic (C=C, C=O) and hydroxyl groups in TAC, respectively. The band at 1022.25 cm^{-1} for TAC which is assigned to C–O groups, shifted to 1042.89 cm^{-1} with lower intensity for Pb-loaded TAC. Moreover, the bands 2918.08 cm^{-1} and 2850.2 cm^{-1} , assigned to aliphatic –CH stretching groups, shifted to 2920.8 cm^{-1} and 2850.68 cm^{-1} after loading Pb on TAC. These shifts also reflect the involvement of C–O and –CH groups in heavy metal surface complexation. After heavy metal adsorption on TAC, the band allocated to aromatic C–H groups showed a shift with lower/higher intensities. For example, after loading Pb on TAC, the bands 779.20 cm^{-1} and 671.1 cm^{-1} shifted to 791.87 and 668.96 cm^{-1} , respectively. These changes may support the interaction of heavy metals with aromatic π - electrons. The weaker peak of oxygen functional groups after loading Pb on the TAC surface, shows that these groups were consumed during the adsorption of Pb ions. Therefore, it can be declared that hydroxyl, carboxylic and phenolic groups are involved in sorption of heavy metals. These results are also in agreement with other studies that confirm oxygen functional groups are taking part in the sorption of heavy metals (Kołodzyńska et al. 2017; Li et al. 2019; Liu et al. 2020; Tan et al. 2020).

The shifting of the functional groups for CAC after loading heavy metals (Figure 3.18b) also confirms the coordination of heavy metals with the functional groups. However, the intensities of these functional groups are lower compared to TAC. This implies that oxygen functional groups on TAC are more involved in heavy metals adsorption by mechanisms such as surface complexation and ion- π electron interaction.

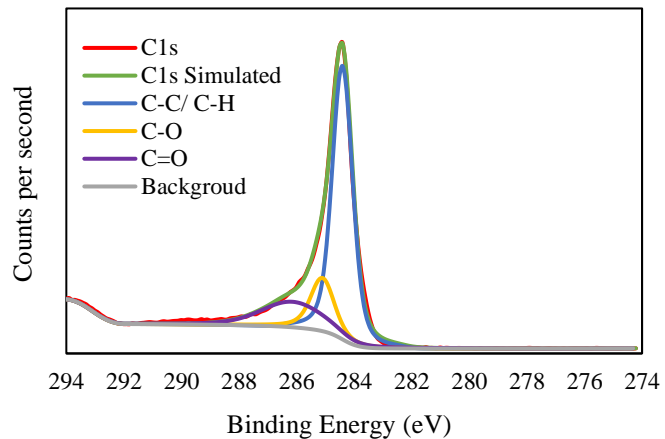
3.3.15 XPS test results

The XPS results of the TAC and CAC before and after Pb adsorption were analyzed to identify the effect of functional groups on coordination with heavy metals (Figure 3.19). As shown in Figure 3.19b, the XPS spectra of C 1s for TAC were divided to three deconvoluted peaks, with binding energies of 284.41 eV (C–C/C–H functionality) 285.10 eV (C–O) and 286.14 eV (C=O) (Liu et al. 2020; Tan et al. 2020; Wu et al. 2019). Three peaks were observed in the O 1s XPS spectra of TAC at 531.1 eV, 532.95 eV, and 533.28 eV, and correspond to (C–O), carbonyl (C=O), and carboxylic acids or lactone (O–C=O), respectively (Guo et al. 2018; Wang et al. 2020; Wu et al. 2019).

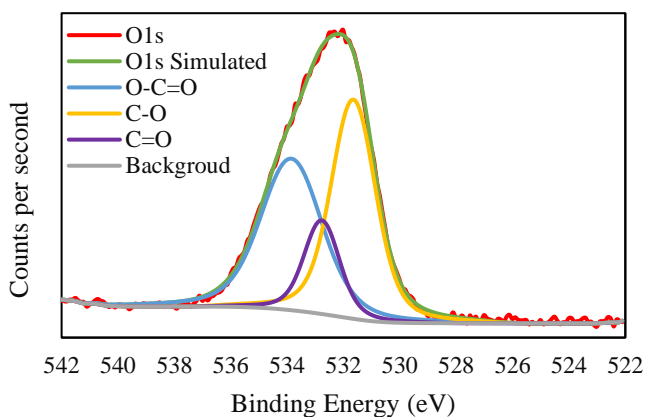
The disappearance and band shifting of some peaks assigned to oxygen functional groups were observed after loading Pb on the TAC. For instance, in C 1s spectrum of Pb loaded TAC, the group with binding energy of 286.14 eV (C=O) disappeared or shifted to a band with higher energy at 289.25 eV, which is representative of O–C=O groups (Jeon et al. 2020; Zhang et al. 2018). This increase in the binding energy may be due to the coordination of oxygen-Pb ions, in which the oxygen in the C=O group shares electrons with Pb, and thus the electron densities of adjacent carbons are reduced, causing an increase in binding energy (Zhang et al. 2019). Instances of band disappearance and shifting confirms the occurrence of coordination between functional groups and Pb ions (Tang et al. 2017). Additionally, after adsorption of Pb by TAC, a new peak at 139.31 eV corresponding to the Pb 4f group was formed in the XPS spectra of the Pb loaded TAC. This indicates that the Pb ion was successfully adsorbed on TAC.



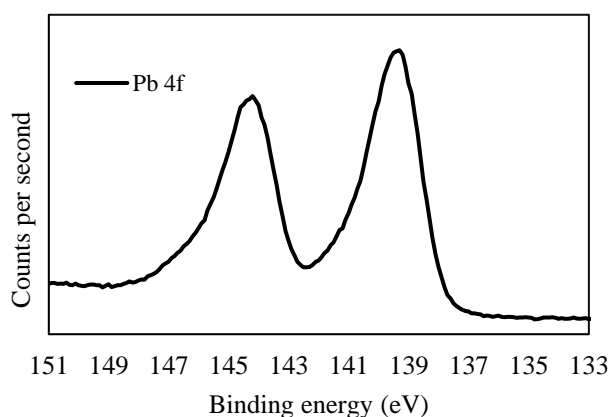
(a)



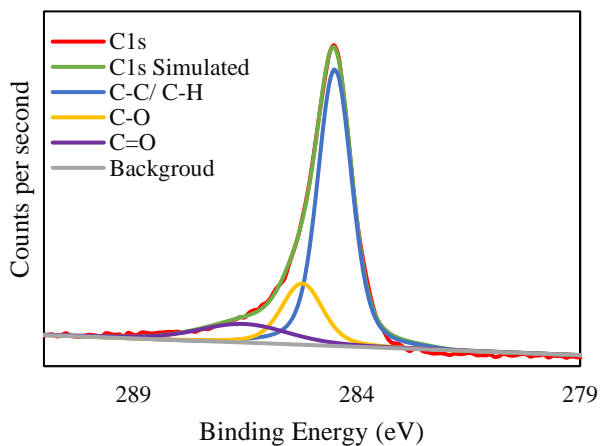
(b)



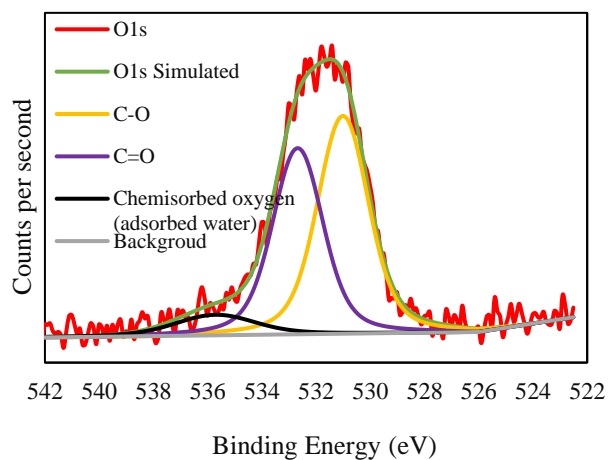
(c)



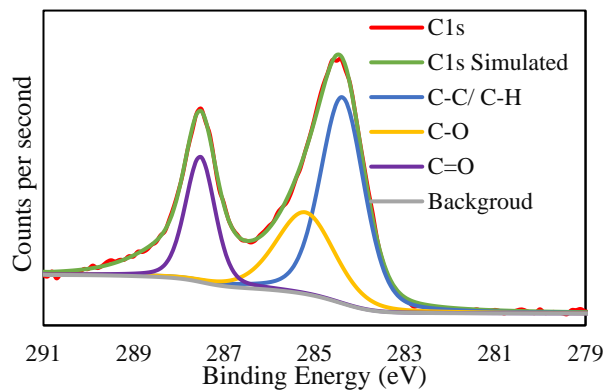
(d)



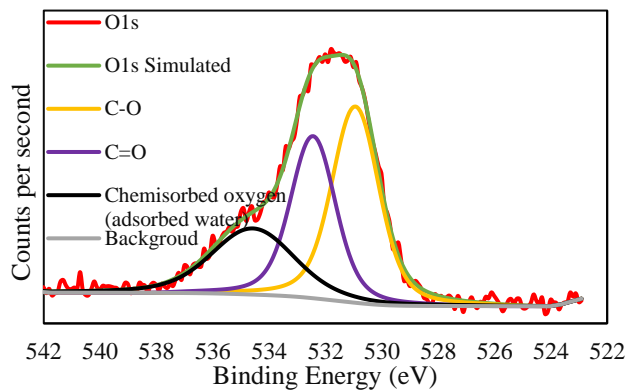
(e)



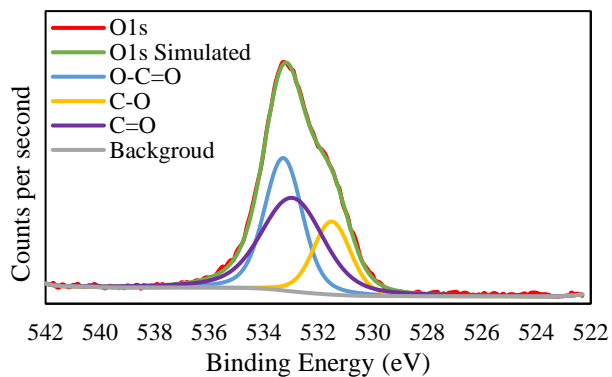
(f)



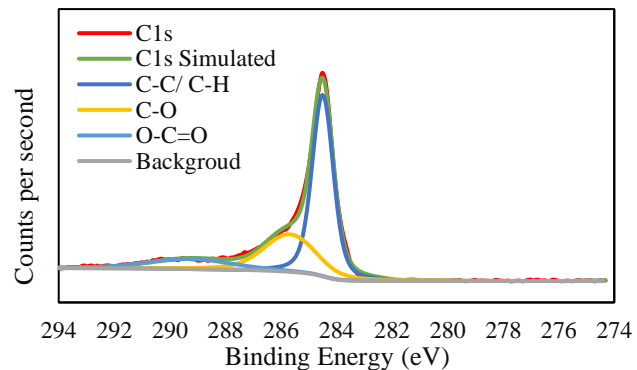
(g)



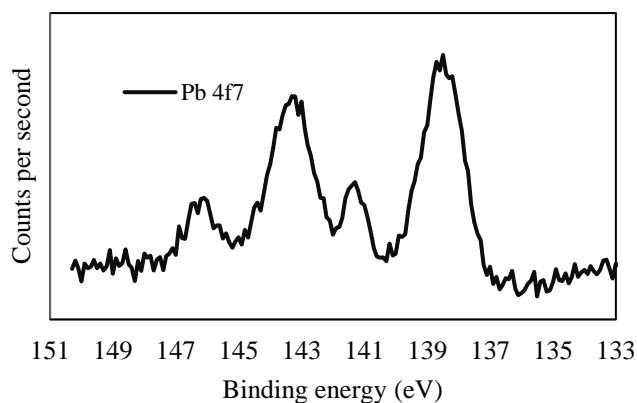
(h)



(k)



(l)



(m)

Fig. 3.19 XPS characterization of TAC and CAC samples (a): XPS survey spectra of TAC and CAC before and after adsorption Pb ion; (b) and (c): C1s and O1s XPS spectra of TAC before loading Pb ion; (d), (e) and (f) : C1s ,O1s and Pb 4f XPS spectra of TAC after loading Pb ion; (g) and (h): C1s and O1s XPS spectra of CAC before loading Pb ion; (k), (l) and (m) : C1s ,O1s and Pb 4f7 XPS spectra of CAC after loading Pb ion

The relative content of functional groups found on TAC and CAC (Figure 3.20) was determined using the XPS plots in combination with AVANTAGE 5.99 software. The content of the TAC functional groups was altered (decrease or increase) after adsorption of Pb. For example, for C 1s, the C–O content increased from 15.08 to 29.39%, whereas the C–C/C–H and C=O contents decreased from 65.86% and 19.06% to 58.39 and 0%, respectively. For the O 1s, the relative content of C=O decreased from 42.76 to 14.92%, while the content of C–O and O–C=O groups increased from 20.11 and 37.13% to 43.54 and 41.54%, respectively. After Pb ion adsorption by TAC, it was observed that the oxygen atom content in the C=O group decreased, while the content of C–O and O–C=O groups increased. This is ascribed to the formation of $\text{Pb}^{2+}\text{-O-C=O}$ or Pb-O groups on the surface of TAC after adsorption of Pb (Guo et al. 2018; Zhang et al. 2019).

High resolution of the C 1s spectra for CAC exhibited three peaks at approximately 284.49, 285.22 and 286.52 cm^{-1} , representing C–C/C–H, C–O, and C=O functional groups, respectively. Also O 1s spectrum for CAC exhibited three major peaks corresponding to C–O at 531.01 eV, C=O at 532.68 eV, and chemisorbed oxygen or water at 535.71 eV (Liu et al. 2008; Velo-Gala et al. 2014). Except for the peak at 535.71 eV, the deconvoluted peaks for raw CAC were similar to those for TAC. However, their relative contents, both before or after Pb loading, were different (see Figure 3.21). In relation to Figure 3.20, when one compares CAC with TAC, it is easy to see that more oxygen functional groups were consumed on the TAC surface during the adsorption of Pb ions. For instance, the relative content of C=O for O 1s of CAC and TAC was 42.34 and 42.76%, and decreased to 32.61 and 14.92%, respectively, after loading Pb on the adsorbent surface. This implies that C=O on the TAC surface was more readily consumed during the adsorption of Pb, which confirms that oxygen functional groups on the TAC surface are more involved during the adsorption of Pb ions.

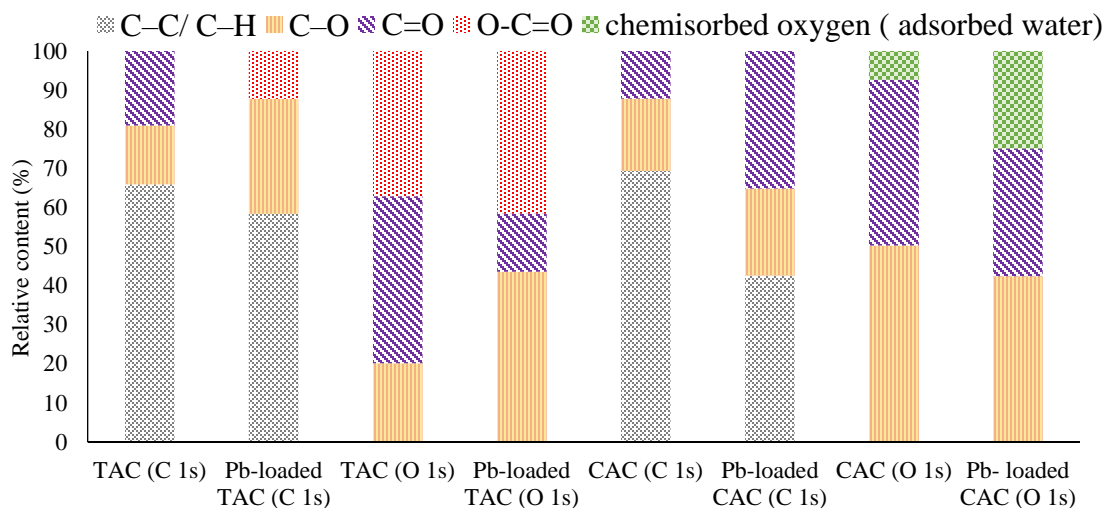


Fig. 3.20 Relative contents of oxygen functional groups for TAC and CAC samples before and after Pb ion adsorption

After sorption of Pb by TAC and CAC samples, the oxygen content increased (Table 3.15). This can be ascribed to the deprotonation of the oxygen functional groups on the adsorbent's surface, which led to ion exchange between Pb^{2+} and the H^+ contained in the oxygen functional groups (Kołodziejka et al. 2017). However, the relative increase of oxygen content for Pb loaded-TAC was higher than that for Pb loaded-CAC (2.39% comparing to 1.25%), indicating that more functional groups on the TAC surface were deprotonated and were able to undergo complexation with more Pb^{2+} ions.

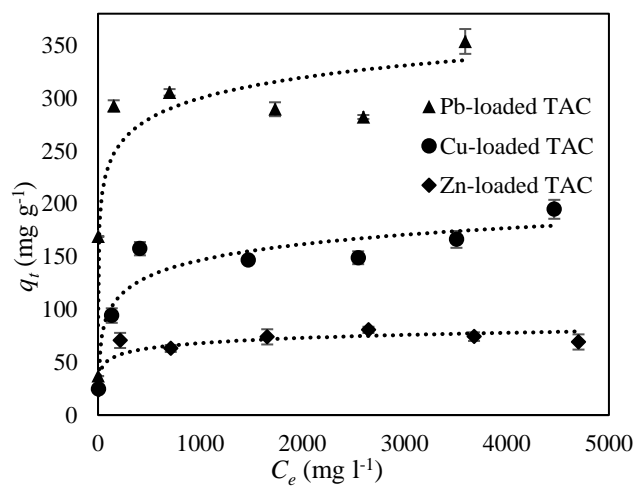
Table 3.15 XPS elemental composition of the TAC and CAC before and after Pb (II) adsorption

Adsorbent	C 1s (Atomic concentration %)	O 1s (Atomic concentration %)	Pb 4f (Atomic concentration %)
TAC	83.87	16.13	–
Pb-loaded TAC	77.88	18.52	3.60
CAC	90.99	9.01	–
Pb-loaded CAC	89.52	10.26	0.22

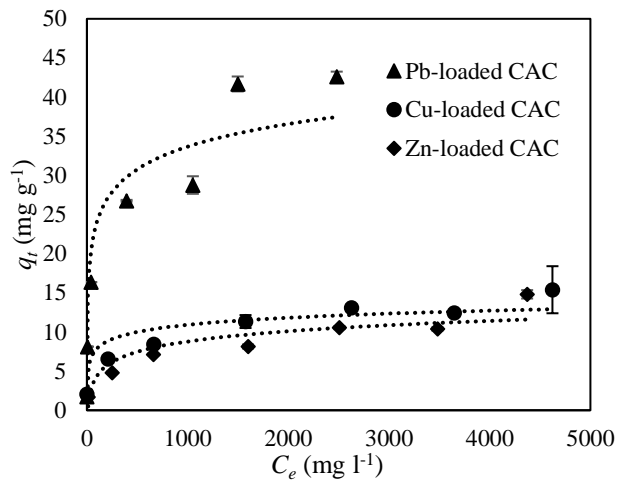
3.3.16 Single batch sorption of TAC and CAC

Figure 3.21 (a-b) shows adsorption curves for TAC and CAC as a function of equilibrium concentration versus adsorbed amount of heavy metals. For all three examined heavy metals, the adsorption capacity increased with increasing equilibrium concentration of metals. However, at higher concentrations, the adsorption rate reached a relatively constant value. This trend was also observed in previous studies with different adsorbents, such as zeolite (Kwon et al. 2019), cellulose beads (Qiao et al. 2020), and agricultural waste -derived activated carbon (Zhang et al. 2020).

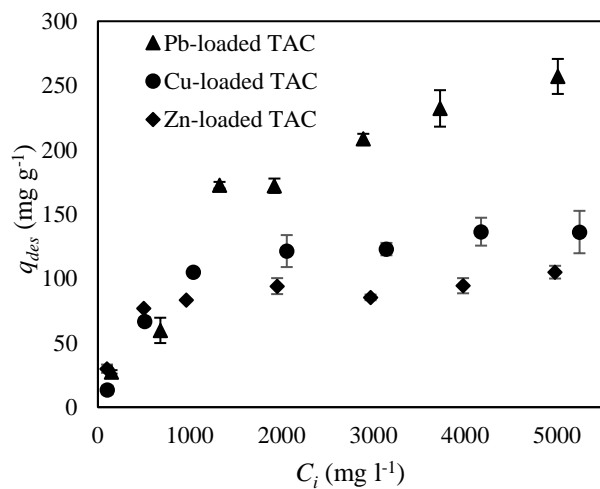
The experimental adsorption data for CAC and TAC samples were fit to the Langmuir, Freundlich, D-R, and Temkin adsorption isotherm models, and the model parameters are presented in Table 3.16. Comparison of the coefficients of determination (R^2) values for adsorption isotherm models of TAC shows that the Langmuir model fit the experimental data better than other three models. Whereas, for CAC the Freundlich model fit the data the best.



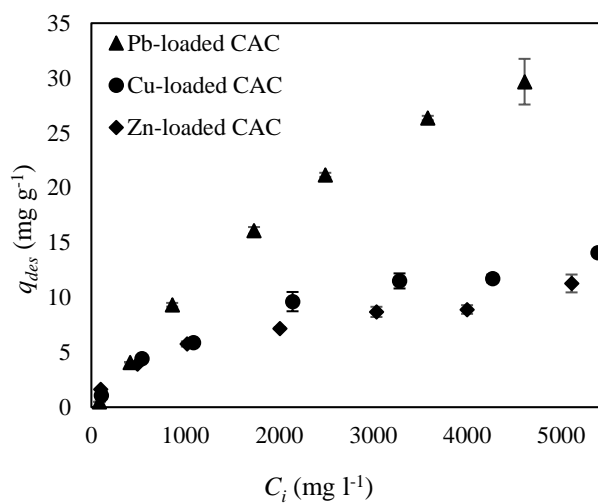
(a)



(b)



(c)



(d)

Fig. 3.21 (a-b) Heavy metals adsorption by TAC and CAC samples, (c-d) heavy metals adsorption from loaded TAC and CAC samples

Table 3.11 Langmuir, Freundlich, D-R, and Temkin isotherm parameters for Pb, Cu and Zn sorption by TAC and CAC samples

Isotherm model	TAC			CAC		
	Pb	Cu	Zn	Pb	Cu	Zn
Langmuir model						
q_{\max} (mg·g ⁻¹)	322.50	185.20	71.90	42.50	15.0	14.0
K_L (L·mg ⁻¹)	0.015	0.005	0.052	0.008	0.003	0.001
R^2	0.978	0.975	0.992	0.962	0.971	0.908
Freundlich model						
K_F (mg·g ⁻¹)	78.50	20.20	21.80	3.87	2.31	1.38
1/n	0.19	0.27	0.15	0.31	0.21	0.34
R^2	0.748	0.906	0.840	0.977	0.987	0.982
D-R model						
q_{\max} (mg·g ⁻¹)	286.90	148.10	71.80	23.90	10.80	8.80
E (kJ·mol ⁻¹)	1.30	0.267	0.353	2.23	1.58	0.10
R^2	0.960	0.903	0.968	0.751	0.824	0.755
Temkin model						
A (L·g ⁻¹)	41.57	0.809	15.08	3.17	4.16	0.102
b (kJ·mol ⁻¹)	0.087	0.113	0.350	0.593	1.89	1.30
R^2	0.911	0.911	0.831	0.891	0.858	0.840

For TAC, the maximum adsorption capacities estimated by the Langmuir isotherm were 322.5, 185.2 and 71.9 mg·g⁻¹ for lead, copper, and zinc, respectively. When converted to mass per surface area (q_{\max} /BET surface area), the calculated values are 3.9, 2.2 and 0.87 mg·m⁻² for lead, copper and zinc, respectively. For CAC, the maximum adsorption capacities were 42.5, 15.0, and 14.0 mg·g⁻¹ for lead, copper and zinc, respectively. Which correspond to mass per surface area values of 0.034, 0.012 and 0.011 mg·m⁻² for lead, copper, and zinc, respectively. As shown in Table 3.16, the estimated Freundlich K_F values for TAC were 78.5, 20.2, and 21.8 mg·g⁻¹ for lead, copper and zinc, respectively. While for CAC these values were 3.87, 2.31, and 1.38 mg·g⁻¹ for lead, copper

and zinc, respectively. Higher K_F values for TAC demonstrated that TAC has a higher uptake capacity for heavy metals compared to CAC.

Obtained R^2 values for D-R and Temkin models for TAC were higher than those for CAC, which shows these two models were fit better for TAC than CAC. For TAC, the maximum adsorption capacities estimated by the D-R model were 286.9, 148.1 and 71.8 $\text{mg}\cdot\text{g}^{-1}$ for lead, copper, and zinc, respectively. Whereas, for CAC these values were 23.9, 10.8, and 8.8 $\text{mg}\cdot\text{g}^{-1}$ for lead, copper and zinc, respectively. The obtained mean free energy values from D-R model for both TAC and CAC samples were lower than 8 $\text{kJ}\cdot\text{mol}^{-1}$, which indicates the sorption of metals on TAC and CAC sorbents happens by physisorption process (Wang and Guo 2020). Additionally, the Temkin adsorption isotherm, which presumes the chemisorption of adsorbate onto the sorbents, was poorly fit with adsorption data ($R^2 < 0.911$). This also supports that the adsorption process is controlled by physical process (Biswas et al. 2007). For both TAC and CAC sorbents, the Temkin constants (b) related to heat of sorption were all positive, which indicates the adsorption is an endothermic process (Inam et al. 2017).

It can be observed that for the three examined heavy metals (Pb, Cu, Zn), TAC displayed a higher adsorption capacity than CAC. Elevated adsorption capacities of TAC may be due to several reasons, including elevated nonspecific adsorption (electrostatic adsorption) capacity, and superior coordination with heavy metals as discussed in Sections 3.3.13, 3.3.14 and 3.3.15.

The adsorption of metals was associated with higher adsorption of Pb ions, where the adsorption sequence of the examined heavy metals was $\text{Pb(II)} > \text{Cu(II)} > \text{Zn(II)}$ for both TAC and CAC samples. The smaller size of the hydrated radius of the Pb ion (4.01 Å) compared to Cu (4.19 Å) and Zn (4.3), could be the reason for this order (Boostani et al. 2019).

Previous studies have documented the modification of waste tires as adsorbent materials. For instance, in a study by Nieto-Márquez et al. (2017), two adsorbents were prepared from waste tires by different activating agent/waste tire ratios for the removal of Pb^{2+} , Cr^{3+} and Cd^{2+} ions. Based on their results, the maximum adsorption capacities of the best adsorbent were 49.7, 29.4, and 10.4 $\text{mg}\cdot\text{g}^{-1}$ for Pb^{2+} , Cr^{3+} and Cd^{2+} , respectively. Gupta et al. (2013) produced a tire activated carbon

for the removal of chromium, and reported a maximum chromium adsorption capacity of 12.08 $\text{mg}\cdot\text{g}^{-1}$. Karmacharya et al. (2016) employed waste tire rubber for synthesizing activated carbon for the removal of Mn(II) and Cr(VI) from aqueous solutions. The authors obtained adsorption capacities of 3.04 and 14.45 $\text{mg}\cdot\text{g}^{-1}$ for Mn (II) and Cr(VI) ions, respectively. In the study by Mouzourakis et al. (2017), a maximum As(III) uptake capacity of 31 $\text{mg}\cdot\text{g}^{-1}$ was achieved by one novel pyrolytic-tire char (PyrC).

The maximum adsorption capacities of tire-derived activated carbons from previous studies were lower than those achieved by the present work. Moreover, compared to other adsorbent materials reported in the literature (Table 3.17), the produced TAC in the present study exhibited higher adsorption capacities. This can be a result of the different pyrolysis procedures and/or different chemical activation agent employed for the present study, which demonstrates the improvement of preparing activated carbon from waste tires for heavy metals removal, due to its relatively high adsorption capacity compared to previous studies.

Table 3.12 Adsorption capacities for different types of adsorbents reported in literature

Adsorbent	Pollutant	Maximum adsorption capacity (mg·g ⁻¹)	Reference
Zeolite	Pb	109.89	(Joseph et al., 2020)
	Zn	36.76	
	Cu	57.80	
NaOH modified fly ash	Pb	126.55	(Huang et al. 2020)
Cellulose nanofibers	Zn	73.90	(Li et al. 2019)
	Cu	102.90	
Cauliflower leaves biochar	Pb	177.82	(Ahmad et al. 2018)
	Cu	53.96	
Granular Activated Carbon	Cu	23.42	(Zheng et al. 2018)
β-cyclodextrin polymers	Pb	196.40	(He et al. 2017)
	Cu	164.40	
Carbon nanotube sheets	Pb	117.64	(Tofighy and Mohammadi 2011)
	Zn	74.62	
	Cu	64.90	
Coconut derived activated carbon	Pb	92.72	(Anirudhan and Sreekumari 2011)
	Cu	73.60	

3.3.17 Competitive sorption of TAC and CAC

Results from competitive adsorption experiments showed that the selectivity adsorption sequence of the examined heavy metals by TAC and CAC samples was in order of Pb(II) > Cu(II) > Zn(II), which is same to the sequence found by single adsorption condition experiments. However, as is clear from Figure 3.22 the obtained maximum adsorption capacities of the three ions under multi-metal condition were reduced compared to those under single adsorption phases. Under the multi-metal adsorption conditions, the maximum adsorption capacities of TAC for Pb, Cu, and Zn ions

were reduced by rates of 12.7, 14.6, and 38.9%, respectively. On the other hand, the reduction rates of maximum adsorption capacity for CAC were 14.3, 24.8, and 49.9% for Pb, Cu, and Zn ions, respectively. Among the three metals the percent reduction of the maximum adsorption capacity for Zn ion was the highest, while the Pb adsorption capacity showed the lowest percent reduction. This can be attributed to higher adsorption interference of Pb when compared to Cu and Zn, which was obtained from the single adsorption experiments. These results were in agreement with the study performed by Park et al. (2016) which demonstrated that the adsorption capacity of sorbents reduce under competitive adsorption conditions.

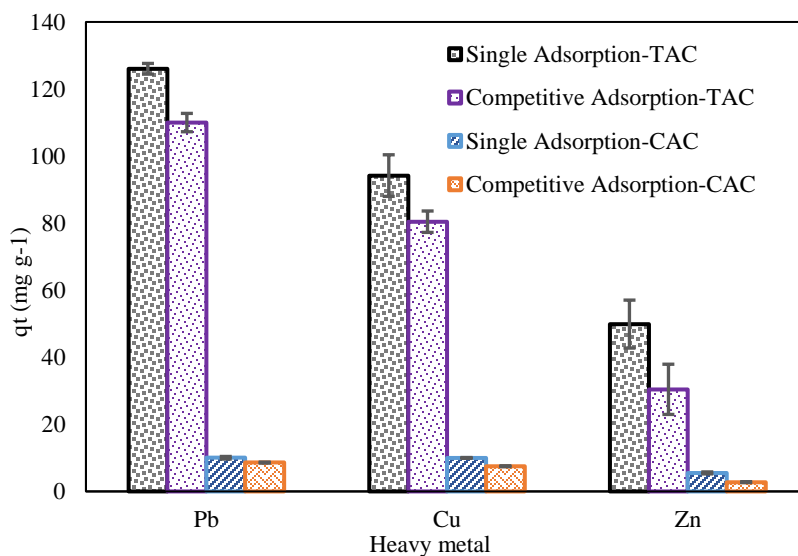


Fig. 3.22 Comparison of the maximum adsorption capacity of the heavy metals in competitive and single adsorption isotherms for TAC and CAC samples (initial concentration of ions: 500 mg·L⁻¹)

3.3.18 Kinetic sorption results of TAC and CAC

As is obvious from the Figure 3.23 (a-b) as the adsorption time increased, the adsorption capacity was increased until the adsorption reached to the equilibrium phase. However, the adsorbents sites were almost occupied with the metal ions at the early hours of contacting time. The TAC sample was saturated faster than CAC, and its equilibrium sorption was almost achieved within 6 h, while the sorption equilibrium of the CAC was reached after 24 h. Also, the initial adsorption rate (v_0)

of heavy metals by TAC and CAC sorbents (Table 3.18), demonstrated that TAC had faster adsorption rate when compared to CAC. Among three metals, Pb showed more rapid adsorption, which can be one reason for its higher adsorption interference to Cu and Zn (Kołodzyńska et al. 2017).

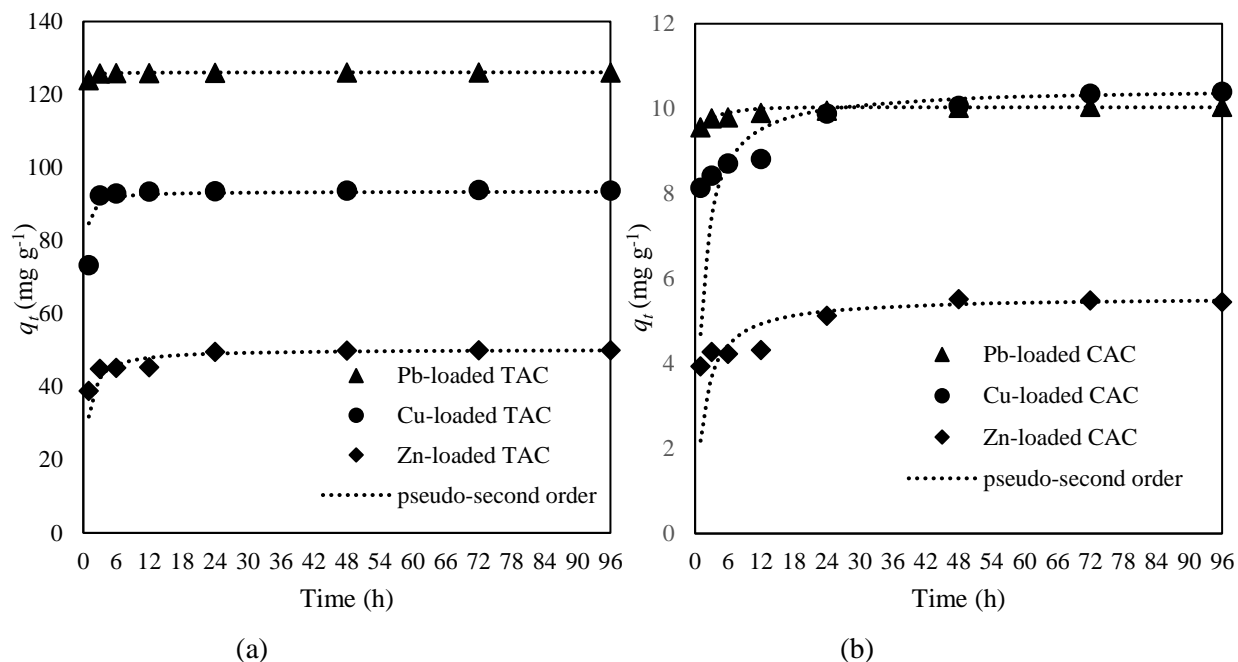


Fig. 3.23 (a-b) Kinetics of heavy metals adsorption by TAC and CAC samples

The analyzed data with pseudo first-order and pseudo second-order models (Table 3.18), showed that the pseudo second-order model was the best fit for adsorption data with the correlation coefficients greater than 0.99. Additionally, the adsorption capacities obtained from pseudo second-order model were well matched with the experimental data (Figure 3.23). Thus, based on pseudo second-order model presumption it can be concluded that the chemisorption is the main adsorption mechanism for heavy metals sorption by TAC and CAC samples (Kołodzyńska et al. 2017).

Table 3.13 Pseudo first-order and pseudo second-order parameters for Pb, Cu and Zn sorption by TAC and CAC samples

Adsorbent	ion	pseudo first-order		pseudo second-order			
		K_1 (min ⁻¹)	R^2	K_2 (g·mg ⁻¹ ·min ⁻¹)	q_e (mg·g ⁻¹)	v_0^a	R^2
TAC	Pb	0.00069	0.748	0.010	126.10	169.49	1
	Cu	0.00069	0.605	0.0017	93.45	15.12	1
	Zn	0.00092	0.889	0.0057	50.25	1.44	0.999
CAC	Pb	0.00069	0.954	0.010	10.77	1.15	1
	Cu	0.00092	0.962	0.0012	10.49	0.14	1
	Zn	0.00069	0.861	0.0019	5.57	0.059	0.999

^a v_0 (mg·g⁻¹·min⁻¹) is the initial adsorption rate, $v_0=k_2q_e^2$.

The intra-particle diffusion model was fit to the adsorption data to describe the adsorption steps of metal ions. As shown in Figure 3.24 and Table 3.19, the adsorption curves exhibited the multi-linear plots with two steps. The primary linear step with sharper slope is related to external diffusion with faster mass transfer through the boundary layer, and the second linear portion with lower slope is due to the internal diffusion which shows the slow rate of diffusion inside the micropores of sorbents. For all adsorption cases the intercept failed to pass through the origin which can also be attributed to different rate of mass transfer in the primary and secondary step of adsorption, and presence of an initial boundary layer resistance (Pan et al. 2020)

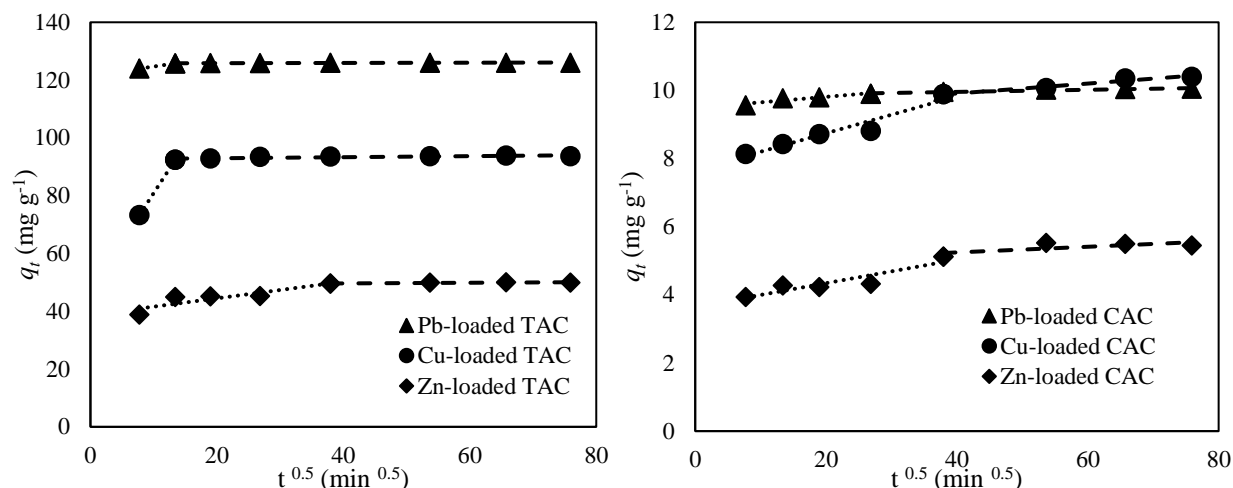


Fig. 3.8 The piecewise fitting curves of heavy metals adsorption kinetics of TAC and CAC by the intra-particle diffusion model

Table 3.19 Fitting parameters of the intra-particle diffusion model for heavy metal adsorption on TAC and CAC

Adsorbent	ion	Intra-particle diffusion model parameters					
		K_{p1}	C_1	R^2	K_{p2}	C_2	R^2
TAC	Pb	0.318	121.50	1	0.0042	125.76	0.865
	Cu	3.36	47.20	1	0.0182	92.58	0.705
	Zn	0.288	38.70	0.792	0.0111	49.19	0.798
CAC	Pb	0.0162	9.48	0.881	0.0031	9.83	0.920
	Cu	0.0543	7.65	0.929	0.0145	9.33	0.956
	Zn	0.0345	3.65	0.843	0.0083	4.91	0.544

Note: k_p ($\text{mg}\cdot\text{g}^{-1}\cdot\text{min}^{-0.5}$) is the intraparticle diffusion rate constant, and C is constant

3.3.20 Chemical stability of TAC

The leaching test results of TAC for pH values ranging from 1.5 – 9 are given in Table 3.20. Among the detected heavy metals, Zn and Cu ions were detected at both acidic and alkaline conditions, and their leaching levels continuously increased with decreasing pH. The leaching levels of Zn ($361.4 \text{ mg}\cdot\text{L}^{-1}$) and Cu ($5.091 \text{ mg}\cdot\text{L}^{-1}$) for the highly acidic condition (pH 1.5) were

markedly higher than the maximum contaminant level (MCL) regulated by the US EPA, as shown in Table 3.20 (EPA 2009). However, the detected levels for the other examined pH values were lower than the US EPA MCL regulation. The highly leachable amounts of Zn from TAC can be ascribed to zinc oxide, which is the main component of waste tire, and remains as a residual after activation of waste tire (Wik and Dave 2009). The detected levels of Pb ions at pH values of 1.5 and 4 were 0.403 and 0.066 mg·L⁻¹, respectively. These values were higher than the US EPA MCL regulation, while for pH values of 7 and 9 there were no detectable Pb ions at the end of the leaching test. Arsenic (As) was only detected at a pH of 1.5, with a concentration of 0.00087 mg·L⁻¹, which was much lower than the US EPA MCL regulation for drinking water. For all other examined pH values, the arsenic and cadmium were not detected at the end of the leaching tests.

Table 3.20 Released metals from TAC at different pH values

Ion of interest	Concentration (mg·L ⁻¹) in solution for given pH value				MCL (mg·L ⁻¹) (EPA, 2009)
	1.5	4	7	9	
Zn	361.40	0.606	0.481	0.222	5.0
Cu	5.091	0.155	0.077	0.062	1.3
Pb	0.403	0.066	ND	ND	0.015
As	0.00087	ND	ND	ND	0.010
Cd	ND	ND	ND	ND	0.005

NOTE: ND, not detected; MCL, maximum contaminant level requirement for drinking water

In addition, SEM EDS analysis (Table 3.13) for TAC and CAC were performed and results were used to evaluate the presence of other toxic heavy metals in the adsorbents. The results showed that the main components of TAC were oxygen and carbon, while the relative content of other metals was less than 5% of its total weight. According to these results, using TAC as an adsorbent material in the field is environmentally safe under neutral and alkaline conditions. Use

of TAC at highly acidic conditions (pH 1.5), although highly rare in nature, should be avoided as much as possible.

3.3.21 Desorption and reusability test of TAC and CAC

Figure 3.21 (c-d) shows the desorbed amounts of Pb, Cu, and Zn as a function of their initial concentrations for both TAC and CAC. The metal ion desorption increased with an increase in the initial concentration of ions for each of the examined heavy metals. That is, the average desorption rates (Table 3.21) for Pb, Cu, and Zn from TAC were 64.5, 72.7 and 125.6%, respectively. Additionally, the desorption efficiency of metal-loaded CAC was 57.5, 73.4 and 84.4%, for Pb, Cu, and Zn, respectively. High deposition rates of Zn from TAC is due to the presence of zinc oxide in the waste tire compositions, which leaches at highly acidic condition (refer to section 3.3.20).

Table 3.21 Desorption rate from ion loaded TAC and CAC samples

Adsorbent	Ion	Desorption (%)
TAC	Pb	64.5
	Cu	72.7
	Zn	125.6
CAC	Pb	57.5
	Cu	73.4
	Zn	84.4

The reusability results (Figure 3.25) showed that after three adsorption-desorption cycles the adsorption capacities of both TAC and CAC sorbents were reduced as compared to their initial maximum adsorption capacities. This can be due to poor recovery of loaded ions during desorption process, which decreases the available active adsorption sites on the sorbents surface. Because of lower recovery of Pb ion as compared to Cu and Zn ions, this reduction was more significant for Pb ion in both TAC and CAC samples.

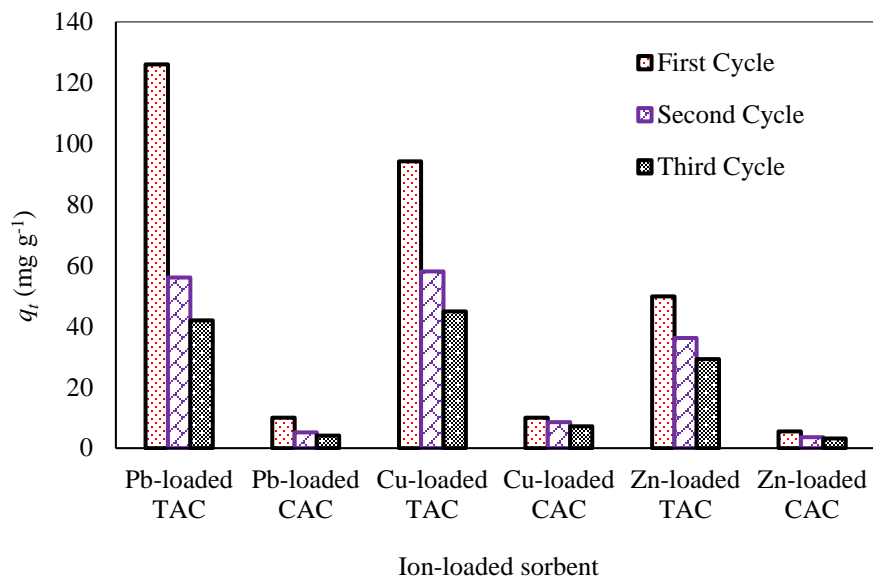


Fig. 3.9 TAC and CAC adsorption capacities for heavy metals after three successive adsorption-desorption cycles

It was revealed that the 0.01M HCl was not an efficient eluent for the recovery of ions, and regeneration of adsorbents was not done successfully. However, after three successive adsorption-desorption cycles, the TAC and CAC samples retained almost half of their initial adsorption capacities (especially for Cu and Zn ions), which confirms that both the TAC and CAC have potential for renewal and subsequent reuse as adsorbent materials.

The results from other studies (Kavand et al. 2020; Kołodyńska et al. 2017) showed better ion recoveries from exhausted activated carbons, which can be attributed to the use of eluents with higher concentrations. Thus, for more efficient recovery of ions and successful sorbents regeneration, further adsorption-desorption studies conducted with eluents with higher concentrations is recommended.

3.3.22 Possible adsorption mechanisms involved for sorption heavy metals by TAC and CAC

Isotherm and kinetics adsorption tests indicated that ion adsorption on TAC and CAC could be the result of both physical and chemical adsorption mechanisms. In particular, the interaction between

ions with adsorbents was accomplished through: (1) physical sorption, (2) ion exchange, (3) electrostatic interaction, and (4) coordination interaction through complexation with oxygen functional groups and interaction with aromatic π - electrons. The higher BET surface area in combination with higher CEC value suggests that physical sorption and ion exchange are the main adsorption mechanisms for CAC. On the other hand, while the physical sorption and ion exchange were also involved in the adsorption of ions by TAC, based on the XPS, FT-IR, and zeta potential analysis, the more predominant mechanisms for adsorption of heavy metals by TAC were electrostatic attraction and surface coordination. Therefore, though CAC had a much higher BET surface area with higher cation exchange capacity, combination of these four above-mentioned sorption mechanisms for TAC were more influential, and as a result the adsorption capacity of TAC was increased compared to the CAC (Figure 3.26).

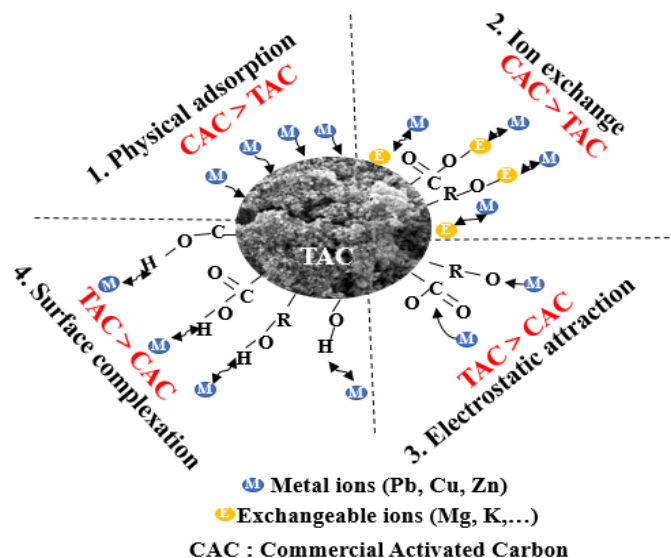


Fig. 3.10 Comparison of TAC and CAC for their dominant sorption mechanism for heavy metals

3.4 Summary

In this chapter, soil- pulverized waste tire (S-PWT) mixtures have been evaluated as adsorptive fill materials. Moreover, tire- derived activated carbon (TAC) and commercial activated carbon

(CAC) were compared in term of their adsorption/desorption capacities for select heavy metals. Key findings from this chapter are as follows:

1) The various S–PWT mixtures showed high sorption capacities towards BTEX, with adsorption of BTEX components in the following order: xylene > ethylbenzene > toluene > benzene. Among the evaluated mixtures, pure PWT displayed the highest removal rate for BTEX, with the removal levels for xylene, ethylbenzene, toluene and benzene at 96, 93, 83 and 78%, respectively. The equilibrium adsorption isotherm of the BTEX component onto the S–PWT media was well described by the Langmuir and Freundlich models, although it was found that the Freundlich model fitted the experimental results better.

2) The experimental results indicated that PWT material is an effective adsorbent for the removal of Pb and Cu from aqueous solutions. In particular, the S–PWT5 mixture showed the highest removal rate among the various mixtures investigated, with removal rates of 62.8 and 37.7% for Pb and Cu, respectively. These results also revealed that the PWT was more effective for the adsorption of BTEX components rather than for Pb and Cu ions.

3) Apart from the highly acidic condition (pH 1), the leaching behavior of selected inorganic constituents in PWT showed that the release of metals was below the detection limit. The inorganics leached more under acidic conditions, while zinc was the most leachable metal from pulverized tire. Based on these findings, the neutral and alkaline pH conditions are preferred for reuse applications of PWT material in the field, while the (highly) acidic condition should be avoided as much as possible.

4) Adding PWT to the soil increases the optimum moisture content for compaction and decreases the achievable maximum dry unit weight.

5) The direct shear test results showed that the shear behavior of the standard Proctor-compacted S–PWT mixtures became more ductile as the PWT content increased. The effective friction angle decreased modestly in value from 39.9° to 34.9° for PWT content increasing from 5 to 25 wt%. That is, the mobilized friction angle values are similar to those of dense sand, indicating that these compacted soil–PWT mixtures are suitable for various engineering fill applications.

6) The adsorption results revealed that TAC is a more effective sorbent for heavy metal removal from aqueous solutions than CAC. The maximum adsorption capacities of TAC were found to be 322.5, 185.2 and 71.9 $\text{mg}\cdot\text{g}^{-1}$ for Pb, Cu, and Zn ions, respectively. These values were higher than the results obtained for CAC. The resulting adsorption capacities for metal ions of both TAC and CAC were in the following order: $\text{Pb(II)} > \text{Cu(II)} > \text{Zn(II)}$.

7) The kinetic sorption results showed that TAC had faster adsorption rate compared to CAC; where the equilibrium times for the TAC and CAC samples were within 6 and 24 h, respectively. Moreover, the pseudo second-order model was fit to the experimental data better than the pseudo first-order and the intra-particle diffusion kinetic models.

8) For both TAC and CAC sorbents, the maximum adsorption capacities of the three ions under competitive condition were reduced compared to those under single sorption. Moreover, the sorption of Zn ion was more affected in multi-metal condition, as it experienced the most reduction in adsorption capacity when compared to that of Pb and Cu metals.

9) The leaching of inorganics from the TAC surface was increased by decreasing the pH value. Zinc was the most leachable metal, with a concentration of $361.4 \text{ mg}\cdot\text{L}^{-1}$ in an acidic environment (pH 1.5). Except for those in highly acidic conditions (pH 1.5), the metals released from TAC were below the MCL given by the US EPA. Consequently, the application of TAC in neutral and alkaline conditions is safe; however, the use of TAC in highly acidic conditions should be considered cautiously.

10) The loaded ions on TAC and CAC surfaces could not be completely recovered using 0.01M HCl, and after three successive adsorption-desorption cycles, the maximum adsorption capacities of both TAC and CAC were reduced to approximately half of their initial values.

11) N_2 adsorption-desorption showed that CAC has a much higher BET surface area with higher cumulative pore volume, which indicate the CAC has an increased physical adsorption capacity for heavy metals in comparison to TAC.

12) The higher CEC values for CAC indicated cation exchange was the predominant mechanism for the adsorption of heavy metals by CAC. The low CEC value for TAC indicated that while ion exchange could also contribute to the adsorption of the metals by TAC, it is not the predominant mechanism for adsorption by TAC. Analysis of the results for the FT-IR, XPS, and zeta potential analyses helped to elucidate the more predominant mechanisms for adsorption of heavy metals by TAC, which were found to be electrostatic attraction and surface complexation. It was found that electrostatic attraction and surface complexation can also contribute to heavy metal adsorption by CAC but to a lesser extent than ion exchange.

Based on the above results, it is recognized that the S–PWT mixture has adsorption potential toward organic/inorganic contaminants, while simultaneously providing adequate shear resistance and hence bearing capacity as fill materials from the geotechnical point of view. These attributes could allow the use of these S–PWT mixtures as efficient adsorptive fill materials for preventing the spread of ground contaminants in industrial areas. Based on the experiments, for satisfying both geotechnical and environmental properties of Soil/Tire mixture, the mixing ratio less than 15% is recommended. Furthermore, tire-derived activated carbon exhibited better performance in adsorbing heavy metals when compared to the commercial activated carbon used in this study. It can be concluded that tire-derived activated carbon has strong potential as an economical alternative adsorbent material for heavy metal removal, which can also help to decrease waste tire disposal problems. In addition, from an environmental perspective, using PWT and TAC in engineering fields could solve their disposal problem while also avoiding the usage of other most expensive materials.

Chapter 4. PFAS removal from contaminated subsurface

4.1 Introduction

4.1.1 Background

Per- and poly-fluoroalkyl substances (PFASs) are classified as a persistent man-made organofluorine compounds with fully or partially substituted hydrogen atoms by fluorine on the carbon skeleton (Park et al. 2020). Because of their unique physico-chemical properties (e.g. resistant to grease, oil, water and heat) they have been widely used as surfactants in many industrial and commercial applications such as cosmetics, lubricants, paints, fire-fighting foams, non-stick cookware, and food contact papers (Ateia et al. 2019). It has been reported that more than 4000 types of PFAS have been identified for various consumption (OECD 2018). While such outstanding attributes make PFASs as valuable compounds, their widespread application and environmental persistence, have resulted in their ubiquitous discharge in the environment with posing a consequent threat to ecosystems and human health (Ahmed et al. 2020; Ateia et al. 2019; Li et al. 2020).

Furthermore, PFASs have demonstrated high bioaccumulation tendencies in plants, invertebrates, birds, fish, and mammals, which lead to human exposure and health risk (Figure 4.1). Studies have indicated that PFASs can cause several adverse health outcomes in humans such as cancer, thyroid hormone disruption, immunotoxicity, hepatotoxicity, and neurodevelopmental problems (Eichler and Little 2020).

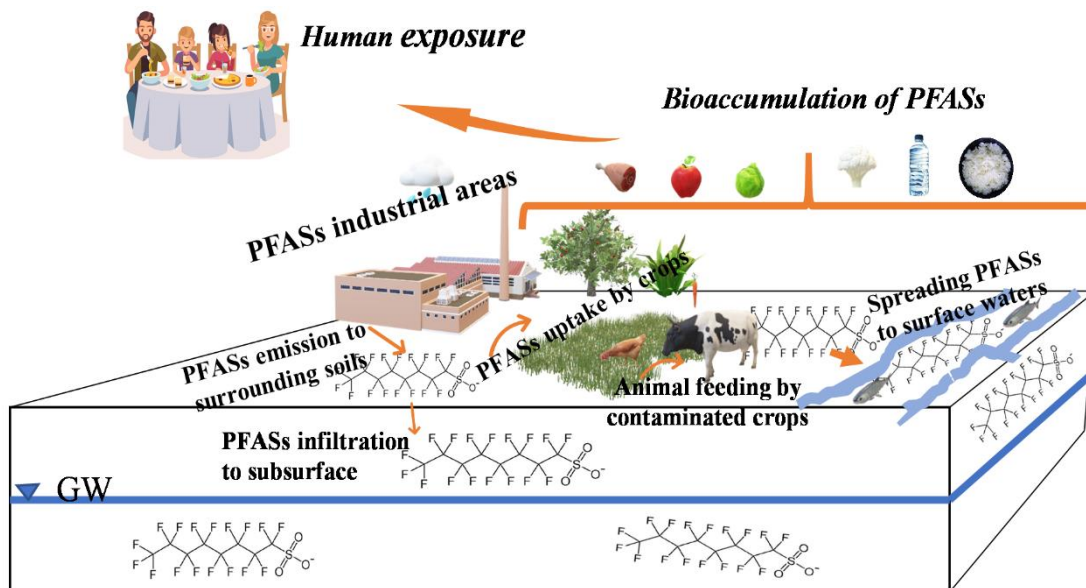


Fig. 4.1 Human exposure to PFASs contaminants

South Korea is a developed country which hosts numerous world-class industries, and they frequently generate substantial quantities of PFASs contaminants. The widespread usage of PFASs compounds in Korea has led to detecting them in different environmental media including soil, groundwater, and sediments in many industrial, agricultural, rivers/lakes, and coastal areas. The nationwide PFASs distribution in Korea has been proven by several studies as mentioned below.

Analyzing the collected soil samples from 243 different agricultural sites adjacent to waste water treatment plants and industrial areas belonging to 81 cities and 5 provinces (Gyeonggi, Gangwon, Chungcheong, Geongsang, and Jeolla) in Korea has demonstrated these areas are contaminated with PFASs pollutants. The PFOA and PFOS with concentrations of <0.05 - $1.573 \mu\text{g.Kg}^{-1}$ soil, and <0.05 - $0.741 \mu\text{g.Kg}^{-1}$ soil were detected in these areas as the main PFASs contaminants (Choi et al. 2017).

The PFASs compounds have been widely distributed in the Asan lake (one of the largest reclaimed estuarine lakes in Korea) with reported concentration of 17.7 - 467ng.L^{-1} in water, 0.04 - 15.0ng.g^{-1} dry weight (dw) in sediment, and 0 - 12.9ng.g^{-1} dw in soils (Figure 4.2) (Lee et al. 2020).

Monitoring the soils in Korea has discovered that PFASs are distributed over industrial, urban, and agricultural soils throughout the Korea (Figure 4.3) (Kim et al. 2014).

The compiled data from more than 2500 PFASs contaminated sites distributed throughout the world (including the Korea) has demonstrated that PFAS are present in soils across the globe, and indicate that soil is a significant reservoir for PFASs. Also, the concentrations reported for PFAS-contaminated sites were generally orders-of-magnitude greater than advisory levels (Brusseau et al. 2020).

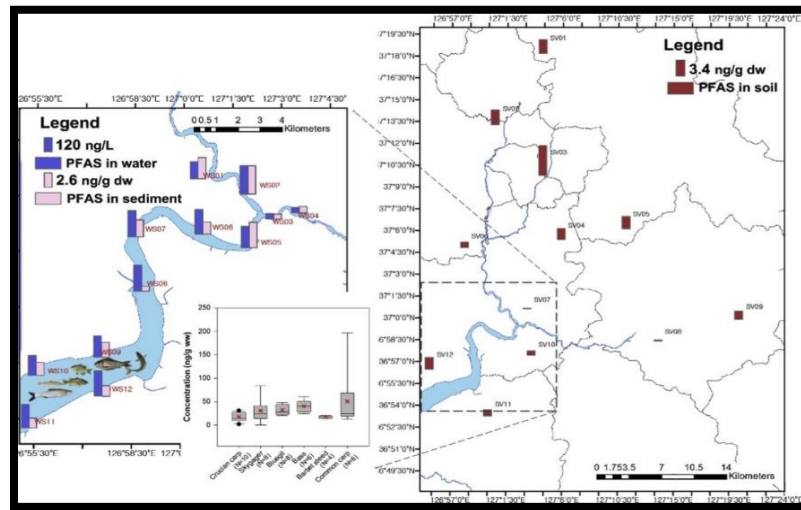


Fig. 4.2 PFASs concentration and distribution in soil, water, and sediment near Asan lake

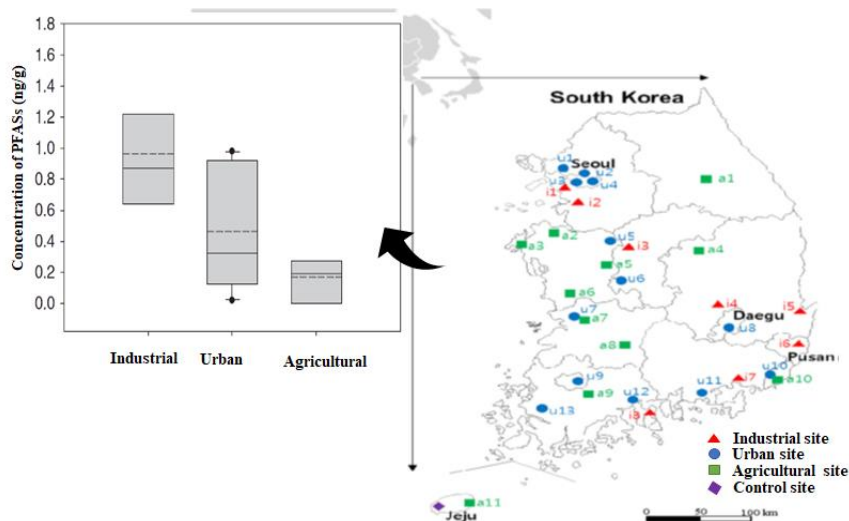


Fig. 4.3 PFASs concentration and distribution in industrial, urban, and agricultural soils throughout the Korea

Also, the PFASs were detected in human's blood from the general population of Korea (Figure 4.4), whereas the level of PFOS (one kind of PFAS) in Koreans has been reported as one of the highest levels among the Asian countries (Harada et al. 2010; Seo et al. 2018).

In addition, Table 4.1 shows brief summary about some studies with their important findings regarding the PFAS distribution in Korea.

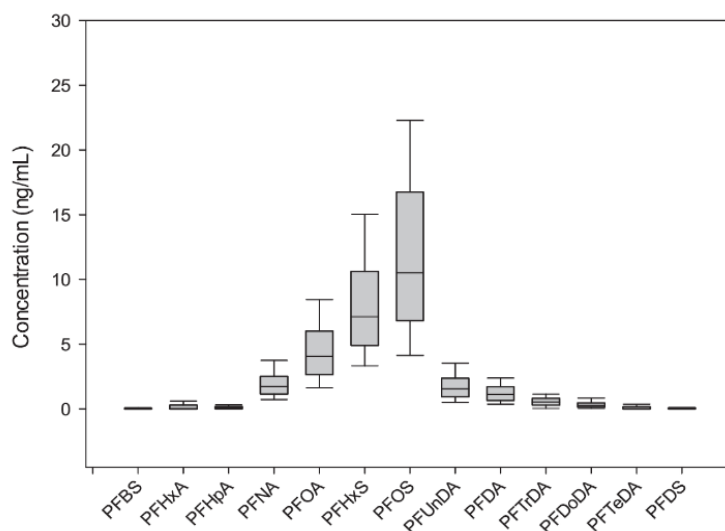


Fig. 4.4 Concentration and distribution of PFASs in the human's blood (n=786) from the general Korean population (Seo et al., 2018)

Table 4.1 Previous research about PFAS distribution in Korea

Sample	Location	Most detected PFASs	Detected concentrations	Remarks	study
Groundwater, Tap water, River water	Nakdong River (Gumi, Daegu, Busan)	PFOA, PFHxA, PFPeA, PFHxS	14.1 – 58.9 ng/L	1. Detection frequency and concentration of PFCA were higher than PFSA. 2. Concentration of PFAS in groundwater was lower than river and tap water. 3. The mean concentrations of PFAS decreased in the order of urban area (17.3 ng/L) > industrial area (13.6 ng/L) > agricultural area (9.2 ng/L)	(Yong et al. 2021)
Paddy soil Void water Brown Rice	Paddy fields located near different complexes	PFOA, PFOS, PFBS, PFHxA, PFBA, PFPeA,		1. The PFCA compounds were the predominant species in all matrices 2. The areas located near textile complex were more contaminated by PFASs	(Kim et al. 2019)
Tap Water	Major metropolitan cities in Korea including Seoul, Incheon, Suwon, Daejeon, Gwangju, Daegu, Andong and Busan	PFHxS, PFPeA, PFHxA, PFOA	2.073- 2.97 ng/L	1. Among eight cities, Daegu and Busan showed the highest PFAS levels in tap water, where these cities are located in the Nakdong river basin. 2. Comparing to past five year, the average PFAS concentrations have noticeably increased, by approximately 2–50 fold. 3. The average human exposure via tap water consumption for PFASs was estimated as 46.8ng/person/day.	(Park et al. 2018)
Sea water, Sediment, Bivalve samples	Coastal areas in Korea	PFOA, PFOS, PFBS, PFHxS, PFHxA, PFUnDA, PFTTrDA, PFTeDA		1. PFCAs and PFSAs were detected as most widespread PFASs. 2. For precursors and alternatives of PFASs in sediment, 8:2 FTS and F-53B were detectable, ranging from <0.005 to 0.30 (mean: 0.03) ng/g dry wt and from <0.002 to 0.013 ng/g dry wt, respectively	(Lee et al. 2020)
Wastewater, Sludge	Five major industrial sectors (chemicals, electronics, metals, paper, and textiles)	PFOA, PFOS	The total discharge loads of 11 PFAAs for the five industries were 0.146 ton/yr	1. The textile industry had the highest discharge load with 0.055 ton/yr (PFOA: 0.039 ton/yr, PFOS: 0.010 ton/yr).	(Kim et al. 2016)
Air, Water, Sediment, Soil, Fish	Asan Lake	PFOA, PFPeA, PFOS	0- 467 ng/L	1. The most frequently detected PFAS were perfluorooctanoic acid (PFOA) in air and soils, perfluoropentanoic acid (PFPeA) in water, and perfluorooctane sulfonate (PFOS) in sediment and fish.	(Lee et al. 2020)
Soil	Industrial areas belonging to 81 cities and 5 provinces (Gyeonggi, Gangwon, Chungcheong, Geongsang, and Jeolla)	PFOA, PFOS	0.05- 1.573 µg/Kg soil		(Choi et al. 2017)

The above-mentioned statements implying that PFASs contaminants have been widely distributed in the environmental nature of Korea. Furthermore, according to previous studies, the most detected PFAS contaminants in Korea are PFOA, PFOS for long-chain PFAS and PFBA, PFBS for short-chain PFAS. The basic properties for these PFAS substance are presented in Table 4.2.

Table 4.2 Most detected PFAS contaminants in Korea with their basic properties

Category	PFAS name	Acronym	Chain length	Log Kow	Molecular Weight (g.mol ⁻¹)	Density (g. cm ⁻³)	Formula
Long-chain	Perfluorooctanic acid	PFOA	8	4.59	414.07	1.8	C ₈ HF ₁₅ O ₂
	Perfluorooctane sulfonic acid	PFOS	8	5.26	538.22	1.85	C ₈ HF ₁₇ SO ₃
Short-chain	Perfluorobutanic acid	PFBA	4	2.32	214.04	1.65	C ₄ HF ₇ O ₂
	Perfluorobutane sulfonic acid	PFBS	4	2.73	338.19	1.82	C ₄ HF ₉ SO ₃

In other developed countries (e.g. USA, Australia, Sweden, Norway), the threat of PFASs to human exposure has been already exposed to people, and the removal of PFASs contaminants from both soil and groundwater has been started in the lab and field scales (Bolan et al. 2021; Bräunig et al. 2017; Söregård et al. 2021) . However, based on our knowledge, although the PFASs compounds have been widely distributed in Korea, the removal of PFASs contaminants from the soil has not been investigated yet.

Therefore, finding a proper remediation technique for cleaning-up the PFASs contaminated soils and groundwater should be considered as one of the most urgent actions in Korea.

4.1.2 PFAS removal difficulties and main objectives of present chapter

Because of high thermal/chemical stability, and strong carbon-fluorine bond dissociation energy of PFOA, most of the conventional remediation techniques such as chemical oxidation, biological degradation, thermal treatment, and reduction are suffering from low PFAS substances removal efficiency (Mahinroosta and Senevirathna 2020; Ross et al. 2018). By contrast, adsorption as a cost-effectiveness, simple, and renewable technology is considering as one the most effective physicochemical approach for encountering the contamination problems caused by PFAS contaminants (Zhang et al. 2019).

Numerous sorbents including the granular/powder activated carbon (Murray et al. 2019; Saeidi et al. 2020), anion-exchange resins (Dixit et al. 2021), mineral materials (Yan et al. 2020), biochars (Askeland et al. 2020), biomaterials (Zhang et al. 2019) , and polymer based synthesized sorbents (Klemes et al. 2019), have been used for PFAS substance sorption (as already discussed in section 1.2.3). Although, some of these sorbents showed good removal efficiency, the prohibitory prices and complicated synthesis procedures of these sorbents restrict their uses for field-scale applications (Vu and Wu 2020). Consequently, developing other affordable and efficient alternative sorbents from agricultural and industrial wastes is vital for PFAS removal.

Chitosan is a cationic biopolymer which is producing through the deacetylation of extracted chitin from crustacean's shell and cell walls of fungi (Crini and Lichtfouse 2019). Due to presence of abundant amino and hydroxyl functional groups on chitosan, as well as its nontoxicity, biodegradability, hydrophilicity, and cost-effectiveness, chitosan has received a considerable attention as a promising candidate to sorb various contaminants such as heavy metals, dyes, fluoride, and humic acid (Wang and Zhuang 2017).

Furthermore, the efficiency of chitosan for capturing the PFAS contaminants from aqueous solutions has been recently examined by several researches. For example, at study by Zhang et al.

(2011) the crosslinked chitosan beads were used for perfluorooctane sulfonate (PFOS) removal from aqueous solution, with reported adsorption capacity of 2500 mg.g^{-1} at equilibrium concentration of 0.33 mmol.L^{-1} .

A developed chitosan-based molecularly imprinted polymer (MIP) has been evaluated for PFOS removal in comparison with non-imprinted chitosan. Results showed the molecularly imprinted chitosan and the non-imprinted chitosan had the sorption capacities of 1460 mg. g^{-1} , and 672.6 mg. g^{-1} for PFOS, respectively. Additionally, this study indicated molecularly imprinted chitosan has more selectivity potential to capture the PFOS in the presence of other contaminants (Yu et al. 2008).

In another study, a synthesized magnetic chitosan, showed removal performance for PFOA and PFOS with maximum adsorption capacities of 16.07 mg.g^{-1} , and 21.64 mg.g^{-1} , respectively, at equilibrium concentration range of $10\text{-}50 \text{ mg.L}^{-1}$ (Elanchezhiyan et al. 2021).

A novel chitosan-based hydrogel has been developed at study by Long et al. (2019) with reported maximum adsorption capacity of 1275.9 mg.g^{-1} for PFOA at initial concentration range of $100\text{-}2000 \text{ mg.L}^{-1}$.

However, majority of these studies have provided the adsorption isotherms at high level of PFAS concentration, and to date, the efficiency of chitosan for PFAS removal has not considered at environmentally relevant concentrations. Another limitation of the existing studies is lack of co-removal of PFAS in the presence of other organic/inorganic contaminants.

Therefore In this section of the current study, crosslinked chitosan beads and grafted chitosan beads were developed for PFAS removal from either aqueous solution or soil by taking into account the following objectives: 1) evaluate the efficiency of chitosan beads by performing the isotherm and kinetic adsorption tests; 2) measuring the adsorption affinity (K_d) value for chitosan at environmentally relevant concentrations; 3) evaluate the effect of pH on sorption efficiency of chitosan; 4) assess the sorption efficiency of chitosan in the presence of other organic and inorganic contaminants; 5) To find the solid- liquid distribution coefficient (k_d) for PFAS components by performing the column sorption tests.

To assess the efficiency of developed chitosan – based sorbents, reference materials such as activated carbon and anionic exchange resin were used at this study.

4.2 Material and Methods

4.2.1 Raw materials

Chitosan (viscosity 200-600mPa.s), Epichlorohydrin (ECH, purity >99%), PEI (polyethylenimine; CAS No 9002-98-6), and Pentadecafluorooctanic Acid (PFOA, $C_8HF_{15}O_2$, purity >98%, molecular weight = 414.07g mol⁻¹) were purchased from Tokyo Chemical Industry (TCI, Japan). N,N,dimethyl acetamide (DMA), Heptadecafluorooctanesulfonic acid potassium salt (PFOS, $CF_3(CF_2)_7SO_3K$, purity >98%, molecular weight = 538.22 g mol⁻¹), Potassium nonafluoro-1-butanesulfonate (PFBS, $CF_3(CF_2)_3SO_3K$, purity >98%, molecular weight = 338.19 g mol⁻¹), Heptafluorobutyric acid (PFBA, $CF_3CF_2CF_2COOH$, purity >98%, molecular weight = 214.04 g mol⁻¹), Diethylenetriamine (DETA), and Poly (diallyldimethylammonium chloride) solution (PDADMAC; Mw 400,000-500,000) were bought from Sigma- Aldrich. The above-mentioned authentic standards of PFOA, PFOS, PFBA, and PFBS were used for preparing the stock solution of PFAS components at 1g L⁻¹. Pulverized activated carbon (PAC) and granular activated carbon (GAC) (20-40 mesh size) have been sourced from Duksan company in Korea. Anion exchange resin (AER) (AE520E) and Montmorillonte (Case No1318-93-0) were purchased from Purolite and sigma-Aldrich companies, respectively.

4.2.2 NaOH concentration

In this study, NaOH aqueous solution with concentration ranging 0.1-3 M was selected as a non-solvent agent for making of chitosan beads. When the concentration of NaOH solution was lower than 0.5 M the chitosan beads were not formed in a proper spherical shape. Moreover, for concentrations higher than 2M the beads were not formed uniformly because of rapid precipitation of chitosan solution inside the NaOH solution. Within range of 0.5-2M for NaOH, the best possible spherical shape of chitosan beads has been formed. This may be due to the most favorable

exchange rate between solvent (acetic acid) and non-solvent (NaOH) during the phase inversion process (Shakeri et al. 2017). Therefore, the NaOH with concentration of 0.5M has been chosen a proper concentration for making chitosan beads.

4.2.3 Chitosan concentration

The first step of bead formation is pouring dropwise of chitosan solution in aqueous NaOH to allow reformation of etheric bonds and regenerate the polymeric structure. At this study, four chitosan concentration (dissolved in acetic acid) including 10, 20, 50, 100 g. L⁻¹ has been examined to evaluate the beads formation. It was observed at very high concentration (>50 g L⁻¹), chitosan solution was extremely viscose and difficult to solve inside the acetic acid. At concentration of 20 g. L⁻¹ chitosan solution was still somewhat viscose for dropwise pouring by pump in NaOH solution. By utilizing the concentration of 10 g. L⁻¹ aggregative and spherically shaped beads have been formed in the NaOH solution. Therefore, the concentration of 10 g. L⁻¹ ensures sufficient intermolecular entanglement and polymerization of chitosan, and was selected for making chitosan beads.

4.2.4 Grafting of chitosan-based sorbents

Electrostatic attraction between PFAS and the adsorbent can be considered as one of the possible adsorption mechanisms involved in the adsorption of PFAS components. The electrostatic attraction between the negatively charged PFAS components and the adsorbent is enhanced when the surface charge of the adsorbent has a higher positive charge. In this study, three cationic surfactants including PDADMAC, DETA, and PEI were selected to improve the positivity of the chitosan- based sorbents.

One of the synthesized chitosan-based sorbents in this study was montmorillonite-chitosan composite. To determine the most influential cationic surfactant, montmorillonite was first modified with each of these surfactants. To modify the montmorillonite, 5gr of montmorillonite

was added to each of these surfactants at a concentration of 5% (V/V) dissolved in DI, and the mixture was agitated for 24 hours before being filtered and dried at 80°C. Finally, to identify the most potent surfactants that will interact with montmorillonite, the dried solid components were characterized using FT-IR and zeta potential tests.

The results of FT-IR tests for modified montmorillonite with each of the surfactants is presented in figure 4.5. Based on these results it looks the PEI had more influence on the montmorillonite surface in comparison of other surfactants. The FT-IR curve of PEI modified showed some new and more peaks comparing to the non- modified montmorillonite, which implies better interaction of PEI with montmorillonite.

Also, the zeta potential results for each modified montmorillonite, which is presented in figure 4.6, shows that PEI-modified has higher point of zero charge in comparison of other surfactants. Higher point of zero charge for PEI modified montmorillonite can increase the electrostatic attraction between montmorillonite and PFAS components.

Additionally, the efficiency of PEI for enhancing the sorption of sorbents has been also confirmed by several previous researches (Chatterjee et al. 2011; Lu et al. 2020; Xie et al. 2019). Therefore, at this study the PEI has been selected for grafting the chitosan-based sorbents.

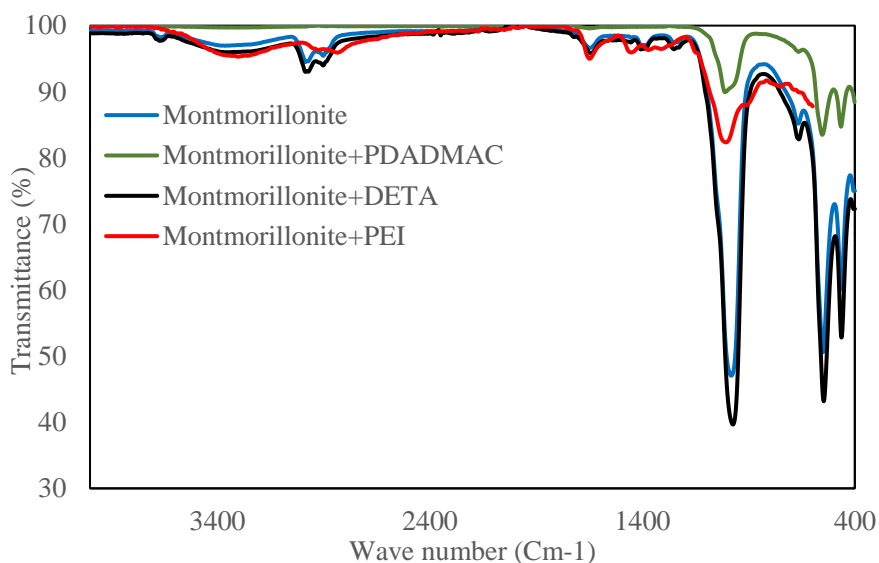


Fig. 4.5 FT-IR results for modified montmorillonite with different cationic surfactants

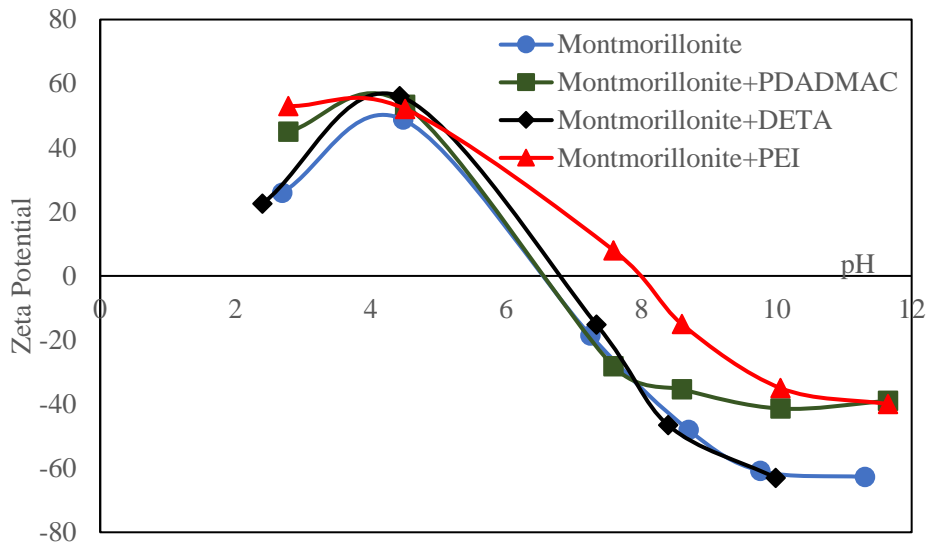


Fig. 4.6 Zeta potential results for modified montmorillonite with different cationic surfactants

4.2.5 Preparation of Chitosan Beads (CB)

First, 1wt% of chitosan powder was dissolved in 100ml of 2% (v/v) acetic acid under mechanical stirring till all air bubbles were completely removed and solution became transparent. Then the homogenous solution was dropped into 500 ml of 0.5M NaOH using peristaltic pump at flow rate of $200\mu\text{l}\cdot\text{min}^{-1}$, and left overnight at ambient temperature to produce the hydrogel beads. For removing the extra NaOH from the chitosan hydrogel beads, they were extensively washed with deionized water (DI) until the pH of solution became similar to pH of DI. To avoid the solubility of hydrogel beads in aqueous solutions, the washed beads were crosslinked with 2% (v/v) ECH dissolved in 100 ml DI under continuous stirring for 12h at 40 °C (Zhang et al. 2011). After crosslinking the beads, to remove unreacted ECH, as well as other possible present pollutants from the beads surface, the beads were activated with methanol 80% (v/v) using Soxhlet Extraction for 12h at 80°C (Yang et al. 2020). The obtained chitosan beads were fully washed with DI water for several times (till the pH was almost natural), and they were dried at 60°C for 24 using vacuum oven. Finally, to make the finer chitosan beads they were crushed by mortar and pestle, and denoted as CB and tested as an adsorbent for PFAS removal.

4.2.6 Preparation of Grafted Chitosan Beads (GCB)

For synthesizing of grafted chitosan, 5gr of the DI washed chitosan hydrogel beads (section 4.2.5) were added to 5 % (v/v) of PEI dissolved in 100 ml of DMA (N, N, dimethyl acetamide) solution. The mixture was reacted for 24 h at 30 °C while stirring at 200 rpm. After grafting, the grafted chitosan beads were crosslinked with 1% (v/v) ECH dissolved in 100 ml DMA under continuous stirring (200rpm) for 6h at 60 °C (Chatterjee et al. 2011). To remove the unbonded PEI with chitosan beads the grafted chitosan beads were purified with methanol 80% (v/v) using soxhlet extraction for 12h at 80°C. After washing the grafted chitosan beads with DI for several times they were vacuum dried at 60°C for 24. The final grafted chitosan beads were crushed, and hereafter referred as GCB. The brief preparation procedure of CB and GCB sorbents is presented in Figure 4.7.

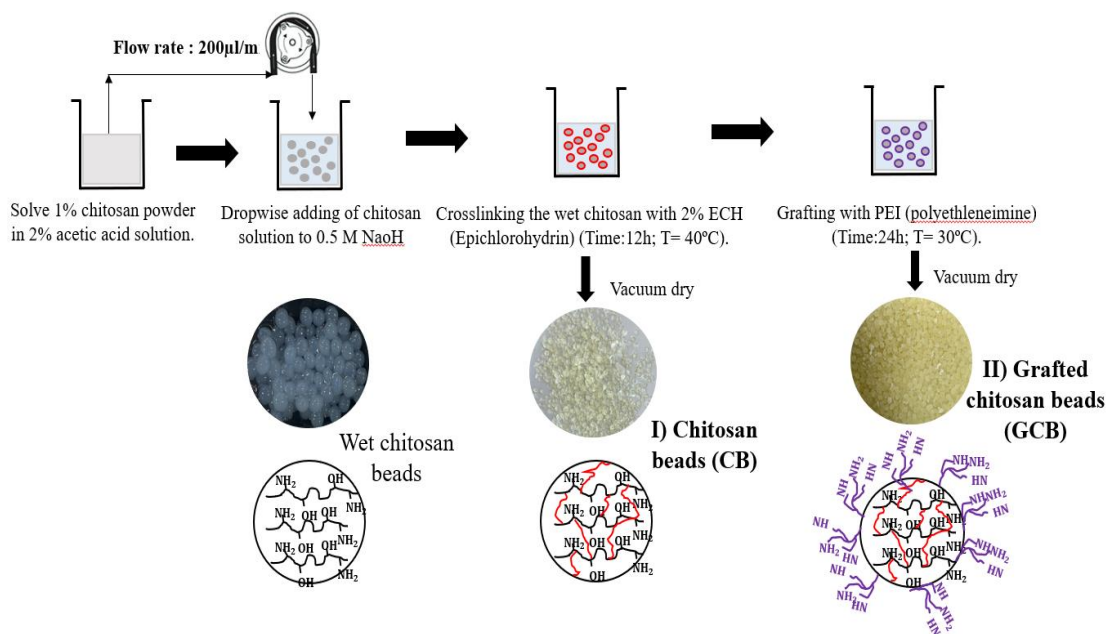


Fig. 4.7 Preparation of chitosan beads (CB) and grafted chitosan beads (GCB)

4.2.7 Preparation of clay chitosan composite

After dissolving 1wt% of chitosan powder in 100ml of 2% (v/v) acetic acid under mechanical stirring, 5gr montmorillonite was added to the solution and stirred till montmorillonite was

homogenously dispersed in chitosan solution. Then the homogenous solution was dropped into 500 ml of 0.5M NaOH using peristaltic pump at flow rate of $200\mu\text{l}\cdot\text{min}^{-1}$, and left overnight at ambient temperature to produce the montmorillonite hydrogel beads. For removing the extra NaOH from the montmorillonite hydrogel beads, they were extensively washed with deionized water (DI) until the pH of solution became similar to pH of DI. To avoid the solubility of montmorillonite hydrogel beads in aqueous solutions, the washed beads were crosslinked with 2% (v/v) ECH dissolved in 100 ml DI under continuous stirring for 12h at 40 °C. The produced montmorillonite hydrogel beads were grafted by 5 % (v/v) of PEI dissolved in 100 ml of DMA (N, N, dimethyl acetamide) solution for 24h at temperature 30°C. Finally, after purifying the beads with methanol 80% (v/v) using soxhlet extraction for 12h at 80°C, they washed with DI for several times and they were vacuum dried at 60°C for 24. The produced sorbent donated as montmorillonite grafted chitosan beads (MT-GCB), and used for PFAS removal from contaminated soils. The brief preparation procedure of MT-GCB is presented in Figure 4.8.

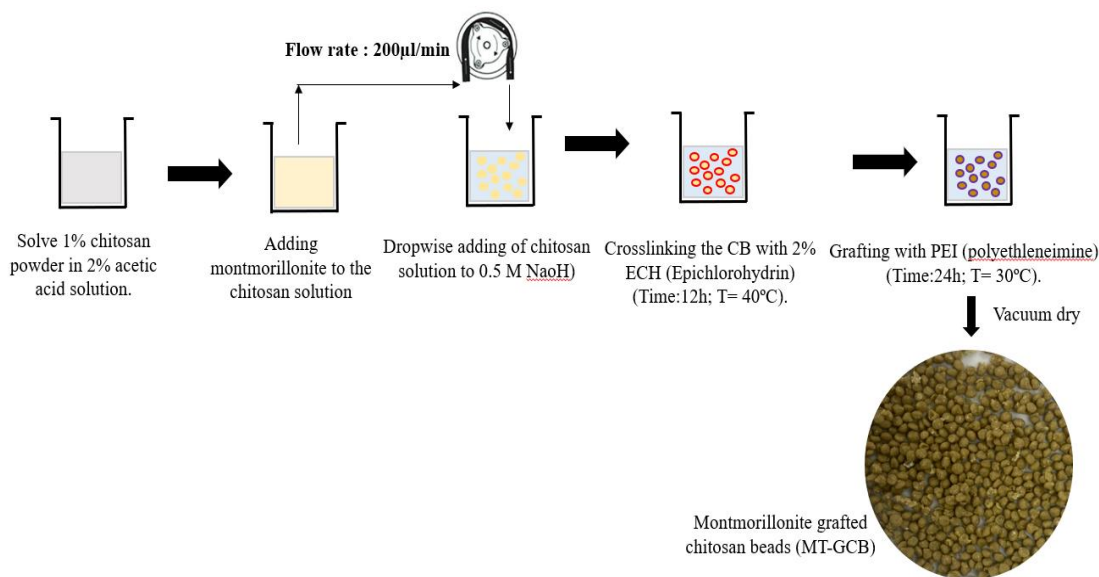


Fig. 4.8 Preparation of montmorillonite grafted chitosan beads (MT-GCB)

4.2.8 Adsorbate solution

A stock solution of 1 g. L⁻¹ of each PFAS substances (PFOA, PFOS, PFBA, and PFBS) was prepared by dissolving of their authentic solid standard in 100% methanol. The prepared stock solution further was diluted at desired working concentrations with appropriate amounts of DI water.

4.2.9 Batch adsorption tests

Adsorption batch experiments were conducted by adding certain amount of adsorbent into 50 ml polypropylene centrifuge tubes containing 45ml of adsorbate solution at pH 6.5 ± 0.2 (except samples for examination the pH effect). The adsorption capacity of each sorbent was determined by preparing single solute of each PFAS substance (PFOA, PFOS, PFBA, and PFBS) at initial concentrations ranging 1-100 mg. l⁻¹, for 24h by loading 220 mg. L⁻¹ of each sorbent. In addition, comparative sorption tests were carried out by preparing a multi-solute solution of four PFAS substances at an initial concentration of 100 µg. L⁻¹ with sorbent dosage of 70 mg. L⁻¹.

In the kinetic experiments, each data point was determined using an individual batch experiment for the contact times ranging 5min to 48h at initial concentration of 100 µg. L⁻¹ with sorbent dosage of 70 mg. L⁻¹.

The effect of pH on PFAS sorption was examined by running adsorption tests at adjusted pH values of 3, 6, 10 using 0.5M HCL or NaOH solutions. The pH effect tests were performed for 24h under initial PFAS concentration of 100 µg. L⁻¹ and sorbent dosage of 70 mg. L⁻¹.

For batch experiments targeting the single point adsorption coefficient (K_d), samples were agitated for 24h under initial concentration of 1000 ng. L⁻¹ and 15 mg. L⁻¹ of each sorbent.

A multi-solute solution including the mixture of PFAS components (PFOA, PFOS, PFBA, PFBS), cationic and anionic metals (Pb²⁺, and NO₃⁻), and two different organic contaminants (TCE, and phenol) has been prepared at initial concentrations of 100 µg L⁻¹, and 1mg. L⁻¹ for PFAS components, and other co-contaminants (Pb²⁺, NO₃⁻, TCE, phenol), respectively.

Subsequently, by adding each sorbent at dosage of 70 mg. L⁻¹ to the multi-solute solution, a series of competitive sorption tests have been conducted for 48h to investigate the selectivity potential of each sorbent for PFAS sorption in presence of other co-existing contaminants.

All samples were mechanically agitated at ambient laboratory temperature (22 ± 2 °C) using a rotary shaker at 150rpm, and after certain agitation time, samples were centrifuged at 3900 rpm for 20 min and then filtered (pore size 0.2 µm), and the supernatants were kept at refrigerator for further analysis. All experiments were run in triplicates, and the mean value with the corresponding standard deviation has been reported as the final results. The adsorption procedures, as well as selecting the adsorbent dosages have been conducted following the methods as described by other previous researches (Ateia et al. 2019; Ching et al. 2020; Du et al. 2017).

4.2.10 Batch adsorption tests by real field water

To evaluate the performance of developed sorbents for PFAS removal in a natural condition, water sample has been taken from Hangang (Han) river in Korea, and used for batch adsorption tests (The Han river is a major river in Korea that provides water to over 12 million South Koreans, so it was chosen to collect water samples for our experimental program). The location for taking sample from Han river was Banpo Hangang Park (Figure 4.9).

After collecting water samples, the Han river water was spiked with PFAS substances (PFOA, PFOS, PFBA, and PFBS) at an initial concentration of 100 µg. L⁻¹ for each of the PFAS substances. Then, the batch sorption experiments were carried out in accordance with the procedure outlined in section 4.2.9.



Fig. 4.9 Location of taking sample from Han river

4.2.11 Reusability tests for the developed sorbents

To evaluate the possibility of recovering PFAS from the loaded sorbents as well as their reusability for subsequent use, five cycle adsorption desorption experiments were performed in a consequence. For this aim at the end of one cycle of sorption tests (sorption tests were conducted at initial concentration of $1 \text{ mg} \cdot \text{L}^{-1}$ multi- solute of PFAS mixture with 10mg sorbent added into 45ml conical tube and agitated for 24h) the exhausted sorbents were regenerated by elute solution consists of 80% ethanol and 1% NH_4Cl (Wang et al. 2019; Zaggia et al. 2016). After drying the regenerated sorbents at $60 \text{ }^\circ\text{C}$ for 24 h, they were placed into a fresh solution containing $1 \text{ mg} \cdot \text{L}^{-1}$ of all four PFAS substances and subject for next sorption cycle. The adsorption-desorption tests were continued for five cycles, and each test was performed in triplicate and the mean was calculated.

4.2.12 Synthesis of the contaminated soil

The soil which was selected for PFAS stabilization by MT-GCB and GAC was classified as SM. The particle size distribution of selected soil is presented in Figure 4.10.

For contaminating the soil first, the soil has been sieved and the larger size over than 4.75mm (sieve number 4) has been removed from the soil. After making the mixed PFAS solution at two different concentration of $1.5\mu\text{g. ml}^{-1}$ and $10\mu\text{g. ml}^{-1}$, the 500gr of dried soil has been mixed with 500ml of PFAS solution. The mixture was homogeneously shaken by shaker for 48h, and it dried at ambient temperature for two weeks. This resulted in a concentration of 1.5 and 10 μg individual PFAS per one gr of dried soil. The dried homogenized soils were stored in air-tight containers at 4 °C for using stabilization experiments. The contamination procedure was carried out following the previous research (Sorengard et al. 2019).

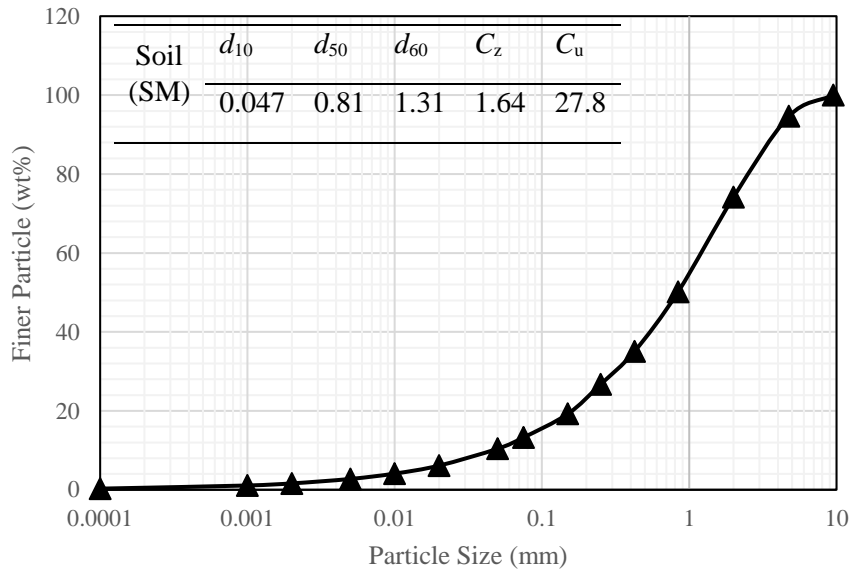


Fig. 4.10 Grain size distribution of soil

4.2.13 Leaching tests for stabilized soils

Two different doses of each sorbents (MT-GCB and GAC) including 0.5 % and 2 % has been used for stabilizing the synthesized contaminated soils. After mixing the soil with sorbents, 2gr of each

sample were transferred to a 50ml conical tube and 40ml of DI water was added to each sample to prepare the liquid: soil ratio (L/S) of 20. The samples were then shaken in an end-over-end shaker at 200 rpm over 7 days (Kabiri et al. 2021; Sorengard et al. 2019). Control samples including soil without any sorbent were prepared in the same way. After shaking, the samples were centrifuged at 6000 rpm for 20min the supernatant was taken for analyze the PFAS concentration.

4.2.14 Rapid Small column test for determining the K_d

Rapid small-scale column tests (RSCCT) has been used for determining the distribution coefficient (K_d) of PFAS substances.

The soil used for column tests was the same as that mentioned in section 4.2.12, with 13% fine content (particles smaller than 75 μm in size). The soil fine content was manually adjusted to have additional 5% and 20% fine contents to investigate the influence of soil fine content on PFAS sorption. Overall, three different fine content percentages of soil were tested: 5, 13, and 20%.

Glass columns with an inner diameter of 15 mm and a length of 120 mm were used for the column experiments. Columns were filled with 25mm of glass beads (0.5 mm diameter zirconia glass silica beads) at the bottom, 40 mm of soil (soil was dried packing in small increments) in the middle, and 20 mm of glass beads on top of the soil media. The control column was only filled with glass beads (no soil) and was used to confirm any PFAS sorption in the absence of soil (Figure 4.11).

In order to detect and fix any leakage before switching to the PFAS-spiked water, and minimizing the trapped air between soil particles, each column was first cleansed with deionized water for several times of bed volume (BV) (~500 times of BV) under upflow movement with flow rate of 1 ml. min⁻¹.

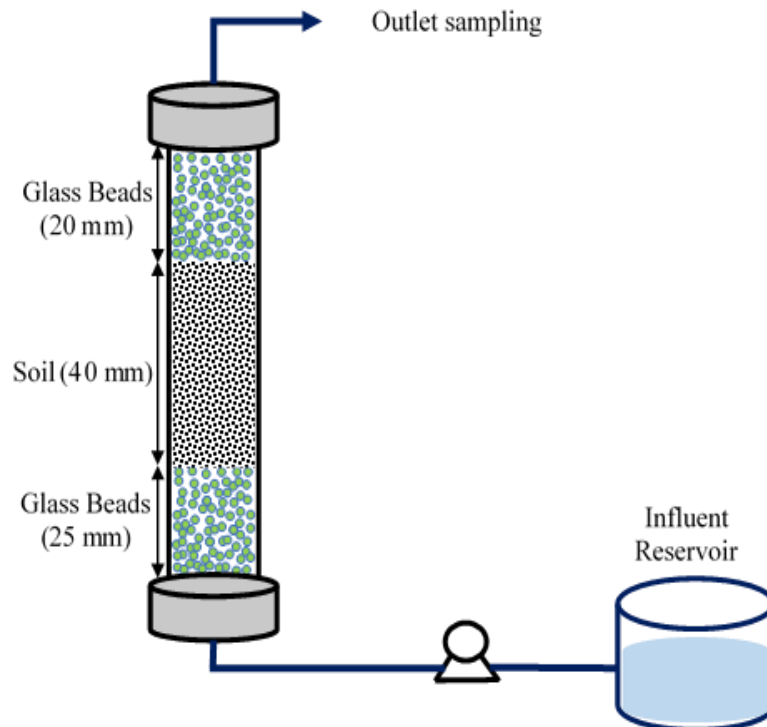


Fig. 4.11 Schematic plan of RSSCT column at this study

The flow rate of PFAS-spiked water (spiked with an initial concentration of 50 mg. L^{-1} for each PFAS component) through the columns for soil was calculated using the EPA-recommended empty bed constant time (EBCT) of 10 minutes based on equation (2.6) (Park et al. 2020; Schaefer et al. 2020). The obtained flow rate was $706 \mu\text{l. min}^{-1}$.

A multi-channel peristaltic pump was used to supply the PFAS-spiked water through the columns. Samples were collected from the outlet until the outlet concentration equaled the inlet concentration. After measuring the PFAS concentration and determining the breakthrough curve for each sample, the retardation factor (R) was determined, and the K_d and K_{oc} values for each PFAS substances was calculated using equations (2.7) and (2.8), respectively.

The density, porosity and organic content for each soil column with different fine contents was based on Table 4.3.

Table 4.3 Properties of soils used for column tests

Fine content	ρ_d (kg. cm ⁻³)	n	f_{oc} (%)
5%	1.87	0.29	
13%	1.66	0.37	0.594 ± 0.008
20%	1.69	0.36	

After calculation the K_{oc} value for each PFAS components, and by having the K_{ow} value of PFAS components from table 4.2, the related sorption equation for estimating the K_{oc} value of PFAS based on their K_{ow} will be derived.

4.2.15 PFAS measurement

After finishing each sorption or leaching experiments, the supernatant of each sample was filtered with a 0.25 polyethersulfone (PES) membrane filter, and 1ml of each supernatant was prepared for measuring the PFAS concentration. The concentration of PFAS was determined by LC-MS/MS equipped with an XDB-C18 guard column.

4.3 Result and Discussion

4.3.1 Characteristics of sorbents

The physicochemical characteristics of four sorbents used for PFAS sorption are shown in Table 4.4. The elemental analyzes for CB, and GCB sorbents showed higher percentage of nitrogen for GCB, which confirm PEI has properly grafted to the chitosan beads (more amino functional groups were properly grafted to the chitosan beads). Moreover, The elemental results display in comparison to GCB, CB had lower carbon and higher oxygen contents. The aromaticity and polarity of the adsorbents were evaluated by calculating the H/C and (O + N)/C molar ratios, respectively. The molar ratio of H/C for CB, GCB, PAC, and AER were 0.17 and 0.193, 0.008 and 0.146, respectively. The fact that PAC had the lowest H/C value of all the sorbents indicates that

it is more hydrophobic than other sorbents. Furthermore, the polarity index $[(O + N)/C]$ for PAC was the lowest, indicating that PAC has a higher hydrophobicity potential (He et al. 2017). However, the obtained low molar ratios for both CB and GCB indicate that both sorbents exhibit significant carbonization and high aromaticity, which make them as an efficient sorbent material. The polarity index $[(O + N)/C]$ for CB and GCB were 1.15 and 0.968, respectively. The lower polarity index for GCB compared to that for CB implies that GCB is more hydrophobic and contains more polar functional groups for coordination with PFAS substances.

The anion exchange capacity (AEC) values for the CB and GCB samples were 14.7 ± 0.42 and $24.23 \pm 0.53 \text{ meq}\cdot\text{L}^{-1}$, respectively. The higher AEC value for GCB reveals that GCB has higher amounts of anions, such as Cl^{-1} , that are available for exchanging with anionic PFAS. Consequently, more PFAS can be adsorbed on the surface of GCB via the anion exchange adsorption mechanism (Saeidi et al. 2020). Additionally, when commercial sorbents (PAC and AER) were compared, AER's AEC was significantly greater than PAC's, demonstrating the presence of more anions on AER for exchanging by fluorine anion in PFAS substances.

Table 4.4 Physicochemical characteristics of developed sorbents

Properties	AER	PAC	CB	GCB
Carbon (C) %	62.07	72.89	39.3	43.21
Hydrogen (H) %	9.08	0.584	6.7	8.34
Nitrogen (N) %	3.56	0.517	5.95	13.82
Sulfur (S)%	0.192	0.565	ND	ND
Oxygen (O) %	16.82	7.717	39.43	28.04
H/C	0.146	0.008	0.17	0.193
O/C	0.27	0.10	1.003	0.65
(O+N)/C	0.328	0.112	1.154	0.969
BET surface area (m ² ·g ⁻¹)	31.37	791.45	3.73	0.474
D ₉₀	858μm	50.3μm	345μm	534μm
Cumulative pore volume (cm ³ ·g ⁻¹) ^a	0.371219	0.38555	0.0109	0.0015
Pore size (nm) ^b	49.36	3.20	16.46	18.95
Anion Exchange Capacity (AEC) (meq·L ⁻¹)	33.13 ± 0.35	1.28 ± 0.6	14.7 ± 0.42	24.23 ± 0.53

NOTE: ND, not detected; ^a P/P0=0.99; ^b Barrett-Joyner-Halenda (BJH) model, desorption data.

4.3.2 Zeta potential

Figure 4.12 shows the results of zeta potential for sorbents at different pH values. As it is obvious from this figure, the GCB had higher positive zeta potential for all examined pH values in comparison of CB. It can be concluded the amino functional groups have been grafted to the surface of chitosan, and as result the zeta potential of the modified chitosan beads has increased positively. This can increase the adsorption capacity of the grafted chitosan beads because of having more electrostatic attraction with anionic PFAS substances. The zeta potential of PAC was positive at acidic pH values however its surface charge has been changed to negative at pH values higher than 5. This is consistent with previous research, which found PZC (Point of Zero Charge) of 5.9 for activated carbons (Saeidi et al. 2020). AER showed almost neutral to positive surface charge at all of the examined pH values.

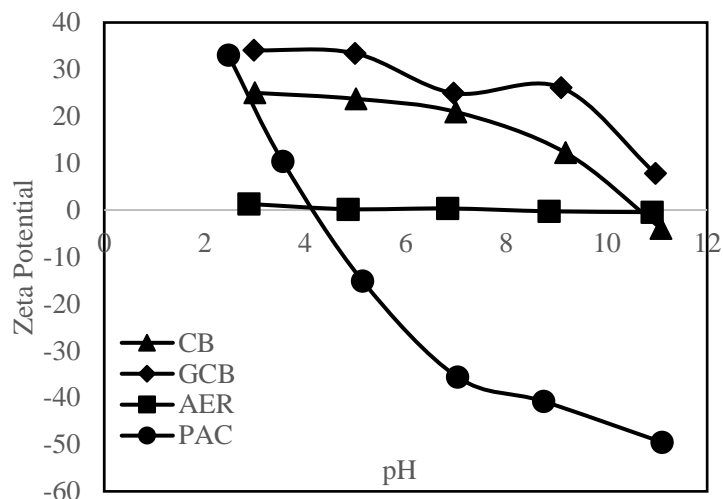


Fig. 4.12 Zeta potential of sorbents at different pH values

4.3.3 Isotherm sorption results

Sorption isotherm as a function of equilibrium concentration versus adsorbed amount of PFAS substances for each sorbent is shown in Figure 4.13. As it is obvious from Figure 4.13 for all four examined PFAS components, the adsorption capacity increased with increasing the equilibrium concentration.

When commercial sorbents were compared, AER performed better sorption removal than PAC, particularly for long-chain PFAS. At the examined concentration of PFAS ($1-100 \text{ mg. L}^{-1}$), PAC had higher sorption capacity for long chain PFAS whereas its sorption capacity for short chain was lower. In research by Fang et al. (2021) the anion-exchange resins (AERs) exhibited significant adsorption of PFASs compared to granular activated carbon which is consistent with obtained results at present research.

The obtained sorption capacities by Langmuir model for AER were 238.09, 263.1, 263.15, and 238.09 mg. g^{-1} for PFOA, PFOS, PFBA, and PFBS, respectively. While, the sorption capacities for PAC were 175.4, 208.3, 52.63, and 72.46 mg. g^{-1} for PFOA, PFOS, PFBA, and PFBS, respectively (see Table 4.5). The reason for higher sorption capacity of PFAS by AER can be attributed to simultaneous removal of PFAS by electrostatic attraction and hydrophobicity

mechanisms by AER (Wang et al. 2019). From obtained results, PFOS was sorbed more than other PFASs because the PFOS with the sulphonic group is more hydrophobic comparing to other PFAS substances (higher K_{ow} for PFOS) (Park et al. 2020).

Figure 4.13, and Table 4.5 have demonstrated that all examined short and long-chain PFAS substances can be captured by both CB and GCB sorbents, while GCB showed more adsorption capacities in comparison of CB. The obtained sorption capacities by Langmuir model for CB were 128.2, 204.08, 102.01, and 101.01 mg. g^{-1} for PFOA, PFOS, PFBA, and PFBS, respectively. While, the sorption capacities for GCB were 238.09, 277.7, 303.03, and 270.27 mg. g^{-1} for PFOA, PFOS, PFBA, and PFBS, respectively (Table 4.5). The obtained higher sorption capacities for GCB shows grafting process of CB is influential for enhancing the sorption capacity of CB.

The sorption capacity of chitosan obtained from other studies also indicates that chitosan can be used as an adsorbent for PFAS removal. For example, at study by Zhang et al. (2011) the crosslinked chitosan beads were used for perfluorooctane sulfonate (PFOS) removal from aqueous solution, with reported adsorption capacity of 2500 mg.g^{-1} at equilibrium concentration of 0.33 mmol. L^{-1} . A novel chitosan-based hydrogel has been developed at study by Long et al. (2019) with reported maximum adsorption capacity of 1275.9 mg.g^{-1} for PFOA at initial concentration range of 100- 2000 mg.L^{-1} . Furthermore, based on Table 4.5, isotherm data were more fit by Langmuir model which presume sorption occurs in monolayer rather than multilayer.

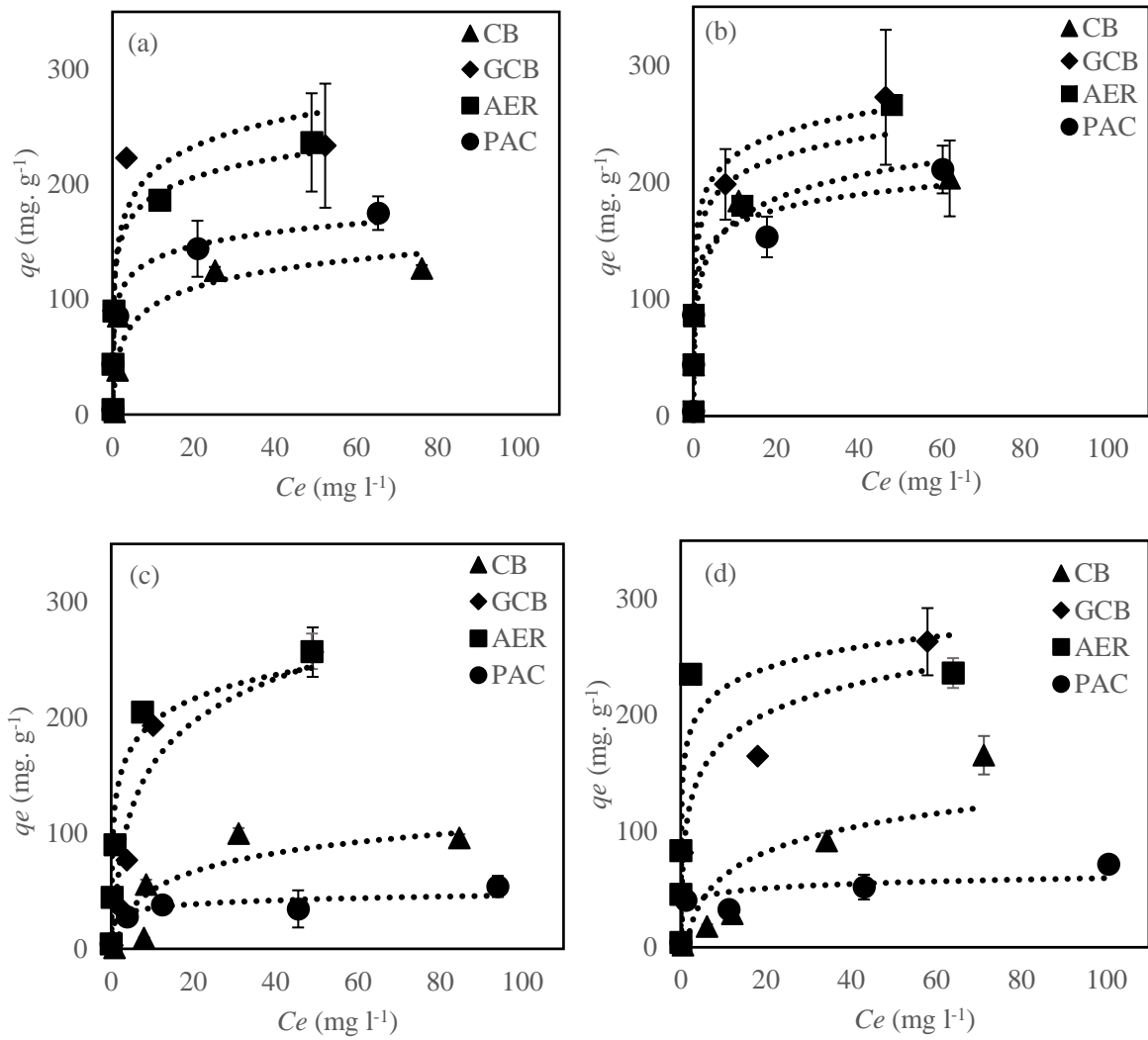


Fig. 4.13 Isotherm sorption results for (a) PFOA, (b) PFOS, (c) PFBA, and (d) PFBS substances

Table 4.5 Langmuir and Freundlich parameters for PFAS substance sorption by each sorbent

PFAS	Sorbent	Langmuir model			Freundlich model		
		q_{\max} (mg. g ⁻¹)	K_L (l. mg ⁻¹)	R^2	K_F (mg. g ⁻¹)	$1/n$	R^2
PFOA	AER	238.09	1.2	0.996	82.88	0.34	0.776
	PAC	175.4	0.77	0.995	56.46	0.33	0.779
	CB	128.2	1.56	1	84.1	0.104	0.946
	GCB	238.09	2	0.999	79.76	0.435	0.704
PFOS	AER	263.1	0.791	0.985	91.81	0.33	0.741
	PAC	208.3	0.716	0.987	74.52	0.28	0.561
	CB	204.08	1.48	0.999	90.54	0.229	0.874
	GCB	277.7	1.33	0.996	103.84	0.32	0.672
PFBA	AER	263.25	0.80	0.998	67.85	0.46	0.936
	PAC	52.63	0.167	0.935	15.99	0.271	0.963
	CB	102.01	0.225	0.993	5.75	0.697	0.507
	GCB	303.03	0.112	0.987	50.39	0.447	0.826
PFBS	AER	238.09	1.4	1	110.85	0.32	0.679
	PAC	72.46	0.148	0.964	22.13	0.258	0.919
	CB	101.01	0.032	0.981	3.067	0.937	0.998
	GCB	270.27	0.256	0.965	45.09	0.498	0.736

4.3.4 Kinetic sorption results

Figure 4.14 shows the kinetic sorption results of PFAS substances by all examined sorbents. As is obvious the PAC has reached to the equilibrium phase much faster than AER. The time for reaching to the equilibrium phase for PAC was less than 5 min, while this time was more than 48h for AER. Moreover, the initial adsorption rate (v_0) of PFAS substances by PAC and AER sorbents (Table 4.6), demonstrated that PAC had faster adsorption rate when compared to AER. Molecular length and carbon chain length can be influential parameters for kinetic sorption of PFAS analytes

(Dixit et al. 2020). Therefore, it seems PFBS with shorter molecular length had the faster adsorption rate through PAC.

The results showed GCB had faster sorption rate in comparison of CB. The obtained initial adsorption rates (v_0) of PFAS substances by GCB were comparable to those date of PAC.

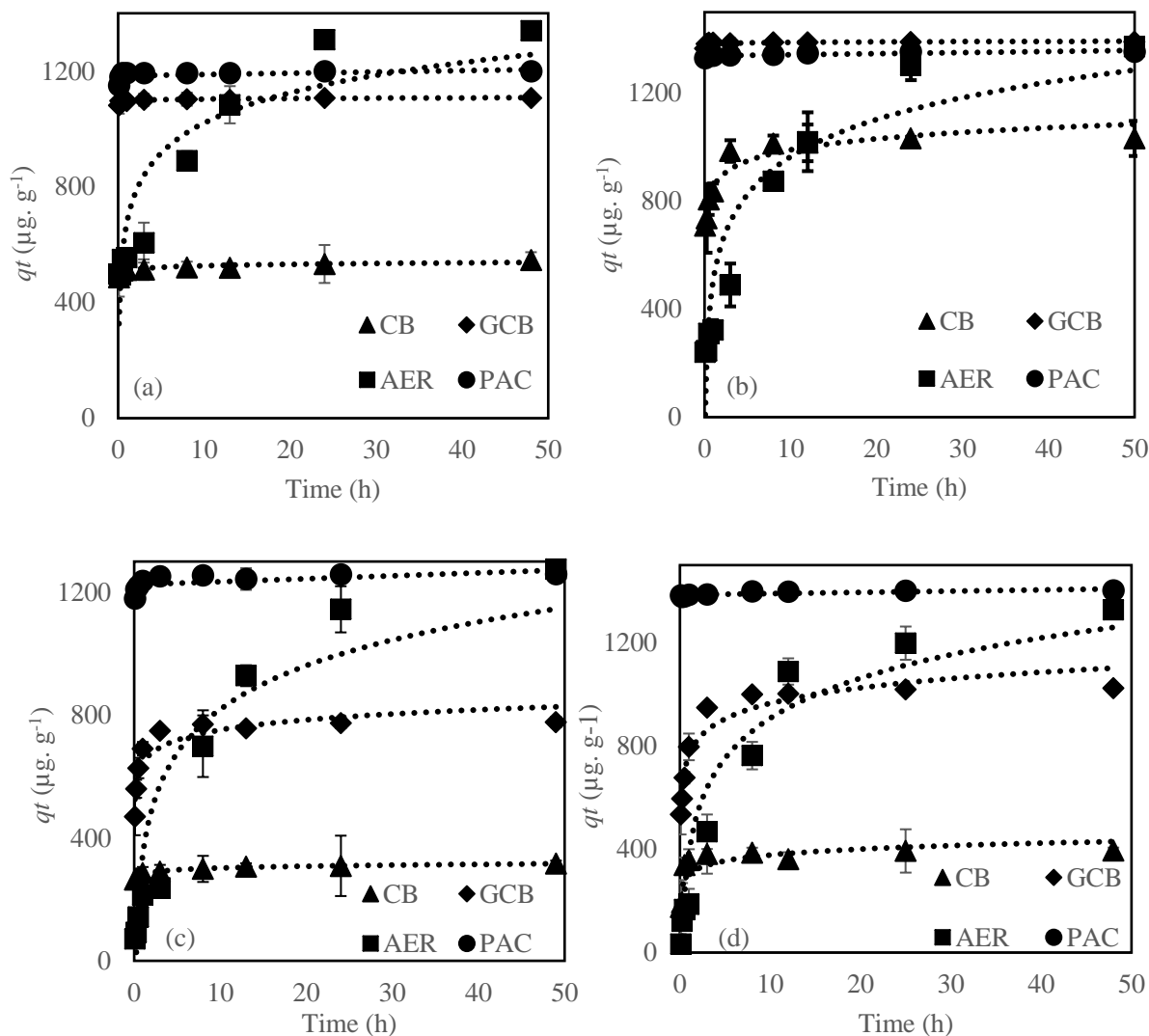


Fig. 4.14 Kinetic sorption results for (a) PFOA, (b) PFOS, (c) PFBA, and (d) PFBS substances

The reason that PAC and GCB had faster sorption rate than AER can be attributed to mass transfer through these sorbents. It looks finer particle size of the PAC (see Table 4.4) increases its

adsorption rate by decreasing the internal PFAS diffusion pathways inside the PACs porous (Wu et al. 2020).

Table 4.6 Pseudo first-order and pseudo second-order parameters for PFAS sorption by sorbents

Adsorbent	PFAS	pseudo first-order			pseudo second-order			
		K_1 (min^{-1})	q_e ($\mu\text{g}\cdot\text{g}^{-1}$)	R^2	K_2 ($\text{g}\cdot\text{mg}^{-1}\cdot\text{min}^{-1}$)	q_e ($\mu\text{g}\cdot\text{g}^{-1}$)	v_0^a	R^2
AER	PFOA	0.0029	1246.5	0.968	5.94×10^{-6}	1428.5	12.12	0.99
	PFOS	0.0029	1658.44	0.96	3.8×10^{-6}	1428.5	7.77	0.987
	PFBA	0.0034	2161.7	0.909	1.83×10^{-6}	1428.6	3.75	0.949
	PFBS	0.0029	1764.0	0.925	2.41×10^{-6}	1428.5	4.93	0.99
PAC	PFOA	0.0023	17.05	0.912	0.0007	1250	1111.1	1
	PFOS	0.002	18.98	0.939	0.00049	1428.5	2	1
	PFBA	0.0023	34.31	0.890	0.0004	1250	1000	1
	PFBS	0.0018	19.373	0.963	0.0007	1428.5	625	1
CB	PFOA	0.002	60.65	0.883	0.00015	555.6	1428.5	1
	PFOS	0.0034	154.49	0.951	0.0001	1000	47.17	0.999
	PFBA	0.0023	52.14	0.94	0.00026	312.5	119.01	1
	PFBS	0.0023	60.17	0.88	0.00016	400	25.38	0.999
GCB	PFOA	0.002	12.65	0.91	0.00081	1111.1	1000	1
	PFOS	0.002	5.3	0.891	0.0024	1428.5	5000	1
	PFBA	0.0027	113.6	0.913	0.00017	769.23	101.01	1
	PFBS	0.0027	251.82	0.956	0.000769	1000	769.23	1

The analyzed data with pseudo first-order and pseudo second-order models (Table 4.6), showed that the pseudo second-order model was the best fit for adsorption data with the correlation coefficients greater than 0.99. Thus, based on pseudo second-order model presumption it can be concluded that the chemisorption is the main adsorption mechanism for PFAS sorption by all examined sorbents at this study (Kołodziejńska et al. 2017).

4.3.5 Influence of pH on sorption capacity of sorbents

Figure 4.15 shows the results of adsorption removal for PFAS components at different pH values. As it is obvious from this figure, for long chain PFAS the sorption efficiency of PAC and AER are not changing with pH while efficiency of PAC is decreasing for short chain PFAS at higher pH values. This can be attributed to the surface charge of PAC and AER. As it was shown in section 4.3.2 surface charge of PAC is changing to the negative after pH~5, while AER holding its positivity because of its high basicity. From other side, since anionic short chain PFAS are adsorbing more by electrostatic attraction, therefore at higher pH values than pHzpc (pH at point of zero charge) possible electrostatic repulsion can occurs between PAC particles and short chain PFAS (Saeidi et al. 2020).

This finding is consistent with previous research, which found that IRA958 and IRA67 resins had high and constant PFOS sorption capacity over a wide pH range of 3 to 10. When the pH of the solution increased above 10, the PFOS sorption capacity on IRA958 changed very little, whereas the sorption capacity on IRA67 decreased significantly (Deng et al. 2010).

The removal efficiency of both CB and GCB sorbents were decreased by increasing the pH value. It looks GCB and CB are more sensitive to pH changing in comparison to other commercial sorbents. This could be because electrostatic attraction is the more dominant sorption mechanism for GCB, whereas PFAS sorption by PAC and AER can occur as a result of a combination of hydrophobicity and electrostatic attraction (Saeidi et al. 2020; Wang et al. 2019). Because the PFAS components are anionic, and the positivity charge of CB and GCB decreases at higher pH (refer to zeta potential results in section 4.3.2), increasing the pH is expected to decrease their adsorption due to electrostatic repulsion.

Overall, the removal of all PFAS substances was greater in acidic than alkaline conditions. The removal efficiency of long-chain PFAS (PFOA, and PFOS) by sorbents was greater than short-chain PFAS (PFBA, and PFBS). This can be attributed to higher hydrophobicity of long chain PFAS because of their higher octanol water partition coefficient in comparison of short chain PFAS (Du et al. 2017).

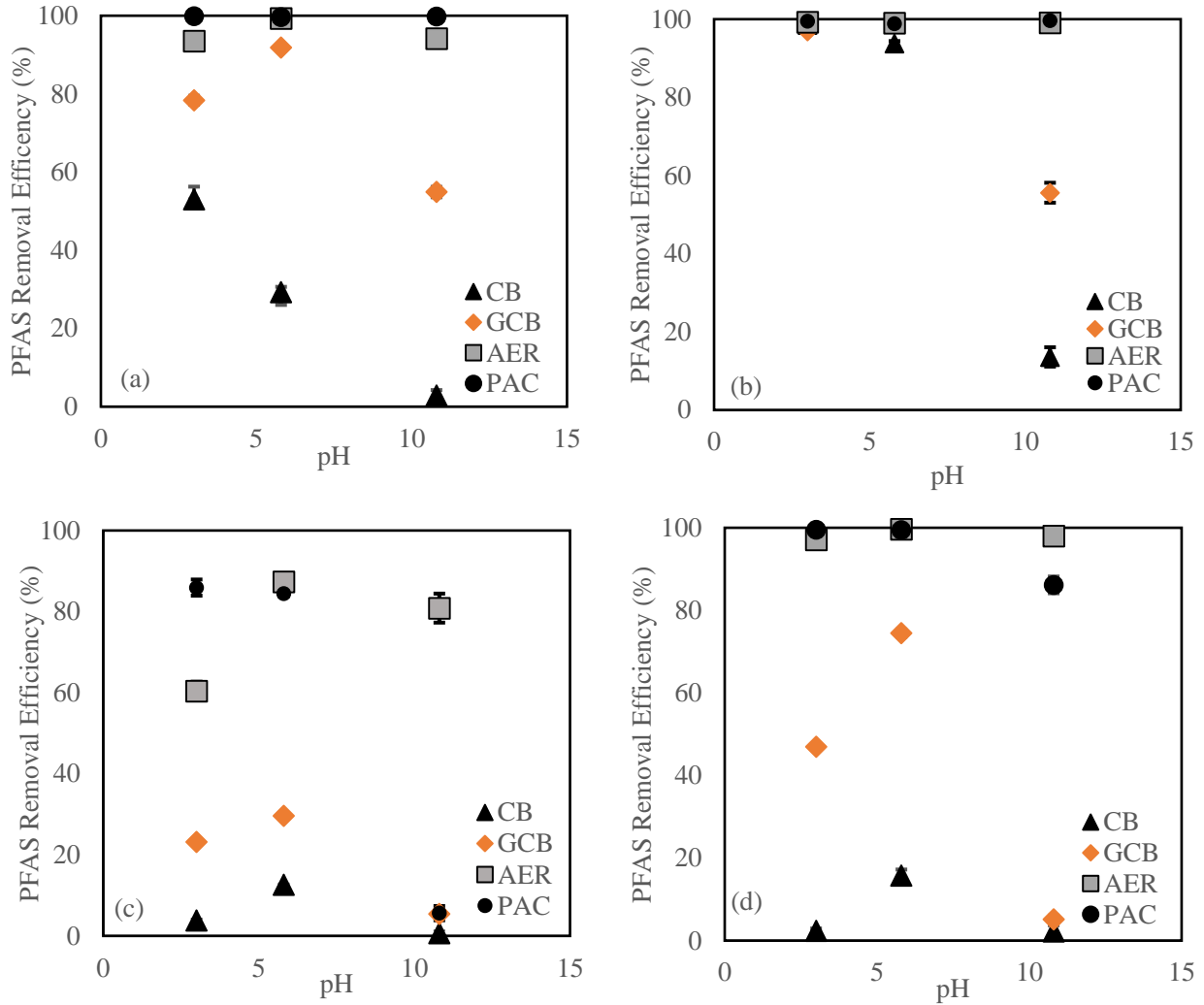


Fig. 4.15 Influence of pH on sorption of (a) PFOA, (b) PFOS, (c) PFBA, and (d) PFBS substances

4.3.6 Single point adsorption coefficient

To evaluate the efficiency of the sorbents for removal of PFAS components at environmentally relevant concentration, single point adsorption test has been performed at the initial concentration of 1000 ng. L⁻¹ for each PFAS components. Figure 4.16 shows the result of single point adsorption for examined adsorbents including AER, PAC, CB and GCB. Based on the Figure 3.16 both PAC and AER showed high K_d values for all PFAS substances. The average K_d value for PAC and AER were 2.5 and 2.3, respectively. It looks PAC showing somewhat better efficiency at lower PFAS

concentration. Maybe, because of finer particles, the PAC exposes more active sites for sorption (Wu et al. 2020). The obtained K_d values for AER and PAC were in the range of reported values with other studies (Ching et al. 2020; Liu et al. 2019)

The GCB showed higher K_d values for PFAS removal in comparison of CB. The obtained average K_d value for GCB was in range of 1.5 -2.5, which is comparable values with PAC and AER. Therefore, it can be concluded that GCB sorbent has efficient performance at concentrations close to the environmental relevant concentrations.

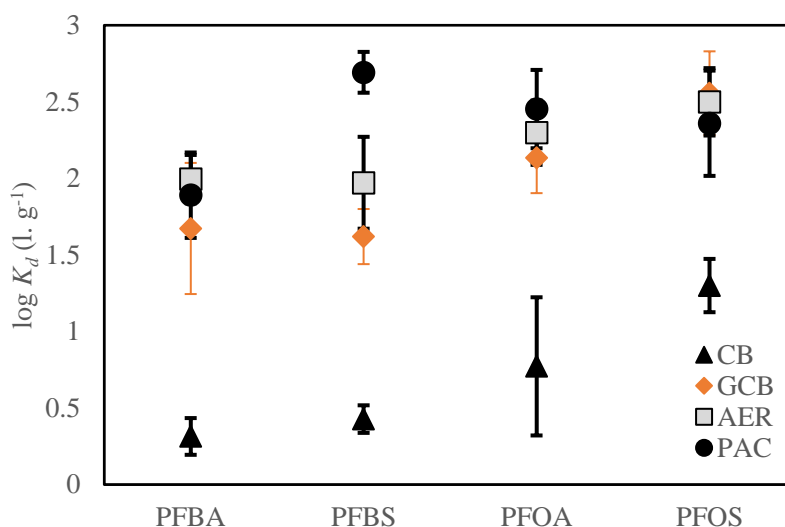


Fig. 4.16 Single point adsorption coefficients for each sorbent at environmentally relevant concentration

4.3.7 Selectivity sorption test results

To evaluate the performance of sorbents for PFAS removal in presence of other organic/inorganic contaminants the selectivity sorption tests has been performed by preparing a multi-solute solution including the mixture of PFAS components (PFOA, PFOS, PFBA, PFBS), cationic and anionic metals (Pb^{2+} , and NO_3^-), and two different organic contaminants (TCE, and phenol) at initial concentrations of $100 \mu g. L^{-1}$, and $1 mg. L^{-1}$ for PFAS components, and other co-contaminants (Pb^{2+} , NO_3^- , TCE, phenol), respectively.

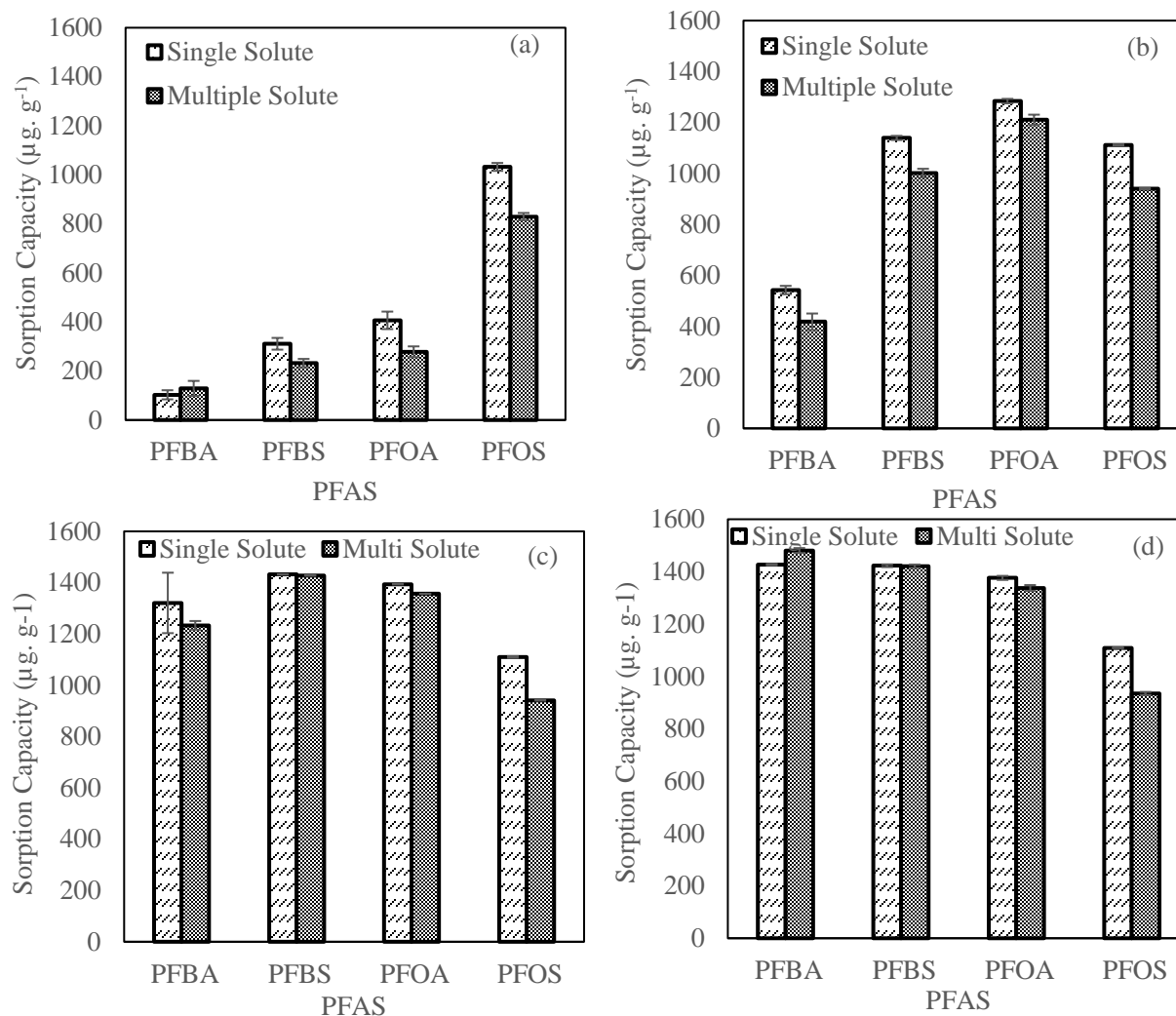


Fig. 4.17 Performance of each sorbents (a) CB, (b) GCB, (c) PAC, and (d) AER for PFAS sorption in single and multi-solute

Figure 4.17 shows the PAC and AER have almost constant sorption efficiency in presence of other organic/ inorganic pollutants. Moreover, efficiency of GCB for PFASs sorption in presence of other pollutants (multiple solute) has not been reduced drastically comparing to single solute (only PFAS substances) sorption tests. This could be because cationic ions bridge between the negatively charged sorbent and the PFAS anionic headgroup and do not compete with PFAS substances for sorbent sorption (Steigerwald and Ray 2021). Another possible explanation is that the examined concentration of other organic/inorganic pollutants ($1 \text{ mg}\cdot\text{l}^{-1}$) is not high enough to

compete with PFAS substances for sorption. These results are in consistent with other study which showed efficiency of activated carbon for PFOS sorption has been increased 24% in the presence of divalent cations (Ca^{2+} and Mg^{2+}) compared to the calcium and magnesium free matrix. In contrast, presence of organic matter (OM) has decreased the PFOS sorption by 60% due to competition for binding sites on the activated carbon between hydrophobic organic matter (OM) and PFOS (Steigerwald and Ray 2021). Another study by Del Moral et al. (2020) showed presence of Suwannee River natural organic matter (SRNOM) had a minimal impact on PFAS removal by anion exchange using polystyrene resin.

4.3.8 Batch adsorption tests by real field water results

To evaluate the performance of developed sorbents for PFAS removal in a natural condition, water sample has been taken from Hangang (Han) river in Korea, and used for batch adsorption tests. First of all, the Han river water quality including its anions and cations has been examined using ICP-MS. The Han river water quality parameters are summarized in Table 4.7. As it is obvious from Table 4.7 different kind of anion and cations are distributed in Han river at high concentration level (total ions concentration $\sim 128 \text{ mg. L}^{-1}$).

Table 4.7 Present anions and cations in the Han river water

	ion	Concentration (mg. L ⁻¹)
Anion	Cl	35.67 ± 0.355
	NO_3^-	135.52 ± 0.239
	SO_4^{2-}	19.06 ± 0.261
	Total	68.26 ± 0.541
Cation	Na	24.22 ± 0.113
	Mg	5.01 ± 0.316
	K	5.78 ± 0.105
	Ca	25.09 ± 2.31
	Total	60.11 ± 2.5

Figure 4.18 shows the results of sorption efficiency of each sorbents in presence of DI water and Han river water. As it shown from this figure, efficiency of all examined sorbent for PFAS removal has been decreased in the Han river water in comparison of the DI. However, CB and GCB had more drastic reduction comparing to other two commercial sorbents. The obtained result is in consistent with the research which showed presence of Sulfate and anionic Cr (VI) has influence on PFOS removal by resins (Deng et al. 2010).

The efficiency of PAC has been decreased more for short chain PFAS (especially for PFBA) comparing to AER. It looks shorter chain PFAS are more competing with other existence anions for sorption by sorbents. This could be because short chain PFAS are more sorbing due to electrostatic attraction, and since PFAS and anions are both negatively surface charged, anions may be more sorbet than PFAS. On the other hand, because longer chain PFAS (PFOA and PFOS) are more sorbing by hydrophobicity attraction, the presence of anions had less influence on their sorption by PAC and AER (Park et al. 2020; Wang et al. 2019).

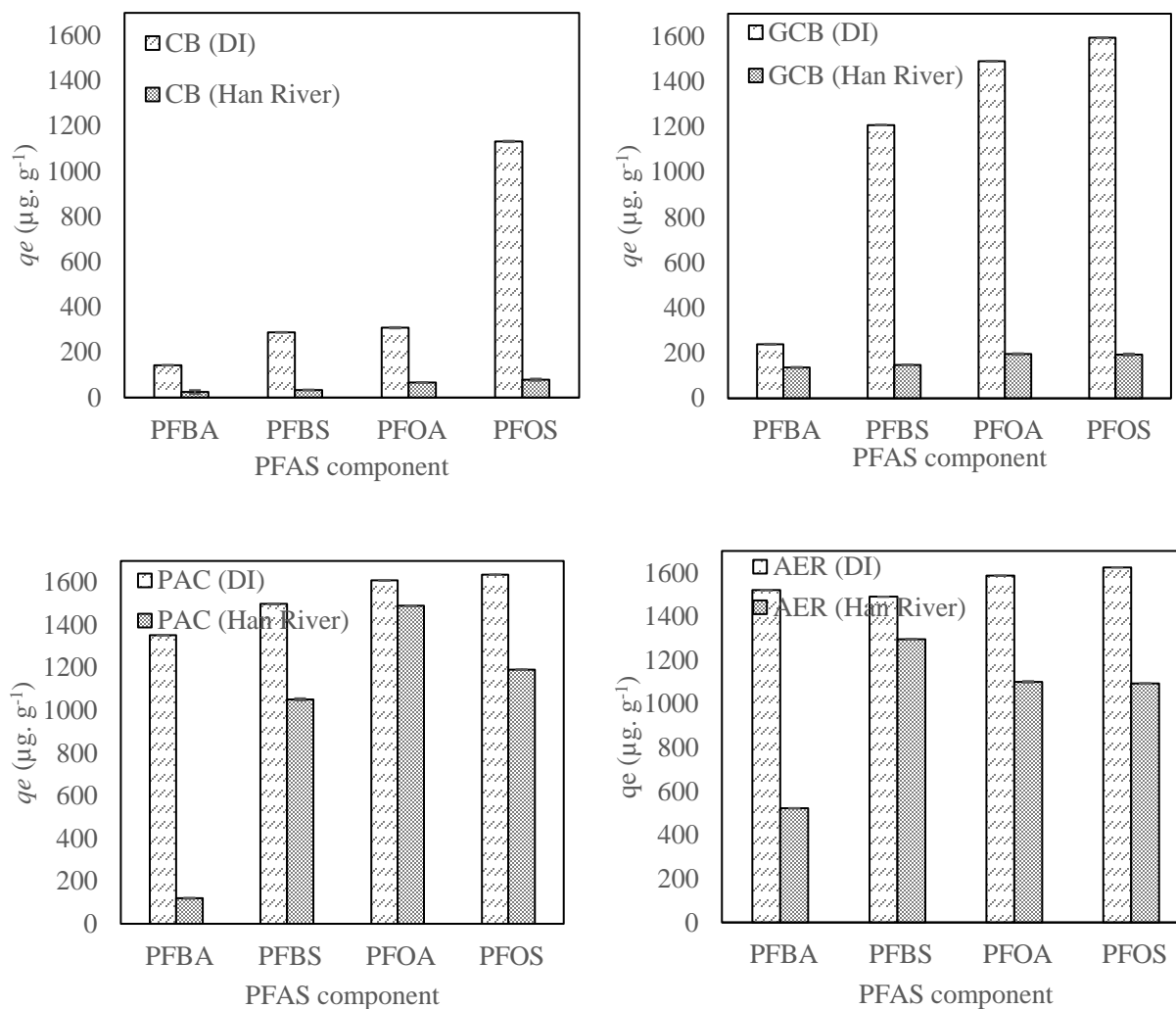
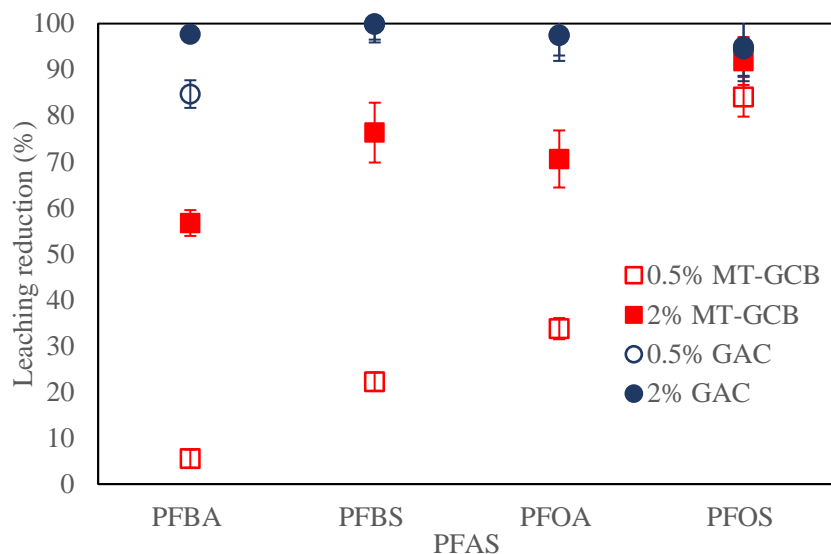


Fig. 4.18 Performance of each sorbents for PFAS sorption in DI an and Han river water

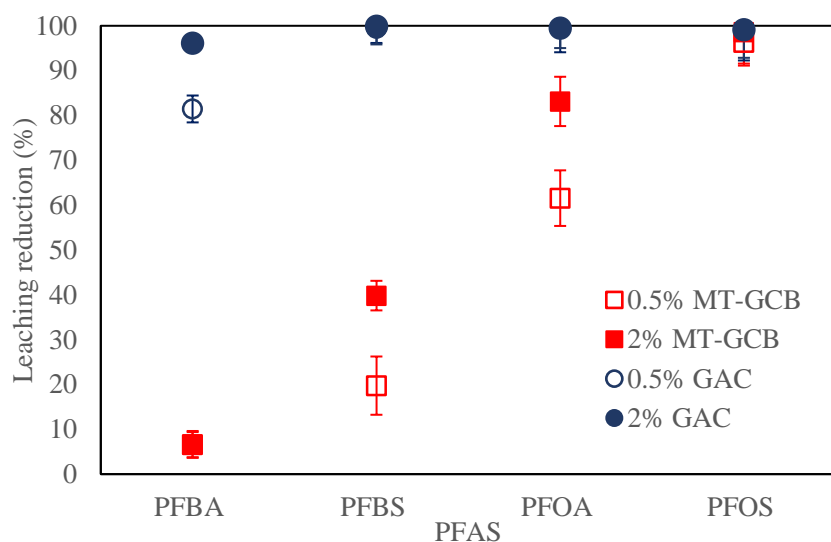
More reduction in sorption removal for CB and GCB sorbents could be attributed to their lower hydrophobicity when compared to PAC and AER (see table 4.4). Given that CB and GCB are less hydrophobic, and their PFAS sorption is primarily due to electrostatic attraction, anions with high concentrations in Han river water are more likely to be sorbet than PFAS substances by CB and GCB sorbents.

4.3.9 Leaching test results

Figure 4.19 depicts MT-GCB and GAC leaching tests on stabilized soil. The results showed that GAC has a high potential for stabilizing PFAS components within contaminated soil. According to figure 4.19, GAC demonstrated leachate reduction rate more than 90% for each PFAS component inside the contaminated soil by $1.5 \mu\text{g. g}^{-1}$ and $10 \mu\text{g. g}^{-1}$ concentrations. It has been demonstrated that 0.5% GAC can remove PFAS components at a rate greater than 90%, which is comparable to 2% GAC removal. However, in the case of PFBA, 0.5% GAC was less effective than 2% GAC. The obtained PFAS removal rate for GAC is consistent with other studies that used activated carbon as a stabilizer in contaminated soil. (Söregård et al. 2021; Sorengard et al. 2019; Sørmo et al. 2021).



(a)



(b)

Fig. 4.19 PFAS stabilization by MT-GCB and GAC inside the soil at (a) contamination level of $1.5 \mu\text{g}\cdot\text{g}^{-1}$, and (b) contamination level of $10 \mu\text{g}\cdot\text{g}^{-1}$

In comparison to GAC, the developed MT-GCB demonstrated lower efficiency for leaching reduction, particularly for short chain PFAS. The MT-GCB with 2% dosage had a higher PFAS component removal rate. The efficiency of MT-GCB for long short chain PFAS (PFOA and PFOS) appears to be comparable to GAC, but at the dosages tested, MT-GCB did not show excellent

removal for short chain PFAS. Adding 2% dosage of MT-GCB to the contaminated soil containing $1.5 \mu\text{g. g}^{-1}$ of each PFAS substances reduced leaching by 56.69%, 76.32%, 70.6%, and 91.87 for PFBA, PFBS, PFOA, and PFOS, respectively.

4.3.10 RSCCT results

Figure 4.20 (a-c) depicts the PFAS component breakthrough for each soil with varying fine content. As can be seen, the PFAS with shorter chains (PFBA, PFBS) exhibited earlier breakthroughs than the ones with longer chains (PFOA, PFOS). It means that, when compared to shorter chain PFASs, longer chain PFASs had a higher retardation factor. For example, for 5% fine content soil, PFBA (C4) showed almost complete breakthrough at $\sim 4\text{BV}$, whereas PFOS with eight carbon chain reached to complete breakthrough at higher BV ($\sim 9\text{BV}$). Also, long- chain PFAS with sulfonate groups showed a slower breakthrough than that one with carboxylic group. For example, for soil with 5% fine content, the PFOS with sulfonate group reached to its breakthrough at $\sim 9\text{BV}$, while for PFOA with carboxylic group breakthrough has completed at $\sim 7\text{BV}$. This is due to the fact that the length of the PFAS chain affects their physicochemical properties. Longer-chain PFAS are more hydrophobic than shorter-chain PFAS, and can be more sorbet by soil particles (Park et al. 2020).

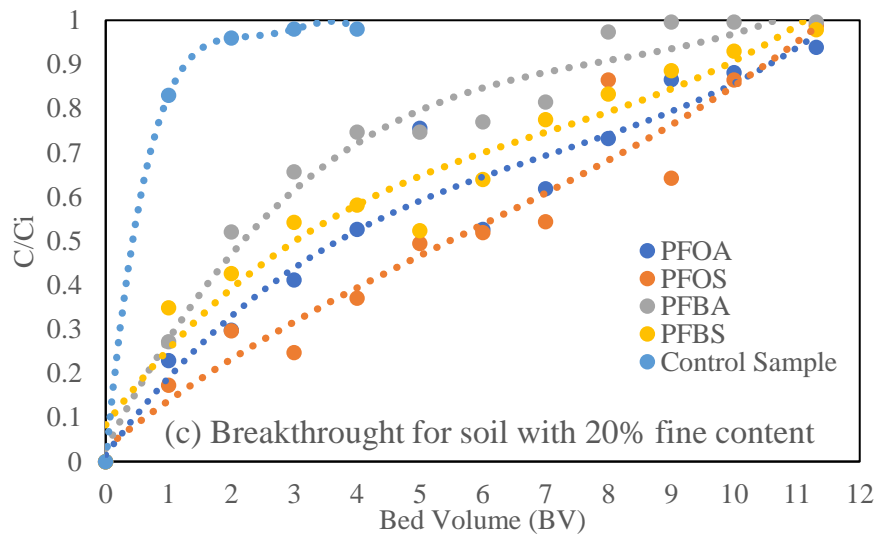
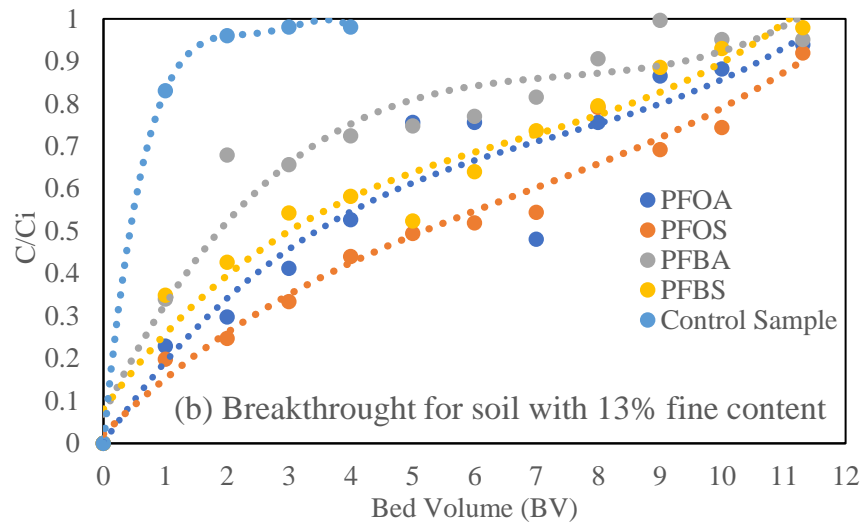
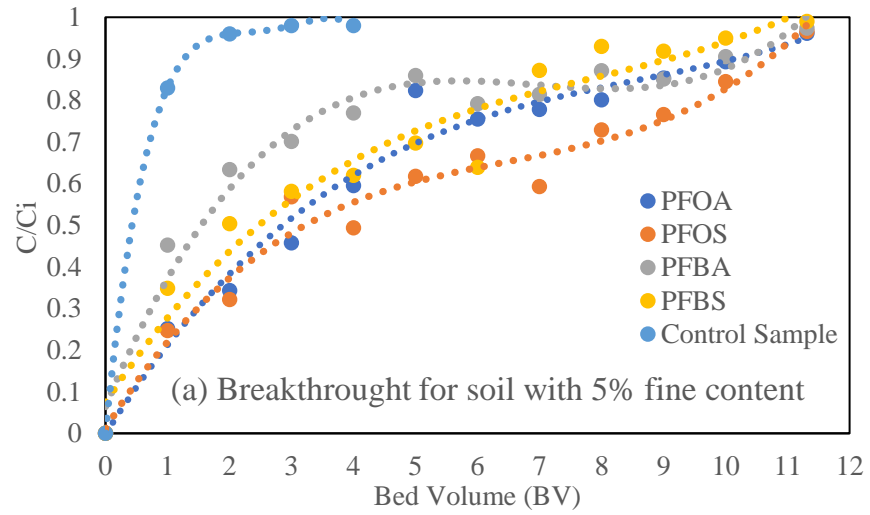


Fig. 4.20 (a-c) Breakthrough curves for PFAS components

Table 4.8 displays the calculated K_d and K_{oc} values for each PFAS component based on their retardation factor. Longer chain PFAS had higher K_d values than shorter chain PFAS, with K_d values decreasing in the sequence of PFOS > PFOA > PFBS > PFBA. This trend in K_d values is consistent with other studies as well (Milinovic et al. 2015; Nguyen et al. 2020). Furthermore, the obtained K_d values in this study were nearly consistent with other studies. For examples the obtained K_d value of Lomay sandy from batch experiments which conducted by Guelfo and Higgins (2013) were 0.61, 0.74, 0.8, and 4.65 L. Kg⁻¹ for PFBA, PFOA, PFBS, and PFOS, respectively. Except for PFOS, the achieved K_d values for the other PFASs were within the range of the current study. The difference in K_d value for PFOS may be due to differences in experimental procedure between this study and others. In another investigation which carried out by Aly et al. (2019) to determine the breakthrough of PFAS substances through Silty sand, the obtained K_d values for PFBS, PFOS, and PFOA were 0.21, 1.23, and 0.55 L. Kg⁻¹, respectively.

Table 4.8 Obtained K_d and K_{oc} values for each PFASs from column tests

Fine content of soil	PFAS	Coefficients	
		K_d (L. Kg ⁻¹)	$Log K_{oc}$ (L. Kg ⁻¹)
5%	PFOA	0.712	2.078
	PFOS	1.161	2.291
	PFBA	0.263	1.646
	PFBS	0.588	1.995
13%	PFOA	0.976	2.215
	PFOS	1.591	2.428
	PFBA	0.360	1.783
	PFBS	0.806	2.132
20%	PFOA	1.037	2.242
	PFOS	1.691	2.454
	PFBA	0.383	1.809
	PFBS	0.857	2.159

Figure 4.21 depicts the relationship between K_{oc} value and K_{ow} for each PFAS substance, along with the equations derived from it. The K_{oc} reported in other studies is primarily based on the batch experiments. The K_{oc} values obtained in this study were within the range of previous

studies, which were mostly estimated using batch sorption experiments. For example, Zhao et al. (2016) used a batch experiments to derive an equation that estimated the K_{oc} values of 1.53, 1.7, 2.5, and 2.8 for PFBA, PFBS, PFOA, and PFOS, respectively.

Almost identical breakthrough trends with the same K_{oc} values were obtained among soils with varying fine contents. It appears that the fine content of soil has not so much influence on the sorption of PFAS components, and overall, PFAS substance breakthrough occurs almost immediately in soils.

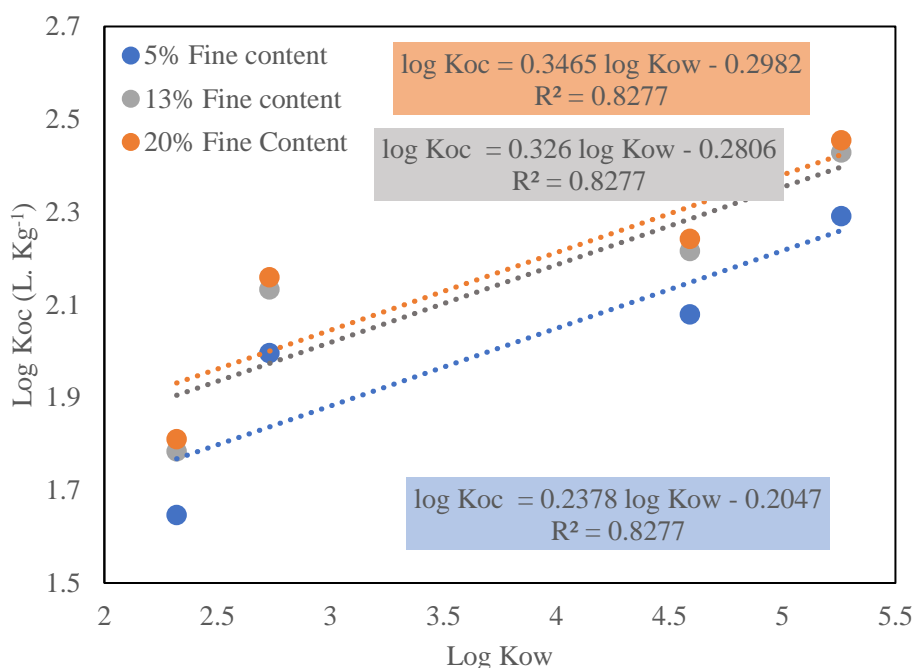


Fig. 4.21 Relationship between K_{oc} and K_{ow} values for each PFAS substance along with the derived equations

4.3.11 Cost comparison of GCB with other common sorbents

As it was discussed in section 4.2.6 chitosan powder, ECH, and PEI are the main three chemical materials for producing the GCB. The chitosan powder, ECH, and PEI can be provided in a market with average price of 14 US\$. Kg⁻¹, 6 US\$. Kg⁻¹, and 5 US\$. Kg⁻¹, respectively (Kim 2022).

Following the section 4.2.6 for making 1kg GCB 10 liter of chitosan solution is required, and the average price of each chitosan powder, ECH, and PEI for making this amount of chitosan

solution is 1.4 US\$, 0.6 US\$, and 2.5 US\$, respectively. Therefore, the total average price for making 1kg GCB in the laboratory will be 4.5 US\$.

It should be noted that this price of GCB is only based on the price of initial materials; by considering other secondary prices or even producing GCB on a commercial scale, the price of GCB could be somewhat reduced or even increased. However, at this step, the price of 4.5 US\$.kg⁻¹ can be considered as a basic average price for producing the GCB and compared to the prices of other commercial sorbents. Based on the reported unit costs, using GCB instead of the common commercial adsorbents could produce estimated cost savings of the order of 25 to 73.3% at 1m³ scale (Table 4.9).

Table 4.9 Cost comparison of GCB with common adsorbents

Material	Cost (US\$.Kg ⁻¹)	Average Bulk Density (Mg.m ⁻³)	Mass of fill material for 1m ³ scale (kg)	Average cost of fill material for 1m ³ scale (US\$)	Saving (%)
GCB	4.5	0.72	720	3240	—
CAC	9 (Kurniawan et al. 2006)	0.48 (Mohammed and Rashid 2012)	480	4320	25
AER	20	0.608 (Ziyang et al. 2001)	608	12160	73.3

Note: CAC, commercial activated carbon; AER, Anion Exchange Resin

4.4. Summary

At This chapter chitosan beads (CB) and grafted chitosan beads (GCB) were developed for removal of short and long chain PFAS at different range of concentration. It was obtained that CB and GCB are both good candidate for using as a sorbent material for PFAS removal, while grafted

chitosan showed better efficiency for PFAS removal. Based on the results, GCB showed the maximum adsorption capacities of 238.09, 277.7, 303.03, and 270.27 mg. g⁻¹ for PFOA, PFOS, PFBA and PFBS, respectively. The PFAS removal efficiency of the synthesized chitosan-based sorbents was compared to that of pulverized activated carbon (PAC) and anion exchange resin (AER), two of the most commonly used commercial sorbents. The summary of key findings from this chapter are as follows:

1. Grafting chitosan beads with PEI improved their sorption performance, either in terms of sorption capacity or sorption rate. The improved sorption performance of grafted chitosan beads was due to the addition of more amino functional groups to the surface of the chitosan beads, which increased their hydrophobicity and positivity surface charge.
2. When commercial sorbents were compared, AER had higher sorption capacity for PFAS removal particularly for short chain PFASs, while PAC had faster sorption rate. The higher sorption capacity of AER was due to its higher anion exchange capacity (AEC) with sufficient hydrophobicity, whereas finer particle size and shorter internal diffusion pathways for PAC could explain its faster PFAS sorption rate.
3. The developed GCB showed high sorption capacity as high as AER with fast sorption rate same as PAC. However, in comparison to PAC and AER, its efficiency has been reduced for PFAS removal in presence of real field water with high concentration of cation/anions.
4. The single point sorption test at environmentally relevant PFAS concentration (1000 ng. L⁻¹) showed that GCB has potential to sorb PFAS contaminates even at low concentrations. The obtained average K_d value from single point sorption test for GCB was in range of 1.5 -2.5, which was comparable values with those of PAC and AER.
5. Batch sorption experiments revealed that AER had constant removal efficiency for long and short-chain PFASs at pH ranges 3-10, whereas PAC removal efficiency decreased as pH increased. Furthermore, the efficiency of both CB and GCB has been decreased by increasing the pH values because of electrostatic repulsion.

6. At this study montmorillonite chitosan composite (MT-GCB) has been developed for stabilizing the PFAS substances inside the contaminated soils. The findings revealed that MT-GCB had comparable sorption efficiency to granular activated carbon (GAC), particularly for long-chain PFAS (PFOA and PFOS). Adding 2% dosage of MT-GCB to the contaminated soil containing $1.5 \mu\text{g. g}^{-1}$ of each PFAS substances reduced leaching by 56.69%, 76.32%, 70.6%, and 91.87 for PFBA, PFBS, PFOA, and PFOS, respectively.
7. PFAS substance breakthrough occurs almost immediately in soils where soil fine content has not significant influence on their breakthrough. The obtained K_{oc} values for soil with 5% fine content were 2.078, 2.291, 1.646, and 1.995 L. Kg^{-1} for PFOA, PFOS, PFBA, and PFBS, respectively.

Chapter 5. Conclusions and Recommendations

5.1 Conclusions

In research work presented in this dissertation some efficient and cost-effective sorbents from recyclable waste materials have been developed for removing the most common and emerging contaminants in Korea such as BTEX, PFAS, Pb, Cu, and Zn. Pulverized waste tire (PWT) and chitosan, two of Korea's most abundant wastes, were chosen to create sorbents for removing contaminants from water or soil. The geotechnical performance of soil-pulverized waste tire (S-PWT) mixtures as engineering fill materials was evaluated while simultaneously PWT mixed with soil was used for removing BTEX components and heavy metals. Furthermore, tire-derived activated carbon (TAC) has been synthesized through carbonization and chemical activation and has been used to remove heavy metals. Long and short chain PFAS were removed from soil and water using newly developed chitosan-based sorbents such as chitosan beads (CB), grafted chitosan beads (GCB), and montmorillonite chitosan composite (MT-GCB). The following are the major conclusions of the research work presented in this dissertation:

1. The experimental findings showed that PWT material is an efficient adsorbent for the removal of both heavy metals and BTEX from aqueous solutions. Based on the direct shear test results the shear behavior of the standard Proctor-compacted S–PWT mixtures became more ductile as the PWT content increased. The effective friction angle decreased modestly in value from 39.9° to 34.9° for PWT content increasing from 5 to 25 wt%. The BTEX sorption and strength properties of the mixture increased and decreased as the PWT content increased. Following the findings, a mixing ratio of less than 15% is recommended as an optimum mixing ratio for satisfying both geotechnical and environmental properties of a Soil/Tire mixture.

2. The sorption results revealed that TAC outperformed commercial activated carbon in terms of sorption capacity and sorption rate for heavy metal removal from aqueous solutions (CAC). The maximum adsorption capacities of TAC were found to be 322.5, 185.2 and 71.9 mg·g⁻¹ for Pb, Cu, and Zn ions, respectively. These values were higher than the results obtained for CAC. Moreover, the equilibrium times for the TAC and CAC samples were within 6 and 24 h, respectively.
3. The leaching of inorganics from the PWT and TAC surface was increased by decreasing the pH value. Zinc was the most leachable metal from both PWT and TAC. Except for those in highly acidic conditions (pH 1), the metals released from PWT and TAC were below the MCL given by the US EPA. Based on these findings, the application of these sorbents in neutral and alkaline conditions is safe, while their usage in highly acidic conditions should be considered cautiously.
4. Comparing to CB, GCB showed better performance for removing both short and long chain PFAS from aqueous phase. The obtained sorption capacities for GCB were 238.09, 277.7, 303.03, and 270.27 mg·g⁻¹ for PFOA, PFOS, PFBA, and PFBS, respectively. These values were comparable with those obtained for anion exchange resin (AER) as one the most efficient commercial sorbent. The obtained sorption capacities by Langmuir model for AER were 238.09, 263.1, 263.15, and 238.09 mg·g⁻¹ for PFOA, PFOS, PFBA, and PFBS, respectively.
5. The kinetic sorption tests revealed GCB has fast sorption rate for sorption the PFAS substance from aqueous phase. The equilibrium time for GCB was less than 5 minutes, which was same as equilibrium time for pulverized activated carbon (PAC).
6. The single point sorption results demonstrated that the developed GCB has the potential to remove PFAS contaminants at concentrations close to those found in the environment. The obtained average K_d value from single point sorption test for GCB was in range of 1.5 -2.5, which was comparable values with those of PAC and AER. However, the efficiency of GCB

for PFAS removal from real field water (Han river water) with high anion/cation concentrations was lower than that of AER and PAC.

7. The leaching tests for PFAS contaminated soil revealed that the synthesized MT-GCB had the potential to stabilize the PFAS substances within the contaminated soils. According to the findings, MT-GCB had comparable sorption efficiency to granular activated carbon (GAC), especially for long-chain PFASs. The leaching of PFBA, PFBS, PFOA, and PFOS was reduced by 56.69%, 76.32%, 70.6%, and 91.87, respectively, by adding 2% MT-GCB to contaminated soil containing $1.5 \mu\text{g} \cdot \text{g}^{-1}$ of each PFAS substance.
8. The obtained K_d and K_{oc} values for PFAS components demonstrated that PFAS breakthrough occurs immediately in soils, indicating that PFAS sorption by soil is not a significant factor for their fate and transport through soils.

5.2 Recommendations for future studies

The experimental studies on batch adsorption presented in this dissertation have helped to introduce some developed sorbents from recyclable wastes for removing organic and inorganic contaminants. Further research on this topic, particularly on PFAS substances, that can be conducted with potential subjects includes the following:

1. Evaluating the geotechnical properties of chitosan-based sorbents for using them as adsorptive fill materials.
2. Developing sorbents from waste material with the goal of having the same removal efficiency for short-chain PFAS as long-chain PFAS.
3. Creating some sorbents with more selective sorption for PFAS substances in the presence of other cations/anions.
4. Estimating the distribution factor (K_d) of PFAS contaminants for soils by considering influential parameter such as pH, organic content of soil and soil mineralogy.

5. Reduction and degradation of PFAS contaminants either from the polluted soil or exhausted sorbents.
6. Performing 3D soil box experiments for sorption and degradation of PFAS components to simulate the real field conditions.

Bibliography

- Abbaspour, M., Aflaki, E., and Nejad, F. M. (2019). "Reuse of waste tire textile fibers as soil reinforcement." *J. Clean. Prod.*, 207, 1059–1071.
- Acosta, R., Fierro, V., De Yuso, A. M., Nabarlantz, D., and Celzard, A. (2016). "Tetracycline adsorption onto activated carbons produced by KOH activation of tyre pyrolysis char." *Chemosphere*, 149, 168–176.
- Acosta, R., Nabarlantz, D., Sánchez-Sánchez, A., Jagiello, J., Gadonneix, P., Celzard, A., and Fierro, V. (2018). "Adsorption of Bisphenol A on KOH-activated tyre pyrolysis char." *J. Environ. Chem. Eng.*, 6(1), 823–833.
- Ahmad, Z., Gao, B., Mosa, A., Yu, H., Yin, X., Bashir, A., Ghozeisi, H., and Wang, S. (2018). "Removal of Cu (II), Cd (II) and Pb (II) ions from aqueous solutions by biochars derived from potassium-rich biomass." *J. Clean. Prod.*, 180, 437–449.
- Ahmed, M., Johir, M., McLaughlan, R., Nguyen, L. N., Xu, B., and Nghiem, L. D. (2020). "Per- and polyfluoroalkyl substances in soil and sediments: Occurrence, fate, remediation and future outlook." *Sci. Total Environ.*, 748, 141251.
- Aivalioti, M., Papoulias, P., Kousaiti, A., and Gidarakos, E. (2012). "Adsorption of BTEX, MTBE and TAME on natural and modified diatomite." *J. Hazard. Mater.*, 207, 117–127.
- Aivalioti, M., Vamvasakis, I., and Gidarakos, E. (2010). "BTEX and MTBE adsorption onto raw and thermally modified diatomite." *J. Hazard. Mater.*, 178(1–3), 136–143.
- Alamo-Nole, L. A., Perales-Perez, O., and Roman-Velazquez, F. R. (2011). "Sorption study of toluene and xylene in aqueous solutions by recycled tires crumb rubber." *J. Hazard. Mater.*, 185(1), 107–111.
- Almeida, I. L. S., Filho, N. R. A., Alves, M. I. R., Carvalho, B. G., and Coelho, N. M. M. (2012). "Removal of BTEX from aqueous solution using Moringa oleifera seed cake." *Environ. Technol.*, 33(11), 1299–1305.
- Aly, Y. H., McInnis, D. P., Lombardo, S. M., Arnold, W. A., Pennell, K. D., Hatton, J., and Simcik, M. F. (2019). "Enhanced adsorption of perfluoro alkyl substances for in situ remediation." *Environ. Sci.: Water Res. Technol.*, 5(11), 1867–1875.
- Amuthan, M., Boominathan, A., and Banerjee, S. (2018). "Density and Shear Strength of Particulate Rubber Mixed with Sand and Fly Ash." *J. Mater. Civ. Eng.*, 30(7), 04018136.
- Anbazhagan, P., Manohar, D., and Rohit, D. (2017). "Influence of size of granulated rubber and tyre chips on the shear strength characteristics of sand-rubber mix." *Geomech. Geoengin.*, 12(4), 266–278.
- Anirudhan, T., and Sreekumari, S. (2011). "Adsorptive removal of heavy metal ions from industrial effluents using activated carbon derived from waste coconut buttons." *J. Environ. Sci.*, 23(12), 1989–1998.
- Anjum, H., Johari, K., Gnanasundaram, N., Appusamy, A., and Thanabalan, M. (2019). "Impact of surface modification on adsorptive removal of BTX onto activated carbon." *J. Mol. Liq.*, 280, 238–251.
- Asenjo, N. G., Álvarez, P., Granda, M., Blanco, C., Santamaría, R., and Menéndez, R. (2011). "High performance activated carbon for benzene/toluene adsorption from industrial wastewater." *J. Hazard. Mater.*, 192(3), 1525–1532.
- Askeland, M., Clarke, B. O., Cheema, S. A., Mendez, A., Gasco, G., and Paz-Ferreiro, J. (2020). "Biochar sorption of PFOS, PFOA, PFHxS and PFHxA in two soils with contrasting texture." *Chemosphere*, 249, 126072.

- ASTM D2434-68 (2006). "Standard test method for permeability of granular soils (constant head)." *ASTM International, West Conshohocken, PA, USA*.
- ASTM D698-12e2 (2007). "Standard test methods for laboratory compaction characteristics of soil using standard effort (12 400 ft-lbf/ft³ (600 kN-m/m³))." *ASTM International, West Conshohocken, PA, USA*.
- ASTM D3080M-11 (2002). "Standard test method for direct shear test of soils under consolidated drained conditions." *ASTM International, West Conshohocken, PA, USA*.
- ASTM D2435M-11 (2011). "Standard test method for one-dimensional consolidation properties of soils." *ASTM International, West Conshohocken, PA, USA*.
- Ateia, M., Alsbaiee, A., Karanfil, T., and Dichtel, W. (2019). "Efficient PFAS removal by amine-functionalized sorbents: critical review of the current literature." *Environ. Sci. Technol. Lett.*, 6(12), 688–695.
- Ateia, M., Arifuzzaman, M., Pellizzeri, S., Attia, M. F., Tharayil, N., Anker, J. N., and Karanfil, T. (2019). "Cationic polymer for selective removal of GenX and short-chain PFAS from surface waters and wastewaters at ng/L levels." *Water Res.*, 163, 114874.
- Ateia, M., Maroli, A., Tharayil, N., and Karanfil, T. (2019). "The overlooked short- and ultrashort-chain poly- and perfluorinated substances: A review." *Chemosphere*, 220, 866–882.
- Babiker, E., Al-Ghouti, M. A., Zouari, N., and McKay, G. (2019). "Removal of boron from water using adsorbents derived from waste tire rubber." *J. Environ. Chem. Eng.*, 7(2), 102948.
- Baimenov, A., Berillo, D. A., Pouloupoulos, S. G., and Inglezakis, V. J. (2020). "A review of cryogels synthesis, characterization and applications on the removal of heavy metals from aqueous solutions." *Adv. Colloid Interface Sci.*, 276, 102088.
- Banaszkiewicz, K., and Badura, M. (2019). "Experimental investigation on the application of recycled tires polymer fibers as a BTEX removal material." *SN Appl. Sci.*, 1(6), 1–10.
- Bansal, R. C., and Goyal, M. (2005). "Activated carbon adsorption." *First ed. Boca Raton: CRC press*.
- Barrett, E. P., Joyner, L. G., and Halenda, P. P. (1951). "The determination of pore volume and area distributions in porous substances. I. Computations from nitrogen isotherms." *J. Am. Chem. Soc.*, 73(1), 373–380.
- Bartilotti, M., Viana, T. S., de Oliveira, D. P., Santos, E. V., Rojas-Mantilla, H. D., Santos, M. C., and Zanoni, M. V. B. (2021). "Assessment of the improved performance of magnetite-modified vermiculite in the reduction of BTEX and metals, as well as toxicity in petroleum-produced water." *J. Water Process. Eng.*, 39, 101749.
- Bhattacharya, P., Banerjee, P., Mallick, K., Ghosh, S., Majumdar, S., Mukhopadhyay, A., and Bandyopadhyay, S. (2013). "Potential of biosorbent developed from fruit peel of *Trewia nudiflora* for removal of hexavalent chromium from synthetic and industrial effluent: Analyzing phytotoxicity in germinating *Vigna* seeds." *J. Environ. Sci. Health A*, 48(7), 706–719.
- Bhattacharyya, K. G., and Gupta, S. S. (2008). "Adsorption of a few heavy metals on natural and modified kaolinite and montmorillonite: a review." *Adv. Colloid Interface Sci.*, 140(2), 114–131.
- Bhatti, I. A., Ahmad, N., Iqbal, N., Zahid, M., and Iqbal, M. (2017). "Chromium adsorption using waste tire and conditions optimization by response surface methodology." *J. Environ. Chem. Eng.*, 5(3), 2740–2751.

- Biswas, K., Saha, S. K., and Ghosh, U. C. (2007). "Adsorption of fluoride from aqueous solution by a synthetic iron (III)–aluminum (III) mixed oxide." *Ind. Eng. Chem. Res.*, 46(16), 5346–5356.
- Boglaienko, D., and Tansel, B. (2017). "Wicking of light hydrophobic liquid phase from water by pulverized rubber: Theoretical and experimental analyses." *J. Hazard. Mater.*, 325, 189–197.
- Bolan, N., Sarkar, B., Yan, Y., Li, Q., Wijesekara, H., Kannan, K., Tsang, D. C., Schauer, M., Bosch, J., and Noll, H. (2021). "Remediation of poly-and perfluoroalkyl substances (PFAS) contaminated soils—To mobilize or to immobilize or to degrade?" *J. Hazard. Mater.*, 401, 123892.
- Boominathan, A., and Banerjee, S. (2019). "Engineering properties of sand–rubber tire shred mixtures." *Int. J. Geotech. Eng.*, 15(9), 1061–1077.
- Boostani, H. R., Najafi-Ghiri, M., and Hardie, A. G. (2019). "Single and competitive adsorption isotherms of some heavy metals onto a light textured calcareous soil amended with agricultural wastes-biochars." *Arch. Agron. Soil Sci.*, 65(3), 360–373.
- Bräunig, J., Baduel, C., and Mueller, J. "Influence of a commercial adsorbent on the leaching behaviour and bioavailability of selected perfluoroalkyl acids (PFAAs) from soil impacted by AFFFs." *37th International Symposium on Halogenated Persistent Organic Pollutants, Dioxin 2017, Vancouver, Canada, 20–25 August 2017*.
- Brunauer, S., Emmett, P. H., and Teller, E. (1938). "Adsorption of gases in multimolecular layers." *J. Am. Chem. Soc.*, 60(2), 309–319.
- Brusseau, M. L., Anderson, R. H., and Guo, B. (2020). "PFAS concentrations in soils: Background levels versus contaminated sites." *Sci. Total Environ.*, 740, 140017.
- Calisir, F., Roman, F., Alamo, L., Perales, O., Arocha, M., and Akman, S. (2009). "Removal of Cu (II) from aqueous solutions by recycled tire rubber." *Desalination*, 249(2), 515–518.
- Çelebi, H., Gök, G., and Gök, O. (2020). "Adsorption capability of brewed tea waste in waters containing toxic lead (II), cadmium (II), nickel (II), and zinc (II) heavy metal ions." *Sci. Rep.*, 10(1), 1–12.
- Cetin, H., Fener, M., and Gunaydin, O. (2006). "Geotechnical properties of tire-cohesive clayey soil mixtures as a fill material." *Eng. Geol.*, 88(1-2), 110–120.
- Chatterjee, S., Chatterjee, T., and Woo, S. H. (2011). "Influence of the polyethyleneimine grafting on the adsorption capacity of chitosan beads for Reactive Black 5 from aqueous solutions." *Chem. Eng. J.*, 166(1), 168–175.
- Chen, T., Zhang, Y., Wang, H., Lu, W., Zhou, Z., Zhang, Y., and Ren, L. (2014). "Influence of pyrolysis temperature on characteristics and heavy metal adsorptive performance of biochar derived from municipal sewage sludge." *Bioresour. Technol.*, 164, 47–54.
- Ching, C., Klemes, M. J., Trang, B., Dichtel, W. R., and Helbling, D. E. (2020). "β-cyclodextrin polymers with different cross-linkers and ion-exchange resins exhibit variable adsorption of anionic, zwitterionic, and nonionic PFASs." *Environ. Sci. Technol.*, 54(19), 12693–12702.
- Choi, G.H., Lee, D.Y., Jeong, D.K., Kuppusamy, S., Lee, Y. B., Park, B. J., and Kim, J.H. (2017). "Perfluorooctanoic acid (PFOA) and perfluorooctanesulfonic acid (PFOS) concentrations in the South Korean agricultural environment: A national survey." *J. Integr. Agric.*, 16(8), 1841–1851.

- Chowdhury, P., Athapaththu, S., Elkamel, A., and Ray, A. K. (2017). "Visible-solar-light-driven photo-reduction and removal of cadmium ion with Eosin Y-sensitized TiO₂ in aqueous solution of triethanolamine." *Sep. Purif. Technol.*, 174, 109–115.
- Crini, G., and Lichtfouse, E. (2019). "Chitin and chitosan: applications in food, agriculture, pharmacy, medicine and wastewater treatment.", *Sustain. Agric. Rev.*, 36, Springer.
- Del Moral, L. L., Choi, Y. J., and Boyer, T. H. (2020). "Comparative removal of Suwannee River natural organic matter and perfluoroalkyl acids by anion exchange: Impact of polymer composition and mobile counterion." *Water Res.*, 178, 115846.
- Deng, S., Nie, Y., Du, Z., Huang, Q., Meng, P., Wang, B., Huang, J., and Yu, G. (2015). "Enhanced adsorption of perfluorooctane sulfonate and perfluorooctanoate by bamboo-derived granular activated carbon." *J. Hazard. Mater.*, 282, 150–157.
- Deng, S., Yu, Q., Huang, J., and Yu, G. (2010). "Removal of perfluorooctane sulfonate from wastewater by anion exchange resins: Effects of resin properties and solution chemistry." *Water Res.*, 44(18), 5188–5195.
- Deng, Y., Morris, C., Rakshit, S., Landa, E., Punamiya, P., and Sarkar, D. (2016). "Water treatment residuals and scrap tire rubber as green sorbents for removal of stormwater metals." *Water Environ. Res.*, 88(6), 500–509.
- Depaolini, A. R., Bianchi, G., Fornai, D., Cardelli, A., Badalassi, M., Cardelli, C., and Davoli, E. (2017). "Physical and chemical characterization of representative samples of recycled rubber from end-of-life tires." *Chemosphere*, 184, 1320–1326.
- Dickson, T. H., Dwyer, D. F., and Humphrey, D. N. (2001). "Prototype tire-shred embankment construction." *Transp. Res. Rec.*, 1755(1), 160–167.
- Disfani, M. M., Tsang, H.H., Arulrajah, A., and Yaghoubi, E. (2017). "Shear and compression characteristics of recycled glass-tire mixtures." *J. M. Civil Eng.*, 29(6), 06017003.
- Dixit, F., Barbeau, B., Mostafavi, S. G., and Mohseni, M. (2020). "Removal of legacy PFAS and other fluorotelomers: optimized regeneration strategies in DOM-rich waters." *Water Res.*, 183, 116098.
- Dixit, F., Dutta, R., Barbeau, B., Berube, P., and Mohseni, M. (2021). "PFAS removal by ion exchange resins: A review." *Chemosphere*, 272, 129777.
- Drescher, A., Newcomb, D., and Heimdahl, T. (1999). "Deformability of shredded tires." Minnesota. Dept. of Transportation.
- Du, Z., Deng, S., Zhang, S., Wang, B., Huang, J., Wang, Y., Yu, G., and Xing, B. (2016). "Selective and high sorption of perfluorooctanesulfonate and perfluorooctanoate by fluorinated alkyl chain modified montmorillonite." *J. Phys. Chem. C.*, 120(30), 16782–16790.
- Du, Z., Deng, S., Zhang, S., Wang, W., Wang, B., Huang, J., Wang, Y., Yu, G., and Xing, B. (2017). "Selective and fast adsorption of perfluorooctanesulfonate from wastewater by magnetic fluorinated vermiculite." *Environ. Sci. Technol.*, 51(14), 8027–8035.
- Eeshwarasinghe, D., Loganathan, P., and Vigneswaran, S. (2019). "Simultaneous removal of polycyclic aromatic hydrocarbons and heavy metals from water using granular activated carbon." *Chemosphere*, 223, 616–627.
- Eichler, C. M., and Little, J. C. (2020). "A framework to model exposure to per- and polyfluoroalkyl substances in indoor environments." *Environ. Sci.: Process. Impacts*, 22(3), 500–511.

- Elanchezhiyan, S. S., Preethi, J., Rathinam, K., Njaramba, L. K., and Park, C. M. (2021). "Synthesis of magnetic chitosan biopolymeric spheres and their adsorption performances for PFOA and PFOS from aqueous environment." *Carbohydr. Polym.*, 267, 118165.
- EPA (1986). "Test methods for evaluating solid waste:physical/chemical methods, SW-846." *U.S. Environmental Protection Agency, Washington, DC.*
- EPA (2006). "Acid rain program 2005 progress report." *EPA-430-R-06-015. Clean Air Markets Division, Office of Air and Radiation, U.S. Environmental Protection Agency, Washington, DC.*
- EPA (2009). "National primary drinking water regulations." *EPA 8106-F-09-004, U.S. Environmental Protection Agency, Washington, DC.*
- Esfandiar, N., Suri, R., and McKenzie, E. R. (2022). "Competitive sorption of Cd, Cr, Cu, Ni, Pb and Zn from stormwater runoff by five low-cost sorbents; Effects of co-contaminants, humic acid, salinity and pH." *J. Hazard. Mater.*, 423, 126938.
- Fang, Y., Ellis, A., Choi, Y. J., Boyer, T. H., Higgins, C. P., Schaefer, C. E., and Strathmann, T. J. (2021). "Removal of per- and polyfluoroalkyl substances (PFASs) in aqueous film-forming foam (AFFF) using ion-exchange and nonionic resins." *Environ. Sci. Technol.*, 55(8), 5001–5011.
- Feizi, M., Jalali, M., Antoniadis, V., Shaheen, S. M., Ok, Y. S., and Rinklebe, J. (2019). "Geo- and nano-materials affect the mono-metal and competitive sorption of Cd, Cu, Ni, and Zn in a sewage sludge-treated alkaline soil." *J. Hazard. Mater.*, 379, 120567.
- Freundlich, H. (1907). "Über die adsorption in lösungen." *Zeitschrift für physikalische Chemie*, 57(1), 385–470.
- Gao, Y., Deng, S., Du, Z., Liu, K., and Yu, G. (2017). "Adsorptive removal of emerging polyfluoroalkyl substances F-53B and PFOS by anion-exchange resin: A comparative study." *J. Hazard. Mater.*, 323, 550–557.
- Gautam, R. K., Mudhoo, A., Lofrano, G., and Chattopadhyaya, M. C. (2014). "Biomass-derived biosorbents for metal ions sequestration: Adsorbent modification and activation methods and adsorbent regeneration." *J. Environ. Chem. Eng.*, 2(1), 239–259.
- Gelder, C., and Fowmes, G. J. (2016). "Mixing and compaction of fibre- and lime-modified cohesive soil." *Proc. Inst. Civ. Eng. Ground Improv.*, 169(2), 98–108.
- Ghazavi, M., Ghaffari, J., and Farshadfar, A. (2011). "Experimental determination of waste tire chip-sand-geogrid interface parameters using large direct shear tests." *Proc. Fifth Symp. Advances in Science and Technology, Mashhad, Iran, paper 0702-995, 9pp.*
- Gong, H., Song, W., Huang, B., Shu, X., Han, B., Wu, H., and Zou, J. (2019). "Direct shear properties of railway ballast mixed with tire derived aggregates: Experimental and numerical investigations." *Constr. Build. Mater.*, 200, 465–473.
- Gualtieri, M., Andrioletti, M., Vismara, C., Milani, M., and Camatini, M. (2005). "Toxicity of tire debris leachates." *Environ. Int.*, 31(5), 723–730.
- Guelfo, J. L., and Higgins, C. P. (2013). "Subsurface transport potential of perfluoroalkyl acids at aqueous film-forming foam (AFFF)-impacted sites." *Environ. Sci. Technol.*, 47(9), 4164–4171.
- Guo, S., Dan, Z., Duan, N., Chen, G., Gao, W., and Zhao, W. (2018). "Zn (II), Pb (II), and Cd (II) adsorption from aqueous solution by magnetic silica gel: preparation, characterization, and adsorption." *Environ. Sci. Pollut. Res.*, 25(31), 30938–30948.

- Gupta, V. K., Ali, I., Saleh, T. A., Siddiqui, M., and Agarwal, S. (2013). "Chromium removal from water by activated carbon developed from waste rubber tires." *Environ. Sci. Pollut. Res.*, 20(3), 1261–1268.
- Gupta, V. K., Ganjali, M., Nayak, A., Bhushan, B., and Agarwal, S. (2012). "Enhanced heavy metals removal and recovery by mesoporous adsorbent prepared from waste rubber tire." *Chem. Eng. J.*, 197, 330–342.
- Harada, K. H., Yang, H.R., Moon, C.S., Hung, N. N., Hitomi, T., Inoue, K., Niisoe, T., Watanabe, T., Kamiyama, S., and Takenaka, K. (2010). "Levels of perfluorooctane sulfonate and perfluorooctanoic acid in female serum samples from Japan in 2008, Korea in 1994–2008 and Vietnam in 2007–2008." *Chemosphere*, 79(3), 314–319.
- He, J., Li, Y., Wang, C., Zhang, K., Lin, D., Kong, L., and Liu, J. (2017). "Rapid adsorption of Pb, Cu and Cd from aqueous solutions by β -cyclodextrin polymers." *Appl. Surf. Sci.*, 426, 29–39.
- He, P., Yu, Q., Zhang, H., Shao, L., and Lü, F. (2017). "Removal of copper (II) by biochar mediated by dissolved organic matter." *Sci. Rep.*, 7(1), 1–10.
- Holtz, R. D., Kovacs, W. D., and Sheahan, T. (2011). "An Introduction to Geotechnical Engineering 2nd." *Pearson plc*.
- Hoppe, E. J., and Mullen, W. G. (2004). "Field study of a shredded-tire embankment in Virginia." Virginia Transportation Research Council.
- Hotová, G., Slovák, V., Zelenka, T., Maršálek, R., and Parchaňská, A. (2020). "The role of the oxygen functional groups in adsorption of copper (II) on carbon surface." *Sci. Total Environ.*, 711, 135436.
- Hou, L., Kumar, D., Yoo, C. G., Gitsov, I., and Majumder, E. L.W. (2021). "Conversion and removal strategies for microplastics in wastewater treatment plants and landfills." *Chem. Eng. J.*, 406, 126715.
- Huang, X., Zhao, H., Zhang, G., Li, J., Yang, Y., and Ji, P. (2020). "Potential of removing Cd (II) and Pb (II) from contaminated water using a newly modified fly ash." *Chemosphere*, 242, 125148.
- Humphrey, D., Whetten, N., Weaver, J., and Recker, K. "Tire shreds as lightweight fill for construction on weak marine clay." *Proc., Proc., Int. Symp. on Coastal Geotechnical Engineering in Practice*, Citeseer, Balkema, Rotterdam, The Netherlands, 611–616.
- Inam, E., Etim, U., Akpabio, E., and Umoren, S. (2017). "Process optimization for the application of carbon from plantain peels in dye abstraction." *J. Taibah Univ. Sci.*, 11(1), 173–185.
- Isinkaralar, K., Gullu, G., and Turkyilmaz, A. (2022). "Experimental study of formaldehyde and BTEX adsorption onto activated carbon from lignocellulosic biomass." *Biomass Convers. Biorefin.*, 1–11.
- Islam, M. N., Taki, G., Nguyen, X. P., Jo, Y. T., Kim, J., and Park, J.H. (2017). "Heavy metal stabilization in contaminated soil by treatment with calcined cockle shell." *Environ. Sci. Pollut. Res.*, 24(8), 7177–7183.
- Jayawardhana, Y., Keerthanan, S., Lam, S. S., and Vithanage, M. (2021). "Ethylbenzene and toluene interactions with biochar from municipal solid waste in single and dual systems." *Environmental Research*, 197, 111102.
- Jeon, C., Solis, K. L., An, H.R., Hong, Y., Igalavithana, A. D., and Ok, Y. S. (2020). "Sustainable Removal of Hg (II) by Sulfur-Modified Pine-Needle Biochar." *J. Hazard. Mater.*, 388, 122048.

- Joseph, I. V., Tosheva, L., and Doyle, A. M. (2020). "Simultaneous removal of Cd (II), Co (II), Cu (II), Pb (II), and Zn (II) ions from aqueous solutions via adsorption on FAU-type zeolites prepared from coal fly ash." *J. Environ. Chem. Eng.*, 8(4), 103895.
- Kabiri, S., Tucker, W., Navarro, D. A., Braunig, J., Thompson, K., Knight, E. R., Nguyen, T. M. H., Grimison, C., Barnes, C. M., and Higgins, C. P. (2021). "Comparing the leaching behavior of per-and polyfluoroalkyl substances from contaminated soils using static and column leaching tests." *Environ. Sci. Technol.*, 56(1), 368–378.
- Karmacharya, M. S., Gupta, V. K., and Jha, V. K. (2016). "Preparation of activated carbon from waste tire rubber for the active removal of Cr (VI) and Mn (II) ions from aqueous solution." *T. Indian Ceram. Soc.*, 75(4), 234–241.
- Kavand, M., Eslami, P., and Rازه, L. (2020). "The adsorption of cadmium and lead ions from the synthesis wastewater with the activated carbon: Optimization of the single and binary systems." *J. Water Process. Eng.*, 34, 101151.
- Kim, E. J., Park, Y. M., Park, J.E., and Kim, J.g. (2014). "Distributions of new Stockholm convention POPs in soils across South Korea." *Sci. Total Environ.*, 476, 327–335.
- Kim, H.K., and Santamarina, J. (2008). "Sand–rubber mixtures (large rubber chips)." *Can. Geotech. J.*, 45(10), 1457–1466.
- Kim, H. Y., Seok, H.W., Kwon, H. O., Choi, S.D., Seok, K.S., and Oh, J. E. (2016). "A national discharge load of perfluoroalkyl acids derived from industrial wastewater treatment plants in Korea." *Sci. Total Environ.*, 563, 530–537.
- Kim, H., Ekpe, O. D., Lee, J.H., Kim, D.H., and Oh, J.E. (2019). "Field-scale evaluation of the uptake of Perfluoroalkyl substances from soil by rice in paddy fields in South Korea." *Sci. Total Environ.*, 671, 714–721.
- Kim, J. Y., Park, J. K., and Edil, T. B. (1997). "Sorption of organic compounds in the aqueous phase onto tire rubber." *J. Environ. Eng.*, 123(9), 827–835.
- Kim, S. (2022). "Blending of waste biomass for cost-effective chitosan-based biosorbents for removal of reactive dye from aqueous solution." *Environ. Eng. Res.*, 27(6), 210457.
- Kim, Y., and Kang, H. (2013). "Effects of rubber and bottom ash inclusion on geotechnical characteristics of composite geomaterial." *Mar. Georesources Geotechnol.*, 31(1), 71–85.
- Klimes, M.J., Ling, Y., Ching, C., Wu, C., Xiao, L., Helbling, D. E., and Dichtel, W. R. (2019). "Reduction of a tetrafluoroterephthalonitrile- β -cyclodextrin polymer to remove anionic micropollutants and perfluorinated alkyl substances from water." *Angew. Chem.*, 131(35), 12177–12181.
- Ko, M.S., Jeon, Y.J., and Kim, K.W. (2022). "Novel application of xanthan gum-based biopolymer for heavy metal immobilization in soil." *J. Environ. Chem. Eng.*, 10(5), 108240.
- Kołodzyńska, D., Krukowska, J. a., and Thomas, P. (2017). "Comparison of sorption and desorption studies of heavy metal ions from biochar and commercial active carbon." *Chem. Eng. J.*, 307, 353–363.
- Kurniawan, T.A., Chan, G.Y., Lo, W.h., and Babel, S. (2006). "Comparisons of low-cost adsorbents for treating wastewaters laden with heavy metals." *Sci. Total Environ.*, 366(2-3), 409–426.
- Kwak, J.H., Islam, M. S., Wang, S., Messele, S. A., Naeth, M. A., El-Din, M. G., and Chang, S. X. (2019). "Biochar properties and lead (II) adsorption capacity depend on feedstock type, pyrolysis temperature, and steam activation." *Chemosphere*, 231, 393–404.
- Kwon, P.S., Shahrokhi, R., Park, J., and Kim, H. (2019). "Zeolite mixtures as adsorptive fill material with sustainable bearing capacity." *WIT Trans. Eco. Envir.*, 231, 91–100.

- Langmuir, I. (1916). "The dissociation of hydrogen into atoms.III. The mechanism of the reaction." *J. Am. Chem. Soc.*, 38(6), 1145–1156.
- Lee, J.W., Lee, H.K., Lim, J.E., and Moon, H.B. (2020). "Legacy and emerging per-and polyfluoroalkyl substances (PFASs) in the coastal environment of Korea: Occurrence, spatial distribution, and bioaccumulation potential." *Chemosphere*, 251, 126633.
- Lee, Y.M., Lee, J.Y., Kim, M.K., Yang, H., Lee, J.E., Son, Y., Kho, Y., Choi, K., and Zoh, K.D. (2020). "Concentration and distribution of per-and polyfluoroalkyl substances (PFAS) in the Asan Lake area of South Korea." *J. Hazard. Mater.*, 381, 120909.
- Li, F., Duan, J., Tian, S., Ji, H., Zhu, Y., Wei, Z., and Zhao, D. (2020). "Short-chain per-and polyfluoroalkyl substances in aquatic systems: Occurrence, impacts and treatment." *Chem. Eng. J.*, 380, 122506.
- Li, H., Dong, X., da Silva, E. B., de Oliveira, L. M., Chen, Y., and Ma, L. Q. (2017). "Mechanisms of metal sorption by biochars: biochar characteristics and modifications." *Chemosphere*, 178, 466–478.
- Li, M., Messele, S. A., Boluk, Y., and El-Din, M. G. (2019). "Isolated cellulose nanofibers for Cu (II) and Zn (II) removal: performance and mechanisms." *Carbohydr. Polym.*, 221, 231–241.
- Li, X., Berger, W., Musante, C., and Mattina, M. I. (2010). "Characterization of substances released from crumb rubber material used on artificial turf fields." *Chemosphere*, 80(3), 279–285.
- Liang, J., Li, X., Yu, Z., Zeng, G., Luo, Y., Jiang, L., Yang, Z., Qian, Y., and Wu, H. (2017). "Amorphous MnO₂ modified biochar derived from aerobically composted swine manure for adsorption of Pb (II) and Cd (II)." *ACS Sustain. Chem. Eng.*, 5(6), 5049–5058.
- Lin, C., Huang, C.L., and Shern, C.C. (2008). "Recycling waste tire powder for the recovery of oil spills." *Resour. Conserv. Recycl.*, 52(10), 1162–1166.
- Liu, C. J., Werner, D., and Bellona, C. (2019). "Removal of per-and polyfluoroalkyl substances (PFASs) from contaminated groundwater using granular activated carbon: a pilot-scale study with breakthrough modeling." *Environ. Sci.: Water Res. Technol.*, 5(11), 1844–1853.
- Liu, M. Y., Tsang, D. C., Hu, J., Ng, K. T., Liu, T., and Lo, I. M. (2008). "Adsorption of methylene blue and phenol by wood waste derived activated carbon." *J. Environ. Eng.*, 134(5), 338–345.
- Liu, N., Zhang, Y., Xu, C., Liu, P., Lv, J., Liu, Y., and Wang, Q. (2020). "Removal mechanisms of aqueous Cr (VI) using apple wood biochar: a spectroscopic study." *J. Hazard. Mater.*, 384, 121371.
- Long, L., Hu, X., Yan, J., Zeng, Y., Zhang, J., and Xue, Y. (2019). "Novel chitosan–ethylene glycol hydrogel for the removal of aqueous perfluorooctanoic acid." *J. Environ. Sci.*, 84, 21–28.
- Lu, Q., de Toledo, R. A., Xie, F., Li, J., and Shim, H. (2015). "Combined removal of a BTEX, TCE, and cis-DCE mixture using *Pseudomonas* sp. immobilized on scrap tyres." *Environ. Sci. Pollut. Res.*, 22(18), 14043–14049.
- Lu, Y., Wang, Z., Ouyang, X.k., Ji, C., Liu, Y., Huang, F., and Yang, L.Y. (2020). "Fabrication of cross-linked chitosan beads grafted by polyethylenimine for efficient adsorption of diclofenac sodium from water." *Int. J. Biol. Macromol.*, 145, 1180–1188.
- Ma, Y., Cheng, L., Zhang, D., Zhang, F., Zhou, S., Ma, Y., Guo, J., Zhang, Y., and Xing, B. (2022). "Stabilization of Pb, Cd, and Zn in soil by modified-zeolite: Mechanisms and evaluation of effectiveness." *Sci. Total Environ.*, 814, 152746.

- Madhusudhan, B., Boominathan, A., and Banerjee, S. (2017). "Static and large-strain dynamic properties of sand–rubber tire shred mixtures." *J. Mat. Civil Eng.*, 29(10), 04017165.
- Madhusudhan, B., Boominathan, A., and Banerjee, S. (2019). "Factors affecting strength and stiffness of dry sand-rubber tire shred mixtures." *Geotech. Geol. Eng.*, 37(4), 2763–2780.
- Mahinroosta, R., and Senevirathna, L. (2020). "A review of the emerging treatment technologies for PFAS contaminated soils." *J. Environ. Manage.*, 255, 109896.
- Makhathini, T. P., and Rathilal, S. (2017). "Investigation of BTEX compounds adsorption onto polystyrenic resin." *S. Afr. J. Chem. Eng.*, 23(1), 71–80.
- Manchón-Vizuete, E., Macías-García, A., Gisbert, A. N., Fernández-González, C., and Gómez-Serrano, V. (2005). "Adsorption of mercury by carbonaceous adsorbents prepared from rubber of tyre wastes." *J. Hazard. Mater.*, 119(1-3), 231–238.
- Martínez, J. D., Puy, N., Murillo, R., García, T., Navarro, M. V., and Mastral, A. M. (2013). "Waste tyre pyrolysis—A review." *Renew. Sust. Energ. Rev.*, 23, 179–213.
- Merck KGaA (2020). "IR spectrum table by frequency range." <https://www.sigmaaldrich.com/technical-documents/articles/biology/ir-spectrum-table.html>.
- Milinic, J., Lacorte, S., Vidal, M., and Rigol, A. (2015). "Sorption behaviour of perfluoroalkyl substances in soils." *Sci. Total Environ.*, 511, 63–71.
- Ministry of Environment Korea (2017). "Soil environmental conservation act. Gwacheon: Ministry of Environment." <https://elaw.klri.re.kr/eng/service/lawView.do?hseq=46236&lang=ENG>.
- Mitra, S., and Roy, P. (2011). "BTEX: A serious ground-water contaminant." *Res. J. Environ. Sci.*, 5(5), 394–398.
- Mohammed, W. T., and Rashid, S. A. (2012). "Phosphorus removal from wastewater using oven-dried alum sludge." *Int. J. Chem. Eng.*, 2012.
- Mouzourakis, E., Georgiou, Y., Louloudi, M., Konstantinou, I., and Deligiannakis, Y. (2017). "Recycled-tire pyrolytic carbon made functional: A high-arsenite [As (III)] uptake material PyrC₃₅₀[®]." *J. Hazard. Mater.*, 326, 177–186.
- Murray, C.C., Vatankhah, H., McDonough, C.A., Nickerson, A., Hedtke, T.T., Cath, T.Y., Higgins, C.P., and Bellona, C.L. (2019). "Removal of per- and polyfluoroalkyl substances using super-fine powder activated carbon and ceramic membrane filtration." *J. Hazard. Mater.*, 366, 160–168.
- Naji, S. Z., and Tye, C. T. (2022). "A review of the synthesis of activated carbon for biodiesel production: Precursor, preparation, and modification." *Energy Convers. Manag.*: X, 13, 100152.
- Nguyen, T. M. H., Bräunig, J., Thompson, K., Thompson, J., Kabiri, S., Navarro, D. A., Kookana, R. S., Grimison, C., Barnes, C. M., and Higgins, C. P. (2020). "Influences of chemical properties, soil properties, and solution pH on soil–water partitioning coefficients of per- and polyfluoroalkyl substances (PFASs)." *Environ. Sci. Technol.*, 54(24), 15883–15892.
- Nieto-Márquez, A., Pinedo-Flores, A., Picasso, G., Atanes, E., and Kou, R. S. (2017). "Selective adsorption of Pb²⁺, Cr³⁺ and Cd²⁺ mixtures on activated carbons prepared from waste tires." *J. Environ. Chem. Eng.*, 5(1), 1060–1067.
- Noorzad, R., and Raveshi, M. (2017). "Mechanical behavior of waste tire crumbs–sand mixtures determined by triaxial tests." *Geotech. Geol. Eng.*, 35(4), 1793–1802.
- Nourmoradi, H., Nikaeen, M., and Khiadani, M. (2012). "Removal of benzene, toluene, ethylbenzene and xylene (BTEX) from aqueous solutions by montmorillonite modified

- with nonionic surfactant: Equilibrium, kinetic and thermodynamic study." *Chem. Eng. J.*, 191, 341–348.
- Ochoa-Herrera, V., and Sierra-Alvarez, R. (2008). "Removal of perfluorinated surfactants by sorption onto granular activated carbon, zeolite and sludge." *Chemosphere*, 72(10), 1588–1593.
- OECD (2018). "Toward a new comprehensive global database of per-and polyfluoroalkyl substances (PFASs): Summary report on updating the OECD 2007 list of per-and polyfluoroalkyl substances (PFASs)." *OECD Environment Directorate, Environment, Health and Safety Division, Paris*.
- Oladoja, N., Ofomaja, A., Idiaghe, J., Akinlabi, A., and Egbon, E. (2010). "Sorption of Cu (II) ion from aqueous solution by scrap tyre." *Desalin. Water Treat.*, 16(1–3), 83–94.
- Pan, S.Y., Syu, W.J., Chang, T.K., and Lee, C.H. (2020). "A multiple model approach for evaluating the performance of time-lapse capsules in trapping heavy metals from water bodies." *RSC Adv.*, 10(28), 16490–16501.
- Park, H., Choo, G., Kim, H., and Oh, J.E. (2018). "Evaluation of the current contamination status of PFASs and OPFRs in South Korean tap water associated with its origin." *Sci. Total Environ.*, 634, 1505–1512.
- Park, J.H., Ok, Y. S., Kim, S.H., Cho, J.S., Heo, J.S., Delaune, R. D., and Seo, D.C. (2016). "Competitive adsorption of heavy metals onto sesame straw biochar in aqueous solutions." *Chemosphere*, 142, 77–83.
- Park, M., Wu, S., Lopez, I. J., Chang, J. Y., Karanfil, T., and Snyder, S. A. (2020). "Adsorption of perfluoroalkyl substances (PFAS) in groundwater by granular activated carbons: Roles of hydrophobicity of PFAS and carbon characteristics." *Water Res.*, 170, 115364.
- Peng, H., Gao, P., Chu, G., Pan, B., Peng, J., and Xing, B. (2017). "Enhanced adsorption of Cu (II) and Cd (II) by phosphoric acid-modified biochars." *Environ. Pollut.*, 229, 846–853.
- Qian, J., Shen, M., Wang, P., Wang, C., Li, K., Liu, J., Lu, B., and Tian, X. (2017). "Perfluorooctane sulfonate adsorption on powder activated carbon: effect of phosphate (P) competition, pH, and temperature." *Chemosphere*, 182, 215–222.
- Qiao, L., Li, S., Li, Y., Liu, Y., and Du, K. (2020). "Fabrication of superporous cellulose beads via enhanced inner cross-linked linkages for high efficient adsorption of heavy metal ions." *J. Clean. Prod.*, 253, 120017.
- Qu, J., Liu, Y., Cheng, L., Jiang, Z., Zhang, G., Deng, F., Wang, L., Han, W., and Zhang, Y. (2021). "Green synthesis of hydrophilic activated carbon supported sulfide nZVI for enhanced Pb (II) scavenging from water: characterization, kinetics, isotherms and mechanisms." *J. Hazard. Mater.*, 403, 123607.
- Ray, J. R., Shabtai, I. A., Teixidó, M., Mishaël, Y. G., and Sedlak, D. L. (2019). "Polymer-clay composite geomedia for sorptive removal of trace organic compounds and metals in urban stormwater." *Water Res.*, 157, 454–462.
- Raychaudhuri, S. S., Pramanick, P., Talukder, P., and Basak, A. (2021). "Polyamines, metallothioneins, and phytochelatin—Natural defense of plants to mitigate heavy metals." *Studies in Natural Products Chemistry*, 69, 227–261.
- Reddy, S., Pradeep Kumar, D., and Murali Krishna, A. (2015). "Evaluation of the optimum mixing ratio of a sand-tire chips mixture for geoenvironmental applications." *J. Mater. Civil Engin.*, 28(2), 06015007.
- Reddy, S. B., Krishna, A. M., and Reddy, K. R. (2018). "Sustainable utilization of scrap tire derived geomaterials for geotechnical applications." *Ind. Geotech. J.*, 48(2), 251–266.

- Ross, I., McDonough, J., Miles, J., Storch, P., Thelakkat Kochunarayanan, P., Kalve, E., Hurst, J., S. Dasgupta, S., and Burdick, J. (2018). "A review of emerging technologies for remediation of PFASs." *Remed. J.*, 28(2), 101–126.
- Rouquerol, J., Rouquerol, F., Llewellyn, P., Maurin, G., and Sing, K. S. (2013). "Adsorption by powders and porous solids: principles, methodology and applications." *Second ed. Academic press.*
- Roy, W., Krapac, I., Chou, S., and Griffin, R. (1986). "Batch-type adsorption procedures for estimating soil attenuation of chemicals." *Environmental Protection Agency, Washington, DC.*
- Saeidi, N., Kopinke, F.D., and Georgi, A. (2020). "Understanding the effect of carbon surface chemistry on adsorption of perfluorinated alkyl substances." *Chem. Eng. J.*, 381, 122689.
- Saleh, T. A., and Gupta, V. K. (2014). "Processing methods, characteristics and adsorption behavior of tire derived carbons: a review." *Adv. Colloid Interface Sci.*, 211, 93–101.
- Salgado, R., Yoon, S., and Siddiki, N. Z. (2003). "Construction of tire shreds test embankment." *Rep. No. FHWA/IN/JTRP-2002/35*, Indiana Dept. of Transportation, Indianapolis
- Schaefer, C. E., Nguyen, D., Culina, V. M., Guelfo, J., and Kumar, N. (2020). "Application of rapid small-scale column tests for treatment of perfluoroalkyl acids using anion-exchange resins and granular activated carbon in groundwater with elevated organic carbon." *Ind. Eng. Chem. Res.*, 59(38), 16832–16837.
- Sekhar, G. (2014). "Proceedings of the Tire Technology Expo." *Cologne, Germany.*
- Selbes, M., Yilmaz, O., Khan, A. A., and Karanfil, T. (2015). "Leaching of DOC, DN, and inorganic constituents from scrap tires." *Chemosphere*, 139, 617–623.
- Seo, S.H., Son, M.H., Choi, S.D., Lee, D.H., and Chang, Y.S. (2018). "Influence of exposure to perfluoroalkyl substances (PFASs) on the Korean general population: 10-year trend and health effects." *Environ. Int.*, 113, 149–161.
- Shaid, M. S. H. M., Zaini, M. A. A., and Nasri, N. S. (2019). "Evaluation of methylene blue dye and phenol removal onto modified CO₂-activated pyrolysis tyre powder." *J. Clean. Prod.*, 223, 487–498.
- Shakeri, A., Salehi, H., and Rastgar, M. (2017). "Chitosan-based thin active layer membrane for forward osmosis desalination." *Carbohydr. Polym.*, 174, 658–668.
- Shakeri, H., Arshadi, M., and Salvacion, J. (2016). "Removal of BTEX by using a surfactant–bio originated composite." *J. colloid and interface sci.*, 466, 186–197.
- Shan, R., Shi, Y., Gu, J., Wang, Y., and Yuan, H. (2020). "Single and competitive adsorption affinity of heavy metals toward peanut shell-derived biochar and its mechanisms in aqueous systems." *Chin. J. Chem. Eng.*, 28(5), 1375–1383.
- Sikder, M. T., Kikuchi, T., Suzuki, J., Hosokawa, T., Saito, T., and Kurasaki, M. (2013). "Removal of cadmium and chromium ions using modified α , β , and γ -cyclodextrin polymers." *Sep. Sci. Technol.*, 48(4), 587–597.
- Simantiraki, F., and Gidarakos, E. (2015). "Comparative assessment of compost and zeolite utilisation for the simultaneous removal of BTEX, Cd and Zn from the aqueous phase: batch and continuous flow study." *J. Environ. Manage.*, 159, 218–226.
- Singh, E., Kumar, A., Mishra, R., You, S., Singh, L., Kumar, S., and Kumar, R. (2021). "Pyrolysis of waste biomass and plastics for production of biochar and its use for removal of heavy metals from aqueous solution." *Bioresour. Technol.*, 320, 124278.
- Smičiklas, I., Dimović, S., Plečaš, I., and Mitrić, M. (2006). "Removal of Co²⁺ from aqueous solutions by hydroxyapatite." *Water Res.*, 40(12), 2267–2274.

- Soganci, A. (2015). "Strength characteristics of tire-sand mixtures." *Soil Mech. Found. Eng.*, 51(6), 306–309.
- Soltani, A., Deng, A., Taheri, A., and O'Kelly, B. C. (2019). "Engineering reactive clay systems by ground rubber replacement and polyacrylamide treatment." *Polymers*, 11(10), article 1675.
- Söregård, M., Gago-Ferrero, P., Kleja, D. B., and Ahrens, L. (2021). "Laboratory-scale and pilot-scale stabilization and solidification (S/S) remediation of soil contaminated with per- and polyfluoroalkyl substances (PFASs)." *J. Hazard. Mater.*, 402, 123453.
- Sorengard, M., Kleja, D. B., and Ahrens, L. (2019). "Stabilization of per- and polyfluoroalkyl substances (PFASs) with colloidal activated carbon (PlumeStop[®]) as a function of soil clay and organic matter content." *J. Environ. Manage.*, 249, 109345.
- Söregård, M., Kleja, D. B., and Ahrens, L. (2019). "Stabilization and solidification remediation of soil contaminated with poly- and perfluoroalkyl substances (PFASs)." *J. Hazard. Mater.*, 367, 639–646.
- Sørmo, E., Silvani, L., Bjerkli, N., Hagemann, N., Zimmerman, A. R., Hale, S. E., Hansen, C. B., Hartnik, T., and Cornelissen, G. (2021). "Stabilization of PFAS-contaminated soil with activated biochar." *Sci. Total Environ.*, 763, 144034.
- Srivastava, A., Dutta, S., Ahuja, S., and Sharma, R. K. (2021). "Green chemistry: key to reducing waste and improving water quality." *Handbook of Water Purity and Quality*, 359–407.
- Steigerwald, J. M., and Ray, J. R. (2021). "Adsorption behavior of perfluorooctanesulfonate (PFOS) onto activated spent coffee grounds biochar in synthetic wastewater effluent." *J. Hazard. Mater. Letters*, 2, 100025.
- Stuart, B. H. (2004). "Infrared Spectroscopy: Fundamentals and Applications." *J. Wiley & Sons*.
- Su, F., Lu, C., and Hu, S. (2010). "Adsorption of benzene, toluene, ethylbenzene and p-xylene by NaOCl-oxidized carbon nanotubes." *Colloids Surf. A: Physicochem. Eng. Asp.*, 353(1), 83–91.
- Su, F., Lu, C., Johnston, K. R., and Hu, S. (2010). "Kinetics, thermodynamics, and regeneration of BTEX adsorption in aqueous solutions via NaOCl-oxidized carbon nanotubes." *Environanotechnology*, Elsevier, 71–97.
- Suneel, M., Konni, G., Chul, I. J., and Dung, N. T. (2018). "Secondary compression index equation for soft clays." *Geotech. Geol. Eng.*, 36(2), 1387–1392.
- Swartjes, F. A. (2011). "Introduction to contaminated site management." *Dealing with contaminated sites*, Springer, 3–89.
- Tan, Z., Yuan, S., Hong, M., Zhang, L., and Huang, Q. (2020). "Mechanism of negative surface charge formation on biochar and its effect on the fixation of soil Cd." *J. Hazard. Mater.*, 384, 121370.
- Tang, C., Shu, Y., Zhang, R., Li, X., Song, J., Li, B., Zhang, Y., and Ou, D. (2017). "Comparison of the removal and adsorption mechanisms of cadmium and lead from aqueous solution by activated carbons prepared from *Typha angustifolia* and *Salix matsudana*." *RSC Adv.*, 7(26), 16092–16103.
- Teng, H., Lin, Y.C., and Hsu, L.Y. (2000). "Production of activated carbons from pyrolysis of waste tires impregnated with potassium hydroxide." *J. Air. Waste. Manag. Assoc.*, 50(11), 1940–1946.
- Tofighy, M. A., and Mohammadi, T. (2011). "Adsorption of divalent heavy metal ions from water using carbon nanotube sheets." *J. Hazard. Mater.*, 185(1), 140–147.

- Uchimiya, M., Wartelle, L. H., Klasson, K. T., Fortier, C. A., and Lima, I. M. (2011). "Influence of pyrolysis temperature on biochar property and function as a heavy metal sorbent in soil." *J. Agric. Food Chem.*, 59(6), 2501–2510.
- Vaezihir, A., Bayanlou, M. B., Ahmadnezhad, Z., and Barzegari, G. (2020). "Remediation of BTEX plume in a continuous flow model using zeolite-PRB." *J. Contam. Hydrol.*, 230, 103604.
- Vardhan, K. H., Kumar, P. S., and Panda, R. C. (2019). "A review on heavy metal pollution, toxicity and remedial measures: Current trends and future perspectives." *J. Mol. Liq.*, 290, 111197.
- Varsha, M., Kumar, P. S., and Rathi, B. S. (2022). "A review on recent trends in the removal of emerging contaminants from aquatic environment using low-cost adsorbents." *Chemosphere*, 287, 132270.
- Velo-Gala, I., López-Peñalver, J. J., Sánchez-Polo, M., and Rivera-Utrilla, J. (2014). "Surface modifications of activated carbon by gamma irradiation." *Carbon*, 67, 236–249.
- Vidal, C. B., Raulino, G. S., Barros, A. L., Lima, A. C., Ribeiro, J. P., Pires, M. J., and Nascimento, R. F. (2012). "BTEX removal from aqueous solutions by HDTMA-modified Y zeolite." *J. Environ. Manage.*, 112, 178–185.
- Vu, C. T., and Wu, T. (2020). "Recent progress in adsorptive removal of per-and poly-fluoroalkyl substances (PFAS) from water/wastewater." *Crit. Rev. Environ. Sci. Technol.*, 52(1), 90–129.
- Wakatsuki, T., Furukawa, H., and Kawaguchi, K. (1974). "Specific and non-specific adsorption of inorganic ions I. Evaluation of specific adsorbability by means of minimum concentration for specific adsorption." *Soil Sci. Plant Nutr.*, 20(4), 353–362.
- Wang, H., Wang, Z., Yue, R., Gao, F., Ren, R., Wei, J., Wang, X., and Kong, Z. (2020). "Functional group-rich hyperbranched magnetic material for simultaneous efficient removal of heavy metal ions from aqueous solution." *J. Hazard. Mater.*, 384, 121288.
- Wang, J., and Guo, X. (2020). "Adsorption isotherm models: Classification, physical meaning, application and solving method." *Chemosphere*, 127279.
- Wang, J., and Zhuang, S. (2017). "Removal of various pollutants from water and wastewater by modified chitosan adsorbents." *Crit. Rev. Environ. Sci. Technol.*, 47(23), 2331–2386.
- Wang, W., Maimaiti, A., Shi, H., Wu, R., Wang, R., Li, Z., Qi, D., Yu, G., and Deng, S. (2019). "Adsorption behavior and mechanism of emerging perfluoro-2-propoxypropanoic acid (GenX) on activated carbons and resins." *Chem. Eng. J.*, 364, 132–138.
- Wartman, J., Natale, M. F., and Strenk, P. M. (2007). "Immediate and time dependent compression of tire derived aggregate." *J. Geotech. Geoenviron.*, 133(3), 245–256.
- Wen, J., Dong, H., and Zeng, G. (2018). "Application of zeolite in removing salinity/sodicity from wastewater: A review of mechanisms, challenges and opportunities." *J. Clean. Prod.*, 197, 1435–1446.
- Wibowo, N., Setyadi, L., Wibowo, D., Setiawan, J., and Ismadji, S. (2007). "Adsorption of benzene and toluene from aqueous solutions onto activated carbon and its acid and heat treated forms: influence of surface chemistry on adsorption." *J. Hazard. Mater.*, 146(1–2), 237–242.
- Wik, A., and Dave, G. (2009). "Occurrence and effects of tire wear particles in the environment—A critical review and an initial risk assessment." *Environ. Pollut.*, 157(1), 1–11.

- Wu, C., Klemes, M. J., Trang, B., Dichtel, W. R., and Helbling, D. E. (2020). "Exploring the factors that influence the adsorption of anionic PFAS on conventional and emerging adsorbents in aquatic matrices." *Water Res.*, 182, 115950.
- Wu, J., Wang, T., Zhang, Y., and Pan, W.-P. (2019). "The distribution of Pb (II)/Cd (II) adsorption mechanisms on biochars from aqueous solution: Considering the increased oxygen functional groups by HCl treatment." *Bioresour. Technol.*, 291, 121859.
- Wu, W., Wu, J., Liu, X., Chen, X., Wu, Y., and Yu, S. (2017). "Inorganic phosphorus fertilizer ameliorates maize growth by reducing metal uptake, improving soil enzyme activity and microbial community structure." *Ecotoxicol. Environ. Saf.*, 143, 322–329.
- Xie, X., Gao, H., Luo, X., Su, T., Zhang, Y., and Qin, Z. (2019). "Polyethyleneimine modified activated carbon for adsorption of Cd (II) in aqueous solution." *J. Environ. Chem. Eng.*, 7(3), 103183.
- Xu, R.k., Xiao, S.c., Yuan, J.h., and Zhao, A.z. (2011). "Adsorption of methyl violet from aqueous solutions by the biochars derived from crop residues." *Bioresour. Technol.*, 102(22), 10293–10298.
- Yadav, V. B., Gadi, R., and Kalra, S. (2019). "Clay based nanocomposites for removal of heavy metals from water: A review." *J. Environ. Manage.*, 232, 803–817.
- Yakout, S., and Daifullah, A. (2014). "Adsorption/desorption of BTEX on activated carbon prepared from rice husk." *Desalin. Water Treat.*, 52(22-24), 4485–4491.
- Yakout, S. M. (2014). "Removal of the hazardous, volatile, and organic compound benzene from aqueous solution using phosphoric acid activated carbon from rice husk." *Chem. Cent. J.*, 8(1), 1–7.
- Yan, B., Munoz, G., Sauvé, S., and Liu, J. (2020). "Molecular mechanisms of per- and polyfluoroalkyl substances on a modified clay: a combined experimental and molecular simulation study." *Water Res.*, 184, 116166.
- Yang, A., Ching, C., Easler, M., Helbling, D. E., and Dichtel, W. R. (2020). "Cyclodextrin polymers with nitrogen-containing tripodal crosslinkers for efficient PFAS adsorption." *ACS Mater. Lett.*, 2(9), 1240–1245.
- Yong, Z. Y., Kim, K. Y., and Oh, J.E. (2021). "The occurrence and distributions of per- and polyfluoroalkyl substances (PFAS) in groundwater after a PFAS leakage incident in 2018." *Environ. Pollut.*, 268, 115395.
- Yu, H., Chen, W., Gong, Z., Tan, X., Ma, Y., Li, X. L., and Sillen, X. (2015). "Creep behavior of boom clay." *Int. J. Rock Mech. Min. Sci.*, 76, 256–264.
- Yu, Q., Deng, S., and Yu, G. (2008). "Selective removal of perfluorooctane sulfonate from aqueous solution using chitosan-based molecularly imprinted polymer adsorbents." *Water Res.*, 42(12), 3089–3097.
- Yu, Q., Zhang, R., Deng, S., Huang, J., and Yu, G. (2009). "Sorption of perfluorooctane sulfonate and perfluorooctanoate on activated carbons and resin: Kinetic and isotherm study." *Water Res.*, 43(4), 1150–1158.
- Zaggia, A., Conte, L., Falletti, L., Fant, M., and Chiorboli, A. (2016). "Use of strong anion exchange resins for the removal of perfluoroalkylated substances from contaminated drinking water in batch and continuous pilot plants." *Water Res.*, 91, 137–146.
- Zhang, D., Zhang, W., and Liang, Y. (2019). "Adsorption of perfluoroalkyl and polyfluoroalkyl substances (PFASs) from aqueous solution-A review." *Sci. Total Environ.*, 694, 133606.

- Zhang, H., Shao, J., Zhang, S., Zhang, X., and Chen, H. (2020). "Effect of phosphorus-modified biochars on immobilization of Cu (II), Cd (II), and As (V) in paddy soil." *J. Hazard. Mater.*, 390, 121349.
- Zhang, L., Guo, J., Huang, X., Wang, W., Sun, P., Li, Y., and Han, J. (2019). "Functionalized biochar-supported magnetic MnFe 2 O 4 nanocomposite for the removal of Pb (ii) and Cd (ii)." *RSC Adv.*, 9(1), 365–376.
- Zhang, L., Tu, L.y., Liang, Y., Chen, Q., Li, Z.-s., Li, C.h., Wang, Z.h., and Li, W. (2018). "Coconut-based activated carbon fibers for efficient adsorption of various organic dyes." *RSC Adv.*, 8(74), 42280–42291.
- Zhang, P., O'Connor, D., Wang, Y., Jiang, L., Xia, T., Wang, L., Tsang, D. C., Ok, Y. S., and Hou, D. (2020). "A green biochar/iron oxide composite for methylene blue removal." *J. Hazard. Mater.*, 384, 121286.
- Zhang, Q., Deng, S., Yu, G., and Huang, J. (2011). "Removal of perfluorooctane sulfonate from aqueous solution by crosslinked chitosan beads: sorption kinetics and uptake mechanism." *Bioresour. Technol.*, 102(3), 2265–2271.
- Zhang, W., Ding, W., and Ying, W. (2013). "Biological activated carbon treatment for removing BTEX from groundwater." *J. Environ. Eng.*, 139(10), 1246–1254.
- Zhang, Y., Song, X., Zhang, P., Gao, H., Ou, C., and Kong, X. (2020). "Production of activated carbons from four wastes via one-step activation and their applications in Pb²⁺ adsorption: Insight of ash content." *Chemosphere*, 245, 125587.
- Zhang, Y., Wang, Y., Zhang, H., Li, Y., Zhang, Z., and Zhang, W. (2020). "Recycling spent lithium-ion battery as adsorbents to remove aqueous heavy metals: Adsorption kinetics, isotherms, and regeneration assessment." *Resour. Conserv. Recycl.*, 156, 104688.
- Zhao, L., Bian, J., Zhang, Y., Zhu, L., and Liu, Z. (2014). "Comparison of the sorption behaviors and mechanisms of perfluorosulfonates and perfluorocarboxylic acids on three kinds of clay minerals." *Chemosphere*, 114, 51–58.
- Zhao, L., Cao, X., Zheng, W., Wang, Q., and Yang, F. (2015). "Endogenous minerals have influences on surface electrochemistry and ion exchange properties of biochar." *Chemosphere*, 136, 133–139.
- Zhao, P., Xia, X., Dong, J., Xia, N., Jiang, X., Li, Y., and Zhu, Y. (2016). "Short-and long-chain perfluoroalkyl substances in the water, suspended particulate matter, and surface sediment of a turbid river." *Sci. Total Environ.*, 568, 57–65.
- Zheng, X., Yu, N., Wang, X., Wang, Y., Wang, L., Li, X., and Hu, X. (2018). "Adsorption properties of granular activated carbon-supported titanium dioxide particles for dyes and copper ions." *Sci. Rep.*, 8(1), 1–9.
- Ziyang, Z., Hidajat, K., and Ray, A. K. (2001). "Determination of adsorption and kinetic parameters for methyl tert-butyl ether synthesis from tert-butyl alcohol and methanol." *J. Catal.*, 200(2), 209–221.
- Zornberg, J. G., Costa, Y. D., and Vollenweider, B. (2004). "Performance of prototype embankment built with tire shreds and nongranular soil." *Transp. Res. Rec.*, 1874(1), 70–77.

초 록

급속한 산업화와 도시화는 생활수준, 생산성 및 경제를 향상시켰으나, 다양한 오염물질을 발생시켜 환경에 악영향을 주고있는것도 사실이다. 산업단지에서는 상당한 수준의 폐수를 유출하고 있고, 이는 토양을 통하여 지하수까지 오염시키고 있다. 여타의 산업국가와 같이 대한민국에서도 다양한 유기화합물과 중금속과 같은 무기물질에 의한 오염문제가 심각한 수준이다. 그러한 유기화합물 중에는 새로이 과불화화합물 (PFAS, per and polyfloroalkyl substances) 과 같은 할로겐족 유기화합물과 더불어 기존의 산업용제인 BTEX (benzene, toluene, ethylbenzene, and xylenes) 가 대표적이다. 또한 산업재료인 중금속 (Pb, Zn, and Cu) 또한 고농도 상태로 자주 발견된다.

흡착성물질을 흙과 혼합하여 조성한 바닥반응층 (Bottom Reactive Layer, BRL) 이러한 오염물질이 지중에서 확산하여 지하수를 오염시키는 상황을 제어할 수 있는 정화공법이다. 본 연구를 통하여 흡착효과가 탁월하고 비용이 저렴한 재활용 폐기물을 활용한 바닥반응층 조성물질을 개발하였다.

본 연구의 첫 부분은 분쇄된 폐타이어 (Pulverized Waste Tires, PWT) 를 활용하여, 폐타이어와 양입도의 모래를 다양한 비율로 혼합하여, 이의 바닥반응층으로서의 흡착능과 지반공학적인 물성을 평가하였다. PWT (0, 5, 10, 15, 25, 그리고 100% 무게비) 로 모래와 혼합하여 각 혼합비의 BTEX 와 두 종류의 중금속 (Pb^{2+} 와 Cu^{2+})에 대한 제거능을 평가하였다. 또한, 탄화과정과 화학적 활성화 기술로 제조된 타이어로 만든 활성탄 (Tire Derived

Activated Carbon, TAC) 으로 세 가지 중금속 (Pb^{2+} , Cu^{2+} 과 Zn^{2+}) 의 혼합액에 대한오염제거능을 조사하였다.

본 연구의 두 번째 부분에서는, 대한민국에서 빈번하게 발견되는 두 종류의 장쇄 (PFOA 및 PFOS) 와 두 종류의 단쇄 (PFBA 및 PFBS) 의 PFAS 물질에 대한 토양 및 수용액 상태에서의 제거를 평가하였는바, 흡착물질로는 키토산비드 (Chitosan Beads, CB) 아민기조성키토산비드 (Amine Functional Grafted Chitosan Beads, GCB) 를 사용하였다. 또한, 컬럼시험을 수행하여 PFAS 의 고액분배계수 (kd) 를 구하였다.

연구의 각 단계에서 대상 오염물질에 대한 흡착물질의 효율성을 평가하고자, 일련의 회분식 등온흡탈착시험, 동적흡착, 선별흡착, pH 영향성시험, 그리고 흡착물질 재활용가능성시험등을 수행하였다.

본 연구수행을 통하여 개발된 흡착물질은 토양 및 수환경에서 해당 유기/무기오염물질을효과적으로 제거 할 수 있는것으로 평가되었다.

주요어: 오염물질, 바닥 반응층, 중금속, BTEX, PFAS

학번: 2017-36819

Acknowledgment

I would like to take this opportunity to express my honest appreciation to all those who supported me through this journey with their supervision, inspiration, encouragement, guidance, assistance, criticism and love.

First and foremost, my sincere acknowledgement goes to my principal supervisor, Professor Junboun Park. Junboun, your insightful and valuable guidance and support always shed light on my PhD journey. You were always available for any discussion, and your office was open even when you were busy. Your kind and patient approach brought me peace of mind. I learned from you a lot. You have my most profound respect and appreciation for your invaluable academic and intellectual support.

I wish to express my appreciation to my co-supervisors, Prof. Choong-Ki Chung and Prof. Sung-Ryul Kim who were excellent mentors. Thank you for your advice, guidance, and detailed feedback which were immensely helpful throughout my candidature. Thank you for your assistance and encouragement. Your support means a lot to me and is very much appreciated.

I would like to acknowledge the all staffs in department of Civil and Environmental Engineering in Seoul National University for their nice and kind attitudes.

I also would like to extend my appreciation to all members of the Geotechnical and geoenvironmental group in Seoul National University. Collaborating and spending time with you made this journey more interesting for me.

I would love to express my special love and gratitude to all of my friends during my PhD. Your inspiration and encouragement made this journey more lovely and unforgettable for me.

Eventually, this dissertation is dedicated to my beloved parents and siblings. I am indebted to my parents, Susan and Farhad, for all of their support over the years. Without them, there was no way I could have gotten where I am today. Mum and Dad, there is no word to express my thankfulness, but I know you have been with me every single moment of my life. Thanks for your unconditional love. Special thanks to my siblings, Nayereh, Nafise and Nasimeh, for their

everyday love and emotional support. I learned and inspired a lot from you. Having you always on my side made everything in my life much easier and more enjoyable.